UNIVERSITY OF CALIFORNIA
RIVERSIDE

Peroxisome Proliferator-Activated Receptor γ (PPARγ): Potential Role During Early Embryonic Development and as a Target for Environmental Chemicals

A Dissertation submitted in partial satisfaction
of the requirements for the degree of

Doctor of Philosophy

in

Environmental Toxicology

by

Vanessa Cheng

September 2021

Dissertation Committee:
Dr. David C Volz, Chairperson
Dr. David Eastmond
Dr. Changcheng Zhou

The Dissertation of Vanessa Cheng is approved:

Committee Chairperson

University of California, Riverside

Acknowledgements

The culmination of this work would not have been possible without the support of many colleagues, friends, and family. I would first like to acknowledge and thank my advisor, Dr. David Volz, for his mentorship, guidance, and training over the past four years. Although I did not start my graduate studies in your lab, I am grateful that it is where I ended up and completed my dissertation. I have gained many research skills, discussed numerous topics, and received valuable advice that have all enhanced the way in which I view and understand the world. I would also like to thank the various committee members for their advice and feedback: Dr. David Eastmond, Dr. Changcheng Zhou, Dr. Tara Nordgren, Dr. Morris Maduro, and Dr. Daniel Schlenk.

Next, I would like to acknowledge past and present lab members and collaborators that have assisted with training and research. Thank you Dr. Subham Dasgupta, Dr. Sara Vliet, Constance Mitchell, and Dr. Aalekhya Reddam for welcoming me into the Volz Lab and training me on zebrafish care, cell culture, and all the other lab techniques used to complete the work presented here. Thank you for your patience as I tried to learn everything you would teach me and for answering all the questions that I had, even after you all had moved on to different careers. Thank you, Dr. Victoria McGruer, Jenna Wiegand, and Sarah Avila-Barnard, for your friendship, advice, and support, all of which made my time as a graduate student enjoyable and memorable.

Lastly, I would like to thank my friends and family for their support. I have been incredibly lucky to have a strong support system. To my parents, thank you for supporting me in all my academic and personal endeavors. To my sister, Katherine, thank you for being a constant source of encouragement. To my partner, Kevin, thank you for being by my side throughout my time at UC Riverside and for having confidence that I could finish my studies even when I didn't.

This research was supported by UCR's Graduate Division and the NRSA T32 Training Program (T32ES018827). Research support was provided by a National Institutes of Health grant (R01ES027576) and USDA National Institute of Food and Agriculture Hatch Project (1009609). Partial funding for attendance to conferences was also provided by the UCR Graduate Student Association Travel Grants and the Teratology Society Student Travel Award.

Copyright Acknowledgements

The text and figures in Chapter 2, in part or in full, are a reprint of the material as it appears in "Ciglitazone- a human PPARγ agonist- disrupts dorsoventral patterning in zebrafish" published in PeerJ, 2019. The coauthors Subham Dasgupta and Aalekhya Reddam assisted in carrying out experiments and analyzing data. Co-author Dr. David Volz directed and supervised this research.

The text and figures in Chapter 3, in part or in full, are a reprint of the materials as it appears in "Utilizing systems biology to reveal cellular responses to peroxisome proliferator-activated receptor γ ligand exposure" published in Current Research in Toxicology, Vol. 2, Pages 169-178, 2021. The co-authors Aalekhya Reddam, Anil Bhatia, Manhoi Hur and, Jay S. Kirkwood assisted in carrying out experiments and analyzing data. Co-author Dr. David Volz directed and supervised this research.

The text and figures in Chapter 4, in part or in full, are currently under review for publication as "Halogenated bisphenol A analogues induce PPARγ-independent toxicity within human hepatocellular carcinoma cells" in Chemical Research in Toxicology. This work was submitted for publication on August 4th, 2021.

ABSTRACT OF THE DISSERTATION

Peroxisome Proliferator-Activated Receptor γ (PPARγ):
Potential Role During Early Embryonic Development and as a Target for Environmental Chemicals

by

Vanessa Cheng

Doctor of Philosophy, Graduate Program in Environmental Toxicology
University of California, Riverside, September 2021
Dr. David C Volz, Chairperson

Peroxisome proliferator-activated receptor γ (PPARγ) is a nuclear receptor that heterodimerizes with retinoid X receptor (RXR), binds to PPAR response elements (PPREs), and activates transcription of genes involved in adipogenesis, fatty acid storage, and glucose metabolism. PPARγ-specific pharmaceuticals (e.g., thiazolidinediones) have been developed to treat Type II diabetes within human populations. However, *in vitro* and *in vivo* (rodent) studies have demonstrated that PPARγ can also be activated by environmental chemicals. Due to the ubiquitous presence of these environmental chemicals, they pose a potential concern for those chronically exposed via inhalation or ingestion of contaminated dust. However, while the potential role of PPARγ in regulating later stages of development has been explored, it is unclear whether 1) exposure to PPARγ agonists may alter early embryonic developmental processes and 2) downstream impacts on cell signaling and physiology are directly associated with PPARγ activation by drugs and environmental chemicals. Therefore, the primary objectives of this dissertation are to 1) test the hypothesis that exposure to a human PPARγ agonist (ciglitazone) disrupts dorsoventral patterning during early embryonic development within zebrafish, 2) map

genomic, transcriptomic, and lipidomic changes in human hepatocarcinoma (HepG2) cells after exposure to a reference PPARγ agonist (ciglitazone) and antagonist (GW 9662), and 3) test the hypothesis that exposure to environmental chemicals (tetrabromobisphenol A and tetrachlorobisphenol A) – suspected PPARγ agonists – results in PPARγ-mediated transcriptional and lipidomic changes within HepG2 cells. For Aim 1, using ciglitazone to activate PPARγ and a pparγ-specific morpholino to knockdown pparγ, we found that ciglitazone affects dorsoventral patterning in developing zebrafish embryos in a PPARγ-independent manner. For Aim 2, using chromatin immunoprecipitation-sequencing, mRNA-sequencing, neutral lipid staining, and lipidomics, we mapped genomic, transcriptomic, and lipidomics changes following exposure to a ciglitazone or GW 9662, but did not find changes at one level to be predictive of changes at other levels. For Aim 3, TBBPA and TCBPA exposure did not result in downstream PPARγ-dependent transcriptomic or neutral lipid changes. Overall, our findings further our understanding about how exogenous PPARγ ligands may alter early embryonic development and affect lipid homeostasis within human cells.

Table of Contents

List of Figures

Chapter 2

Chapter 3

Chapter 4

List of Tables

Chapter 1: Introduction

1.1 The PPAR class of Receptors

In 1983, scientists discovered that administering rat liver cytosolic fractions with nafenopin or clofibrate resulted in an increase in peroxisomes (Lalwani et al., 1983). While the mechanism by which these peroxisomes proliferated was yet to be determined, this class of receptors was named after the observed physiological result: peroxisome proliferator-activated receptor (PPAR). While the activation of this class of receptors does not induce an increase in peroxisomes in humans, PPARs are conserved between humans and rodents. The human isoforms of PPARs were subsequently cloned and have been found in species across the animal kingdom (Issemann and Green, 1990).

To date, there are three types of PPARs within this steroid hormone nuclear receptor superfamily: alpha (α), beta/delta (β/δ), and gamma (γ). While PPAR function and localization to cell types differ, all PPARs respond to ligand binding, recruit cofactors, heterodimerize with retinoid X receptor (RXR), bind to peroxisome proliferator response elements (PPREs), and induce transcription of downstream genes (Kliewer et al., 1992). All three PPAR types bind to the following PPRE consensus sequence: AGGTCANAGGTCA (IJpenber et al., 1997).

PPARα, the first of this family to be discovered, is found in relatively high amounts in heart, skeletal, liver, and brown adipose tissue (Brasissant et al., 1996; Su et al., 2009). Endogenous ligands for PPARα include polyunsaturated fatty acids, leukotriene B4, and 8-hydroxy-eicosatetraenoic acid (Narala et al., 2010; Forman et al., 1997; Kliewer et al., 1997). Gene targets of PPARα include acyl-CoA oxidase, thiolase, CYP 8B1, fatty acid transport protein, lipoprotein lipase, and apolipoprotein A-I and A-II (Muerhoff et al., 1992). Based on these gene targets and studies performed in rodent models, PPARα mediates processes such as beta-oxidation and fatty acid metabolism (Aoyama et al., 1998).

PPARβ/δ is expressed ubiquitously, but higher levels are found in heart, skeletal, and brain tissue (Braissant et al., 1996; Kliewer et al., 1994; Auboeuf et al., 1997). Similar to PPARα, PPARβ/δ can also be activated by unsaturated fatty acids (Forman et al., 1997). Other endogenous ligands for PPARβ/δ include prostacyclin and components of very low-density lipoprotein (VLDL) (Xu et al., 1999; Gupta et al., 2000). PPARβ/δ-specific target genes include those that are involved in lipid uptake, metabolism, and efflux. In skeletal and cardiac muscle, PPARβ/δ participates in fatty acid oxidation (Wang et al., 2004). In other tissues, PPARβ/δ regulates blood cholesterol concentrations and glucose levels (Lee et al., 2006).

PPARγ, the third receptor of this class to be discovered, has two human isoforms. PPARγ1 is expressed in various tissue types, including adipose, muscle, liver, and cardiac tissue (Braissant et al., 1996; Kliewer et al., 2001). PPARγ2, which contains 30 additional amino acids at the N-terminal domain, is highly expressed in adipose tissue (Tontonoz et al., 1994). Similar to the other two receptors in this class, endogenous ligands of PPAR include 15-deoxy-delta 12, 14-prostaglandin J2 (Forman et al., 1995; Kliewer et al., 1995) and oxidized low-density lipoproteins (Nagy et al., 1998). Activation of PPARγ has shown to transcribe genes such as Cd36, Fabp4/aP2, Plin2/Adrp, Fsp27, and monoacylglycerol O-acyltransferase 1 (Nagy et al., 1998; Lee et al., 2012). These genes are involved in adipogenesis, lipid metabolism, and glucose metabolism (Tontonoz et al., 1994).

Taken together, the PPAR class of nuclear receptors function as lipid and glucose regulators. While PPARα and PPARβ/δ are involved in the transcription of genes that oxidize fatty acids to provide energy for other tissues, PPARγ is involved in transcription of genes that store lipids. An imbalance of these transcription factors can have effects at the tissue- and organism-level. PPAR expression can be altered in disease states and, as such, has been the focus for various metabolic syndromes and potential treatments.

1.2 PPARγ Expression, Regulation, and Function

Within humans, there are four splice variants of PPARγ mRNA, with three of these mRNA transcripts that are translated into an identical protein (Fajas et al., 1997). This results in two isoforms of PPARγ: PPARγ1 and PPARγ2. PPARγ2 differs from PPARγ1 in that it contains 30 additional amino acids at the N-terminal domain. The additional amino acids at the N-terminus play a role in ligand-independent transcriptional activation, making PPARγ2 more active than PPARγ1 (Werman et al., 1997). PPARγ1 is expressed in various tissue types, such as adipose, muscle, liver, and cardiac tissues at low levels, while PPARγ2 is exclusively found at high levels in adipose tissue (Elbrecht et al., 1996). The translated PPARγ protein contains six domains, including a ligand-independent transactivation function 1 (AF-1) domain, containing two domains, a DNA-binding domain, hinge domain, ligand-binding domain, and cofactor domain (Chandra et al., 2008).

Endogenous ligands for PPARγ were discovered in 1995 after the receptor had been identified. PPARγ ligands are polyunsaturated fatty acids and include prostaglandin PGJ2, linolenic acid, eicosapentaeonic acid, docosahexaenoic acid, and arachidonic acids (Forman et al., 1995; Kliewer et al., 1995; Nagy et al., 1998). These fatty acids bind PPARγ at relatively low affinity. Based on structural studies, the PPARγ binding site accommodates lipophilic carboxylic acids and other acidic ligands that can bind to polar residues, consistent with its proposed physiological role as a fatty acid sensor (Velkov, 2013).

PPARγ activity is regulated by a number of coactivators and corepressors. When no ligand is bound, PPARγ is bound to corepressors, such as silencing mediator of retinoic and thyroid hormone receptors (SMRT) and nuclear receptor corepressor (Ncor) (Yu et al., 2005). These corepressors bind other repressive enzymes, such as histone deacetylase (HDAC) and histone methyl transferase (HMT), which play a role in chromatin remodeling (Jiang et al., 2014).

Upon ligand activation, coactivators such as CREB binding protein (CBP)/p300, PPARγ coactivator-1 (PGC-1a), and thyroid hormone receptor-associated protein (TRAP 200) are recruited, allowing gene transcription (Ge et al., 2002). There are several corepressors and coactivators that interact with PPARγ, and these differ depending on tissue type, allowing tissue-specific regulation and transcription of target genes.

PPARγ can also be regulated by post-transcriptional modifications such as phosphorylation, acetylation, and SUMOylation. Phosphorylation of PPARγ by 5'-AMP-activated protein kinase (AMPK) or extracellular receptor kinase-mitogen activated protein kinase (ERK-MAPK) at Serine112 represses PPARγ by decreasing ligand binding affinity, reducing transcriptional activity, and reducing adipogenesis (Hu et al., 1996; Adams et al., 1997). In addition to phosphorylation, PPARγ can be regulated by acetylation of lysine residues. Acetylation represses PPARγ activity by enhancing interactions with NCor (Han et al., 2010; Qiang et al., 2012). Finally, SUMOylation of PPARγ lysine residues also negatively regulates transcriptional activity (Yamashita et al., 2004). For example, SUMOylation of Lysine107 inhibits PPARγ-dependent adipogenesis in white adipose tissue of FGF210KO mice (Ohshima et al., 2004). Overall, multiple post-transcriptional modifications suppress PPARγ activity through a variety of mechanisms.

Upon activation by ligand binding, PPARγ heterodimerizes with retinoid X receptor (RXR). Similar to PPARγ, the RXR class of nuclear receptors also contains 3 subtypes: α, β, and γ; expression levels of these isoforms vary by cell type. RXR is activated by 9-cis-retinoic acid (Heyman et al., 1992), and aside from dimerizing with PPARs, RXR can form homodimers as well as heterodimers with a number of nuclear receptors including constitutive androstane receptor (CAR), farnesoid X receptor (FXR), liver X receptor (LXR), pregnane X receptor (PXR), steroid and xenobiotic receptor (SXR), and retinoic acid receptor (RAR) (Honkakoski et

al., 1998; Willy et al., 1995; Blumberg et al., 1998; Zechel et al., 1994). Activation of RXR results in additive activity compared to activation of PPARγ ligand activation alone (Cha et al., 2001). Once activated, the PPARγ:RXR heterodimer binds to PPRE on the DNA and increases transcription of various genes, including adipocyte fatty acid binding protein and cytochrome P450 4B1, many of which are implicated in adipocyte differentiation, adipogenesis, and lipid biosynthesis (Tontonoz et al., 1994; Yu et al., 2003).

1.3 Tissue-Specific Roles of PPARγ: Early Development, Adipose Tissues, and Liver Tissue

Studies within mice have shown that PPARγ is necessary for embryonic development. In mouse models, PPARγ knockout identified two important stages of development that are PPARγ-dependent. In early stages of development, lack of PPARγ resulted in deficient placental vascularization, myocardial thinning, and death by embryonic day 10 (Barak et al., 1999; Kubota et al., 1999; Michalik et al., 2001). In order to study the effects of loss of PPARγ at later stages of development, PPARγ-null embryos were aggregated with tetraploid embryos and wildtype placenta to overcome cardiac defects. These embryos survived to term, but eventually died of lipodystrophy and hemorrhages (Barak et al., 1999). While heterozygous PPARγ-deficient mice survived through later stages of development, male mice had reduced body weight compared to controls (Rieusset et al., 2004).

As PPARγ is highly expressed in adipose tissue, animal models have been used to study to effects of PPARγ knockout on this specific tissue. Studies using heterozygous PPARγ-deficient mice were found to have smaller adipocytes and decreased fat mass compared to wildtype mice (Kubota et al., 1999). Chimeric mice with wildtype and PPARγ-null cells showed that the PPARγ-null cells did not contribute to adipose tissue. Additionally, PPARγ is required to differentiate embryonic stem cells into fat cells, indicating PPARγ's role as a main regulator of adipogenesis (Rosen et al., 1999). Selective knockout studies of PPARγ in mice adipose tissue

also showed decreased adipocyte number, lipoatrophy, and insulin resistance (He et al., 2003). Furthermore, these brown adipose tissue depots of these mice were reduced in size, had abnormal morphology, and displayed abnormal organization (Wang et al., 2013).

PPARγ levels in normal liver remain relatively low, however, increases are found in steatotic liver (Pettinelli and Videla, 2011). Overexpression of hepatic PPARγ results in the formation of lipid droplets in the liver (Yu et al., 2003). In both humans and rodent obesity and diabetes models, developing fatty liver is associated with increased PPARγ expression (Matsusue et al., 2003; Gavrilova et al., 2003). Models utilizing specific knockouts of PPARγ in adult mice liver show that hepatic PPARγ plays a major role in pathways for hepatic fatty acid uptake and monoacylglycerol pathway-mediated fatty acid esterification but does not play as large of a role in hepatic *de novo* lipogenesis, triacylglycerol uptake, triacylglycerol export, or fatty acid oxidation (Greenstein et al., 2017). Overall, PPARγ activity within liver tissue is induced by systemic fatty acid levels and works to store fatty acids in the form of lipids.

1.4 PPARs as Targets for Drug Therapy

Due to the role that PPARs play in glucose and lipid homeostasis, PPARs have been targets for drug therapy for metabolic syndromes such as obesity, diabetes, and cardiovascular disease. Fibrates, such as clofibrate and fenofibrate, are selective PPARα ligands. Through activation of PPARα, these synthetic agonists have been shown to lower triglyceride levels by inducing hepatic fatty acid uptake and reducing hepatic triglyceride production (Martin et al., 1997). These physiological results are attributed to an increase in fatty acid transporter protein levels and acyl-CoA synthetase activity (Schoonjans et al., 1995). This results in less available fatty acids for uptake into muscle tissue. Fibrates also increase high-density lipoprotein (HDL) production, but do not decrease low-density lipoprotein (LDL) cholesterol (Tilly-Kiesi and

Tikkanen, 1991). Currently, gemfibrozil and fenofibrate are used to help patients lower blood triglyceride levels (Jackevicius et al., 2011).

Another class of compounds are the thiazolidinediones, which were first synthesized in 1980 and are selective PPARγ agonists (Lehmann et al., 1995). By 1997, three compounds from this class of drugs – rosiglitazone, pioglitazone, and troglitazone – were being used to treat diabetes (Kumar et al., 1996). Patients taking these compounds showed an increase in insulin sensitization and reduction of blood sugar levels (Nolan et al., 1994). Subcutaneous adipocytes also increased fatty acid storage due to PPARγ activation, reducing triglyceride concentrations in muscle and liver tissue (Gurnell et al., 2003). However, patients also experienced weight gain while taking these drugs and due to incidences of liver toxicity, fluid retention, and bladder toxicity, the use of these compounds was restricted by the FDA in 2010. While they are no longer commonly used therapeutically, several thiazolidinedione compounds are used as tools to elucidate effects of PPARγ activation in animal-based and *in vitro* studies.

In addition to PPARγ- or PPARα-specific ligands, some compounds are able to activate more than one PPAR. The glitazar class of compounds bind to both PPARα and PPARγ. While glitazars have the combined benefits of PPARα and PPARγ agonists on lowering plasma triglycerides and reducing insulin resistance, side effects, such as higher risk for cardiovascular events and weight gain, resulted in termination of many of these compounds for therapeutic use (Dietz et al., 2012). As of 2013, saroglitazar has been approved for use in India as a treatment for Type 2 diabetes (Agrawal, 2014). Compounds that can activate all three PPARs, or pan-PPAR agonists, have also been investigated for the potential to improve lipid homeostasis due to disease-related changes. Studies in mice have shown that pan-PPAR agonists can reduce body weight, improve glucose tolerance, and decrease triglyceride levels (Fernandes-Santos et al., 2009; Wettstein et al., 2017).

1.5 PPARγ as a Target for Environmental Chemicals

Due to the relatively large ligand-binding domain of PPARγ, there is potential for xenobiotic binding and modulation of PPARγ-regulated genes. Various studies have shown that a number of environmental chemicals are able to activate PPARγ *in vitro*. These include some organophosphate-based flame retardants, bisphenol A derivatives, and phthalate compounds. These compounds are not chemically bound to end-use products, resulting in migration over time and dermal exposure, inhalation, or ingestion. Many of these compounds or corresponding metabolites are found in human serum and urine samples (Schauer et al., 2006; Hogberg et al., 2008; Zhao et al., 2019). It is likely that these environmental compounds have other effects that may be indirectly modulating PPARγ in addition to direct PPARγ binding. While these studies show that PPARγ is a potential target for environmental contaminants, it is still unclear whether exogenous ligand binding by environmental chemicals can modulate the function of PPARγ and corresponding downstream effects.

Organophosphate-based flame retardants are compounds used to delay combustion and are commonly applied in electronic devices, furniture, and vehicles to meet flammability standards. Organophosphate-based flame retardants have become more prevalent due to the phase-out of polybrominated diphenyl ether flame retardants (Stapleton et al., 2009). Within this class of organophosphate compounds, triphenyl phosphate (TPHP) has been shown to bind PPARγ in cell-based reporter assays. *In vitro* studies utilizing Gal4 reporter assays show that TPHP was able to activate transfected human PPARγ in HepG2 cells (Wang et al., 2016). Studies utilizing 3T3-L1 cells show that TPHP induces adipogenesis through PPARγ activation (Cano-Sancho et al., 2017; Kim et al., 2019). TPHP is also able to activate PPARγ and alter metabolism in organisms. In rodent studies, perinatal exposure to TPHP increased body fat in rats and accelerated the onset of type 2 diabetes (Green et al., 2017).

Phthalates are a class of plasticizers used to manufacture flexible polyvinyl chloride-containing products. Over 470 million pounds of phthalates are produced every year (EPA 2006). Within this class of compounds, multiple phthalates have been shown to activate PPARα and PPARγ (Maloney and Waxman, 1999; Hurst and Waxman, 2003). Di(2-ethylhexyl) phthalate (DEHP) is one of the cheapest and most commonly used phthalates, making up about 40% of polyvinyl chloride products. Mono-ethylhexyl phthalate (MEHP), a metabolite of DEHP, along with other phthalate monoesters are commonly found in urine samples (Blount et al., 2000; Kato et al., 2004; Silva et al., 2004). Cell-based transactivation assays showed that MEHP could activate both PPARα and PPARγ and was more active than its parent compound (DEHP) (Hurst and Waxman, 2003; Bility et al., 2004). In studies where rodents were administered DEHP, authors observed an increase in a number of adipogenic markers, such as PPARγ, adipocyte-specific fatty acid binding protein, and fatty acid synthetase. In addition, mice exposed to DEHP perinatally from gestation day 12 to lactation day 7 exhibited increased body weight, liver weight, and epididymal fat pad weight compared to control mice (Hao et al., 2013).

Tetrabromobisphenol A (TBBPA) and tetrachlorobisphenol A (TCBPA) – two halogenated bisphenol analogs – have also been shown to activate PPARγ *in vitro*. While bisphenol A, a xenoestrogen compound, is used in the manufacture of polycarbonate and epoxy resins, TBBPA and TCBPA are mainly used as flame retardants in electronic devices. Roughly 20% of TBBPA applications are not chemically bound and able to migrate into indoor dust (Leisewitz et al., 2001). TBBPA in house dust samples ranged from 1 to 3600 ng/g (Wang et al., 2015). Studies utilizing PPARγ-transfected luciferase activity have shown that TBBPA and TCBPA are able to bind to the ligand-binding domain of PPARγ, with TBBPA binding to PPARγ with greater affinity than TCBPA (Riu et al., 2011). While several studies have shown that exposure of rodents to TBBPA and TBCPA can cause uterine epithelial tumors (Dunnick et al.,

2015), to date no studies have evaluated the potential for TBBPA- or TCBPA-induced PPARγ activation within rodent models.

1.6 Overview of Research Aims

While much of PPARγ's physiological role has been well studied, there are still knowledge gaps in its role during early development and as a target of environmental chemicals. To address knowledge gaps of PPARγ's role during early stages of development, such as blastula, gastrula, and segmentation, Chapter 2 of my work will utilize zebrafish embryos to determine whether developmental defects may occur during these early stages following exposure to a PPARγ agonist, ciglitazone, or knockdown of PPARγ mRNA transcripts by morpholino injection. Within Chapter 3, I will characterize the genomic, transcriptomic, and metabolomic changes following exposure to a PPARγ agonist or antagonist within hepatocellular carcinoma (HepG2) cells, once again relying on ciglitazone as a PPARγ agonist and including GW 9662 as a PPARγ antagonist. In Chapter 4, I will utilize readouts based on results from Chapter 3 in order to screen environmental chemicals (TBBPA and TCBPA) and understand the extent to which they may modulate PPARγ within HepG2 cells. While the use of HepG2 cells do not recapitulate normal liver biology, these cells do provide a cost-effective model for screening potential PPARγ activity of compounds and better understanding mechanisms of chemically-induced toxicity.

Chapter 2: Ciglitazone – a Human PPARγ Agonist – Disrupts Dorsoventral Patterning in Zebrafish

2.0 Abstract

Peroxisome proliferator-activated receptor γ (PPARγ) is a ligand-activated transcription factor that regulates lipid/glucose homeostasis and adipocyte differentiation. While the role of PPARγ in adipogenesis and diabetes has been extensively studied, little is known about PPARγ function during early embryonic development. Within zebrafish, maternally-loaded pparγ transcripts are present within the first 6 h post-fertilization (hpf), and de novo transcription of zygotic pparγ commences at ~48 hpf. Since maternal pparγ transcripts are elevated during a critical window of cell fate specification, the objective of this study was to test the hypothesis that PPARγ regulates gastrulation and dorsoventral patterning during zebrafish embryogenesis. To accomplish this objective, we relied on 1) ciglitazone as a potent PPARγ agonist and 2) a splice-blocking, pparγ-specific morpholino to knockdown pparγ. We found that initiation of ciglitazone – a potent human PPARγ agonist – exposure by 4 hpf resulted in concentration-dependent effects on dorsoventral patterning in the absence of epiboly defects during gastrulation, leading to ventralized embryos by 24 hpf. Interestingly, ciglitazone-induced ventralization was reversed by co-exposure with dorsomorphin (DMP), a bone morphogenetic protein (BMP) signaling inhibitor that induces strong dorsalization within zebrafish embryos. Moreover, mRNA-sequencing revealed that lipid- and cholesterol-related processes were affected by exposure to ciglitazone. However, pparγ knockdown did not block ciglitazone-induced ventralization, suggesting that PPARγ is not required for dorsoventral patterning nor involved in ciglitazone-induced toxicity within zebrafish embryos. Our findings point to a novel, PPARγ-independent mechanism of action and phenotype following ciglitazone exposure during early embryonic development.

2.1 Introduction

Peroxisome proliferator-activated receptor gamma (PPARγ) is a nuclear receptor that, upon activation by endogenous (e.g., fatty acids, prostaglandins) or exogenous (e.g., thiazolidinediones) ligands, heterodimerizes with retinoid X receptor (RXR) and binds to PPAR response elements (PPREs) in order to regulate transcription of genes such as adipocyte fatty acid binding protein (A-FABP/aP2) and cytochrome P450 4B1 (CYP4B1) (Issemann and Green, 1990; Kliewer et al., 1997). PPARγ plays a central role in lipid/glucose homeostasis, adipocyte differentiation, proliferation, and immune response (Chawla et al., 1994; Tontonoz, Hu, and Spiegelman, 1994; Ricote et al., 1998; Martin et al., 1998). As a mediator of adipogenesis, PPARγ plays a role in the progression of pathological diseases such as obesity, diabetes, atherosclerosis, cancer, and chronic inflammation (Vidal-Puig et al., 1996; Tontonoz et al., 1997; Gilroy et al., 1999). As such, PPARγ is a promising target for small molecule drugs. For example, PPARγ agonists (e.g., rosiglitazone and pioglitazone) have been used for nearly 20 years for treatment of type II diabetes mellitus (Lehmann et al., 1995; Martens et al., 2002).

While the expression and function of PPARγ has mainly been studied within adult adipose, muscle, heart, pancreatic, and liver tissues, several studies have demonstrated that PPARγ also plays a role in normal development and is expressed within human primary trophoblast cells and placental tissue (Storvik et al., 2014; El Dairi et al., 2018). Based on PPARγ knockout mice, PPARγ is essential for trophoblast differentiation and placental vascularization, and embryos lacking either of these processes leads to myocardial thinning and, ultimately, prenatal death (Barak et al., 1999). Based on ruminant and porcine studies, PPARγ also plays a role in conceptus elongation, the process by which the trophoblast of the spherical blastocyst elongates, differentiates, and secretes products that change the physiology of the endometrium for implantation and placental development (Brooks, Burns, and Spencer, 2015; Ribeiro et al., 2016;

Blitek and Szymanska, 2019). Within Western clawed frog (*Xenopus tropicalis*) embryos, knockdown of PPARγ by morpholino injection results in defects of eye development as well as disruption of lipid and glucose homeostasis (Zhu et al., 2018).

Dorsoventral patterning – a highly-conserved process that governs how dorsal and ventral structures are determined within vertebrate and invertebrate embryoes – is controlled by a complex array of maternal and zygotic factors and signaling pathways, including retinoic acid (RA), Wnt, fibroblast growth factor (FGF), Sonic hedgehog (Shh), and bone morphogenetic protein (BMP) signaling (Chazaud et al., 1996; Furthauer, Thisse, and Thisse, 1997; Furthauer et al., 2004; Chiang et al., 1996; Kishimoto et al., 1997). A gradient of BMP agonists (e.g., Bmp2b/7) and BMP antagonists (e.g., chordin) organize the development and differentiation of cells into ventral and dorsal structures, respectively (Dick et al., 2000). As an embryo progresses through development, strict regulation of these various factors is required for proper dorsoventral patterning. Indeed, this process is sensitive to environmental chemicals that disrupt signaling pathways regulating dorsoventral patterning, resulting in dorsalized or ventralized embryos (Dasgupta et al., 2017).

Within the first 24 h post-fertilization (hpf), zebrafish embryos rapidly progress through cleavage, blastula, gastrula, and segmentation (Kimmel et al., 1995), resulting in a properly formed embryo with dorsal and ventral structures by 24 hpf. Within zebrafish, maternally-loaded PPARγ transcripts are only present within the first 6 h post-fertilization (hpf), and de novo transcription of zygotic PPARγ does not commence until ~48 hpf (White et al., 2017). Within mice and in vitro studies, PPARγ is known to interact with BMP signaling during differentiation of mesenchymal cells into different osteogenic cell fates (Nishii et al., 2009; Shen et al., 2010; Stechschulte et al., 2016; Chung et al., 2016; Wang et al., 2018). Therefore, since maternal PPARγ transcripts are elevated during a critical window of cell fate specification, the objective of

this study was to test the hypothesis that PPARγ regulates gastrulation and dorsoventral patterning during zebrafish embryogenesis.

2.2 Materials and Methods

Animals

Adult wildtype (strain 5D) zebrafish were maintained and bred on a recirculating system using previously described procedures (Mitchell et al., 2018). All adult breeders were handled and treated in accordance with Institutional Animal Care and Use Committee-approved animal use protocols (#20150035 and #20180063) at the University of California, Riverside.

Chemicals

Ciglitazone (>99.4% purity) was purchased from Tocris Bioscience (Bristol, UK), and dorsomorphin (DMP) (99.7% purity) was purchased from Millipore Sigma (St. Louis, MO, USA). For both chemicals, stock solutions were prepared in high performance liquid chromatography (HPLC)-grade dimethyl sulfoxide (DMSO) and stored in 2-mL amber glass vials with polytetrafluoroethylene-lined caps. Working solutions were prepared by spiking stock solutions into particulate-free water from our recirculating system (pH and conductivity of ~7.2 and ~950 μS, respectively) immediately prior to each experiment, resulting in 0.2% DMSO within all vehicle control and treatment groups. Propylene glycol (>99.5% purity) and Oil Red O (>75% dye content) were purchased from Fisher Scientific (Hampton, NH, USA) and Sigma-Aldrich (St. Louis, MO, USA), respectively.

Bioinformatics

Zebrafish-specific pparγ, pparαa, pparαb, pparδa, and pparδb transcript abundance (transcripts per million, or TPM) across developmental stages were obtained from White et al. (2017) (provided within White et al., 2017 as Supplementary File 3, RNA-seq TPM; .tsv file), and stages were converted into hpf per Kimmel et al. (1995). Five replicate TPM values per

developmental stage were used to calculate the mean TPM ± standard deviation at each developmental stage. PPARα, PPARδ, and PPARγ amino acid sequences for *Homo sapiens* (NP_005027.2; NP_006229.1; NP_056953.2), *Mus musculus* (NP_035274.2; NP_035275.1; NP_035276.2), *Rattus norvegicus* (NP_037328.1; NP_037273.2; NP_001138838.1), and *Danio rerio* (NP_001154805.1 (αa); NP_001096037.1 (αb); XP_699900.6 (δa); NP_571543.1 (δb); NP_571542.1) were obtained from the National Center for Biotechnology Information (www.ncbi.nlm.nih.gov). Sequences were aligned using the Multiple Sequence Alignment Tool within Clustal Omega (https://www.ebi.ac.uk/Tools/msa/clustalo/), and the aligned file was used to generate a cladogram within Clustal Omega. Pairwise sequence alignments were also performed to obtain percent amino acid similarity using EMBOSS Matcher (https://www.ebi.ac.uk/Tools/psa/emboss_matcher/). The following default options were used for all pairwise alignments: Matrix = BLOSUM62; Gap Open = 1; Gap Extend = 4; and Alternatives = 1.

Embryo Exposures and Phenotyping

Embryos were sorted and exposed to either vehicle (0.2% DMSO) or ciglitazone (9.375, 12.5, 15, or 20 μM) from 4 to 24 hpf in glass petri dishes (20 embryos per replicate; 3 replicates per treatment). Ciglitazone concentrations were selected based on the maximum tolerated concentration (based on survival as an endpoint) in zebrafish embryos following a 4-24 hpf exposure. At 24 hpf, embryos were imaged under transmitted light at 2X magnification using a Leica MZ10 F stereomicroscope equipped with a DMC2900 camera and assessed for survival and dorsoventral patterning abnormalities (ventralization, dorsalization, or delayed development). Following previously described protocols (Dasgupta et al., 2017), ventralized embryos were defined as embryos with a swollen yolk sac extension; dorsalized embryos were defined as

embryos with a tail deformity; and delayed embryos were defined as embryos that phenocopied embryos at a developmental stage prior to 24 hpf.

Morpholino Injections

Morpholino (MO) antisense oligos were synthesized and obtained from Gene Tools, Inc. (Philomath, OR, USA). A fluorescein-tagged splice-blocking MO was designed to target the first exon-intron boundary (E1I1) of zebrafish pparγ-specific pre-mRNA (NCBI Gene ID: 557037), leading to insertion of intron 1 within pparγ mRNA (pparγ-MO sequence: 5'-TCAGCTCCTCTCTGACACTTACCAG-3'). We did not rely on a pparγ-specific translational morpholino due to the lack of a commercially available PPARγ-specific antibody that cross reacts with zebrafish PPARγ and, as such, inability to confirm knockdown of PPARγ protein. Gene Tools' standard fluorescein-tagged negative control MO (nc-MO) – a MO that targets a human β-globin intron mutation – was used in order to account for potential non-target MO toxicity, and a zebrafish-specific, fluorescein-tagged chordin MO (chd-MO sequence: 5'-ATCCACAGCAGCCCCTCCATCATCC-3') was used as a positive control for disruption of dorsoventral patterning (ventralization) at 24 hpf. Water injections were performed in order to account for potential toxicity associated with injection-related stress. MO stock solutions (1 mM) were prepared by resuspending lyophilized MOs in molecular biology-grade (MBG) water, and stocks were stored at room temperature in the dark.

Working solutions of nc-MOs and pparγ-MOs were diluted to 0.5 mM in MBG water and working solutions of chd-MOs were diluted to 0.125 mM in MBG water. Newly fertilized (1- to 8-cell stage, or before 1.25 hpf) zebrafish embryos were microinjected with MOs (~3 nL per embryo) using a motorized Eppendorf Injectman NI2 and FemtoJet 4x similar to previously described protocols (McGee et al., 2013; Dasgupta et al., 2017). At 3 hpf, MO delivery in embryos was confirmed using a Leica MZ10 F stereomicroscope equipped with a DMC2900

camera and a GFP filter cube; non-fluorescent and/or coagulated embryos were discarded. Fluorescent embryos were then exposed to either vehicle (0.2% DMSO) or 12.5 μM ciglitazone from 4 to 24 hpf and assessed for dorsoventral patterning abnormalities as described above.

To confirm pparγ knockdown, injected embryos (20 per pool; 3 replicate pools per group) were snap-frozen in liquid nitrogen at 24 hpf and stored at -80ºC. Total RNA was extracted using an SV Total RNA Isolation System (Promega, Madison WI, USA) and eluted in 30 μL of nuclease-free water. RNA quality and quantity were confirmed using an Agilent 2100 Bioanalyzer system and Qubit 4.0 Fluorometer (Thermo Fisher Scientific, Waltman, MA, USA), respectively. A total of ~140 ng RNA per replicate sample was reverse-transcribed into cDNA using a GoScript Reverse Transcription System (Promega, Madison WI, USA). An E1E2 pparγ fragment (~228 bp) was then amplified (forward primer: 5'-CACATCTACAGTAGTGCAGTCAT-3'; reverse primer: 5'- TGTTGGGTTGTTCTCGTAGTC-3') using approximately 50 ng of cDNA per sample, ZymoTaq PreMix (Zymo Research, Irvine, CA, USA), and an Eppendorf Mastercycler Nexus Thermocycler with the following conditions: 2 min at 95ºC followed by 45 cycles of 95ºC for 30 s, 49.5ºC for 1 min, and 72ºC for 30 s. PCR products were visualized using an Agilent 2100 Bioanalyzer system.

Oil Red O Staining

To determine whether pparγ knockdown affected lipid homeostasis, embryos were injected with either water, nc-MOs, or pparγ-MOs, reared in particulate-free system water, and imaged under transmitted light at 6, 24, 48, 72, and 96 hpf. At each stage, a subset of embryos (7 per stage) were fixed in 4% paraformaldehyde (PFA)/1X phosphate-buffered saline (PBS) for 24 h and then transferred to 1X PBS. Fixed embryos were stained with Oil Red O (ORO) using previously described protocols (Passeri et al., 2009). Stained embryos were then imaged under

transmitted light at 4X magnification using a Leica MZ10 F stereomicroscope equipped with a DMC2900 camera.

Ciglitazone and DMP Co-exposures

Embryos were exposed to either vehicle (0.2% DMSO), 12.5 μM ciglitazone, 0.078 μM DMP, or 12 μM ciglitazone + 0.078 μM DMP from 4 to 24 hpf in glass petri dishes (20 embryos per replicate per timepoint; 3 replicates per treatment). Maximum tolerated concentrations for DMP and ciglitazone co-exposures were optimized based on preliminary experiments that tested combinations of 0.078 or 1.56 μM DMP in the presence or absence of 9.375, 12.5, or 15 μM ciglitazone. Although 0.625 μM DMP was used in our prior studies (Dasgupta et al., 2017; Dasgupta et al., 2018), we relied on 0.078 μM DMP since co-exposure with 0.625 μM DMP and 12.5 μM ciglitazone resulted in a significant increase in mortality. At 8 hpf, embryos were fixed overnight in 4% PFA/1X PBS. Fixed embryos were manually dechorionated and then incubated overnight with anti-phosphoSMAD 1/5/9 IgG antibody (1:100 dilution; Cell Signaling Technology, Danvers, MA, USA) using previously described protocols (Yozzo, McGee, and Volz, 2013; Dasgupta et al., 2018). Embryos were then incubated overnight with an IgG-specific Alexa Fluor-conjugated secondary antibody (1:500 dilution; Millipore Sigma, St. Louis, MO, USA). Embryos were imaged at 8X magnification using a Leica MZ10 F stereomicroscope equipped with a GFP filter and DMC2900 camera. At 24 hpf, embryos were imaged under transmitted light at 2X magnification using a Leica MZ10 stereomicroscope equipped with a DMC2900 camera and assessed for survival and dorsoventral patterning abnormalities as described above.

mRNA-Sequencing

To quantify potential effects of ciglitazone on the transcriptome, embryos were exposed to vehicle (0.2% DMSO), 12.5 μM ciglitazone, 0.078 μM DMP, or 12.5 μM ciglitazone + 0.078

μM DMP (20 embryos per dish; 2 dishes per replicate; 4 replicates per treatment) from 4 to 24 hpf and then immediately snap-frozen in liquid nitrogen at 24 hpf and stored at -80ºC. All embryos were homogenized in 2-mL cryovials using a PowerGen Homogenizer (Thermo Fisher Scientific, Waltman, MA, USA). Following homogenization, an SV Total RNA Isolation System (Promega, Madison, WI, USA) was used to extract total RNA from each replicate sample per the manufacturer's instructions. RNA quantity and quality were confirmed using a Qubit 4.0 Fluorometer and 2100 Bioanalyzer system, respectively. Based on sample-specific Bioanalyzer traces, the RNA Integrity Number (RIN) was >8 for all RNA samples used for library preparations.

Libraries were prepared using a QuantSeq 3' mRNA-Seq Library Prep Kit FWD (Lexogen, Vienna, Austria) and indexed by treatment replicate per manufacturer's instructions. Library quantity and quality were confirmed using a Qubit 4.0 Fluorometer and 2100 Bioanalyzer system, respectively. Raw Illumina (fastq.gz) sequencing files (16 files) are available via NCBI's BioProject database under BioProject ID PRJNA544341, and a summary of sequencing run metrics are provided in Table S1 (>87.17% of reads were ≥Q30 across all runs). All 16 raw and indexed Illumina (fastq.gz) sequencing files were downloaded from Illumina's BaseSpace and uploaded to Bluebee's genomics analysis platform to align reads against zebrafish genome assembly GRCz10. After combining treatment replicate files, a DESeq2 application within Bluebee (Lexogen Quantseq DE1.2) was used to identify significant treatment-related effects on transcript abundance (relative to control) based on a false discovery rate (FDR) *p*-adjusted value ≤0.05. Significantly affected transcripts were imported into the Database for Annotation, Visualization, and Integrated Discovery (DAVID) v6.8 for Gene Ontology (GO) enrichment analysis. Individual transcripts from significant GO terms (Benjamini score ≤ 0.05) were consolidated into a list of unique transcripts.

Statistical Analysis

For data derived from exposures and MO injections, a general linear model (GLM) analysis of variance (ANOVA) ($\alpha = 0.05$) was performed using SPSS Statistics 24, as these data did not meet the equal variance assumption for non-GLM ANOVAs. Treatment groups were compared with vehicle controls using pair-wise Tukey based multiple comparisons of least square means to identify significant treatment-related differences.

2.3 Results

Zebrafish and mammalian PPARs are highly conserved

As expected, when comparing protein sequences of PPARs from human, mouse, rat, and zebrafish, we found that zebrafish PPARα (a/b), PPARδ (a/b), and PPARγ are closely related to mammalian PPARα, PPARδ, and PPARγ, respectively (Figure 1A). For each PPAR, the DNA binding domain (DBD) and ligand binding domain (LBD) were highly conserved across all four species (Figure 1B, 2A, and 2B). For example, the percent similarity between full-length zebrafish and human PPARγ was 74.9%, whereas the similarity between the DBD and LBD was 97.6% and 80.3%, respectively (Figures 1B) – a finding that was similar to PPARα and PPARδ (Figure 2A and 2B). When comparing similarity across zebrafish-specific PPARs, similarity in the LBD was highest (72.7%) between PPARγ and PPARδb (Figure 3). Finally, when comparing ligand binding pocket amino acid residues involved with rosiglitazone binding to human PPARγ (Sheu et al., 2005), we found that 8 out of 13 residues that interact with thiazolidinediones are conserved between humans and zebrafish (Figure 4).

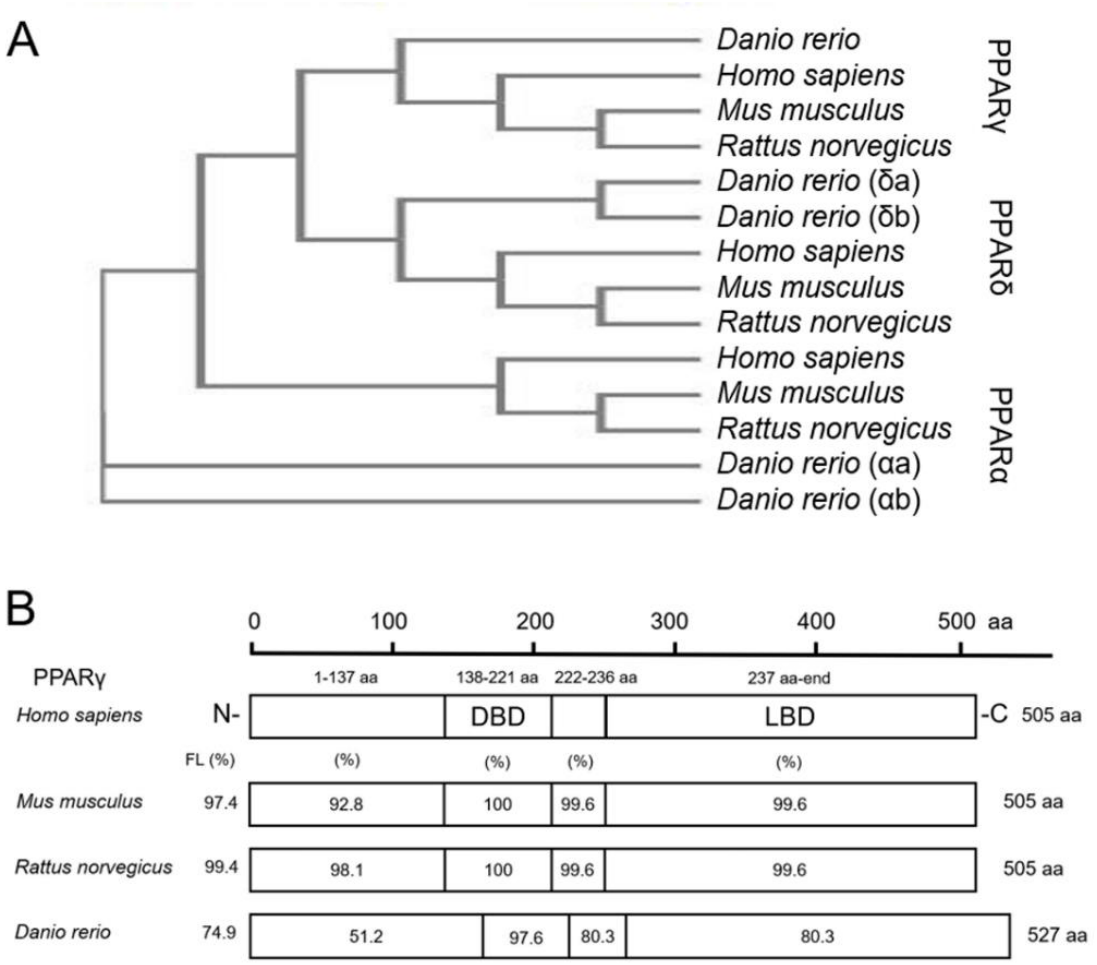

Figure 1: Phylogenetic tree showing relationship between *Homo sapiens* (human), *Mus musculus* (mouse), *Rattus norvegicus* (rat), and *Danio rerio* (zebrafish) PPARs (A). Percent similarity of mouse, rat, and zebrafish PPARγ relative to human PPARγ; FL = full length; DBD = DNA binding domain; and LBD = ligand binding domain (B).

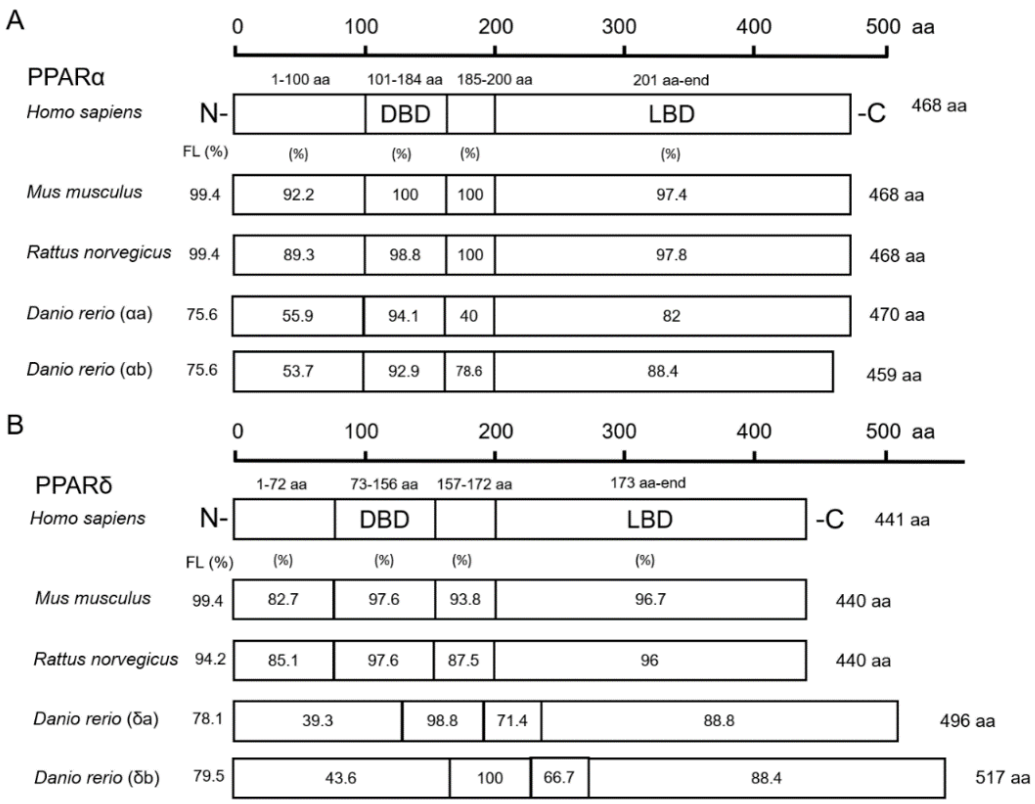

Figure 2: PPARα (A) and PPARδ (B) sequence similarity relative to human amino acid sequences. Percent similarity of mouse, rat, and zebrafish PPARα (A) and PPARδ (B) relative to human PPARα and PPARδ; FL = full length; DBD = DNA binding domain; and LBD = ligand binding domain.

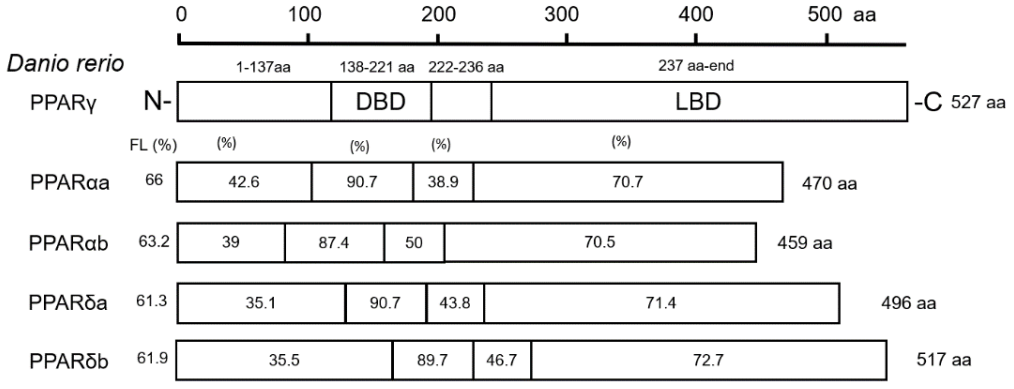

Figure 3: Percent similarity of zebrafish PPARα (a and b) and PPARδ (a and b) relative to PPARγ; FL = full length; DBD = DNA binding domain; and LBD = ligand binding domain (B).

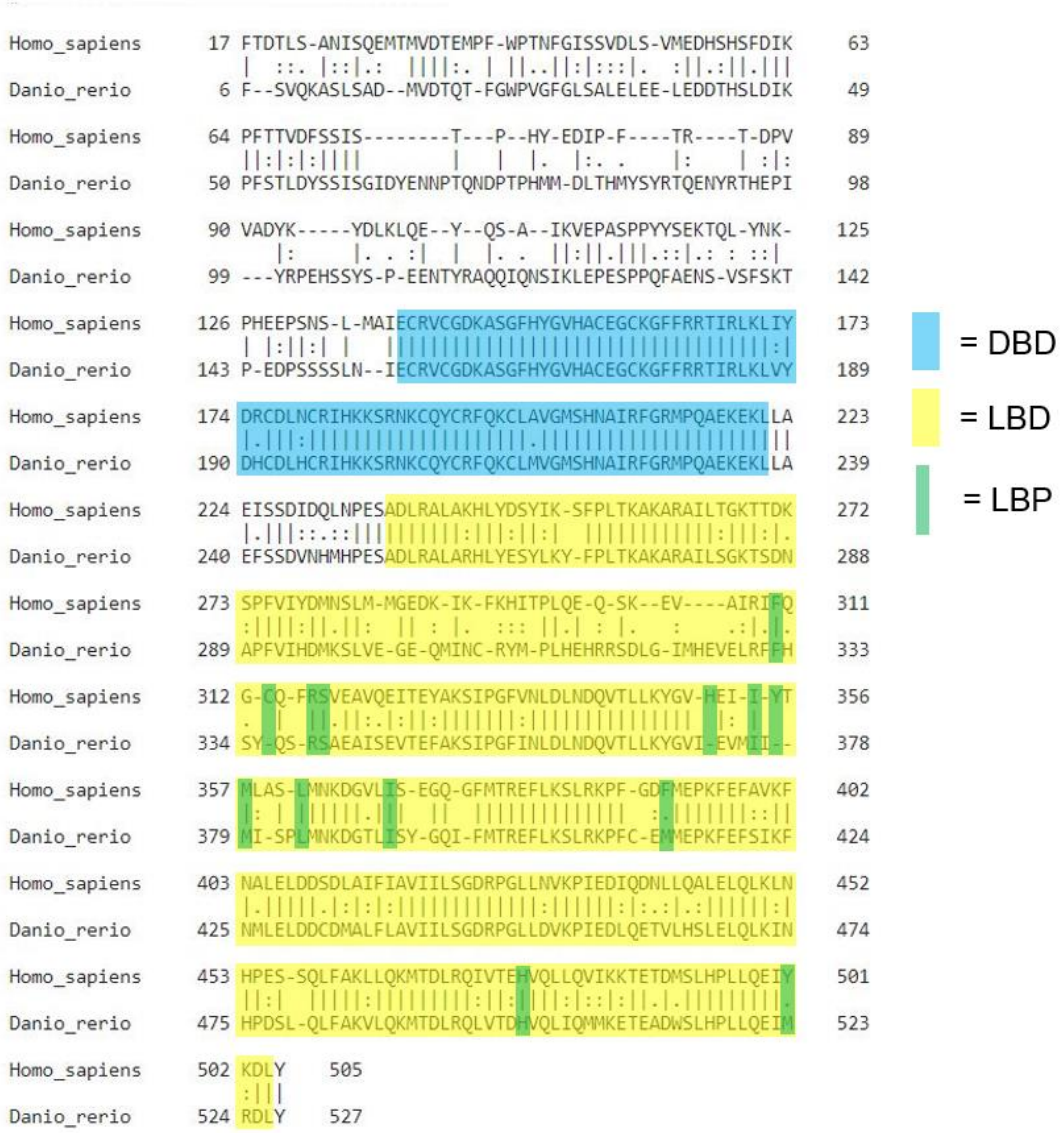

Figure 4: Sequence alignment between human and zebrafish PPARγ; DNA binding domain (DBD) is highlighted in blue, ligand binding domain (LBD) is highlighted in yellow, and amino acid residues in the ligand binding pocket (LBP) involved with thiazolidinediones binding are highlighted in green.

Knockdown of pparγ adversely affects development within the first 96 h

Although there are elevated levels of pparγ transcripts between 0.75 and 5 hpf (due to maternally-loaded pparγ mRNA), zygotic transcription of pparγ mRNA does not occur until ~48 hpf (Figure 6A). Similarly, maternally-loaded pparαa, pparαb, pparδa, and pparδb are all present within the embryo until 5 hpf (Figure 5A-5D). While zygotic transcription of pparαa, pparαb, and pparδa is not initiated until ~24-30 hpf (Figure 5A-5C), zygotic transcription of pparδb is initiated at 5 hpf and peaks at approximately 24 hpf (Figure 5D).

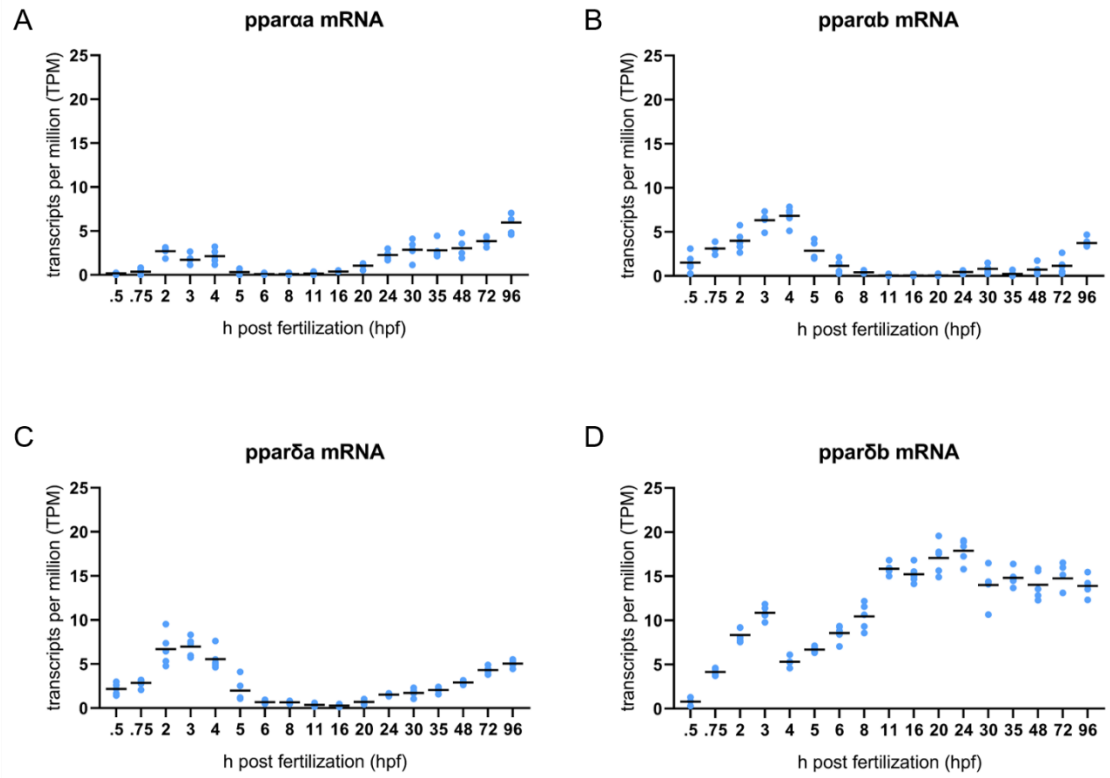

Figure 5: Abundance of pparαa (A), pparαb (B), pparδa (C), and pparδb (D) mRNA within whole zebrafish embryos from 0.75 hpf to 96 hpf.

Injection of pparγ-MO resulted in insertion of intronic sequence within zygotic pparγ transcripts by 24 hpf (Figure 6B). Within the first 48 h of development, injection of nc-MOs and pparγ-MOs resulted in mild defects on dorsoventral patterning relative to water-injected embryos (Figures 6C). However, unlike nc-MO-injected embryos, injection of pparγ-MOs resulted in more severe developmental abnormalities including pericardial edema, cardiac looping defects, and stunted growth at 72 and 96 hpf (Figure 6C) – a stage that coincides with a sharp increase in transcription of zygotic pparγ mRNA (Figure 6A). However, the abundance of neutral lipids (as determined by Oil Red O staining) within pparγ-MO-injected embryos was not qualitatively different across all stages (Figure 6C).

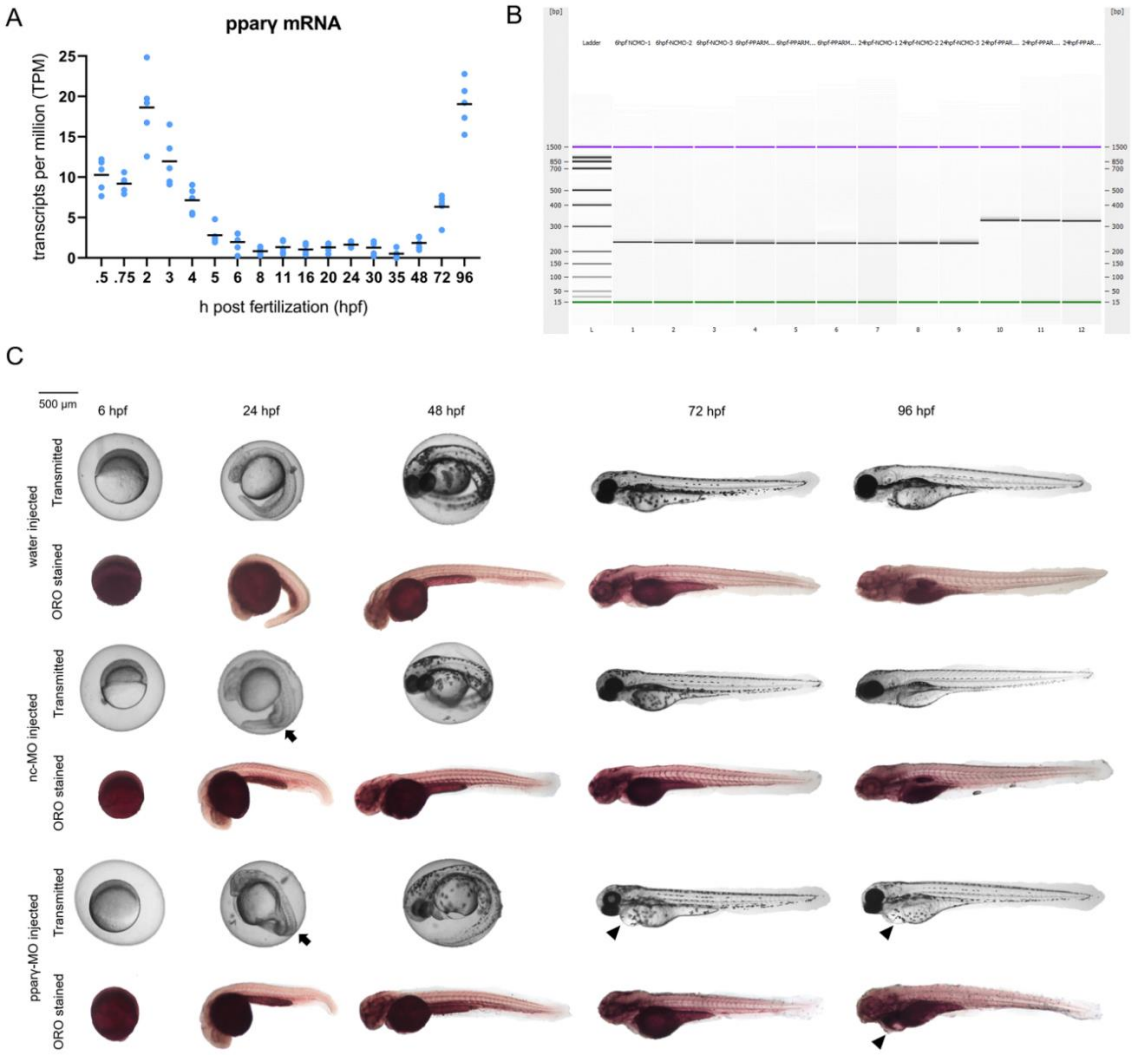

Figure 6: Abundance of pparγ mRNA within whole zebrafish embryos from 0.75 to 96 hpf (A). Confirmation of knockdown by 24 hpf following injection of splice-blocking pparγ-MOs. Lanes 1-3: 6-hpf embryos injected with nc-MO; lanes 4-6: 6-hpf embryos injected with pparγ-MO; lanes 7-9: 24-hpf embryos injected with nc-MO; and lanes 10-12: 24-hpf embryos injected with pparγ-MO (B). Representative images of water-, nc-MO- or pparγ-MO-injected embryos from 6 to 96 hpf before and after staining with Oil Red O (ORO) (C). Arrows point to mild dorsoventral patterning defects (ventralization), whereas arrowheads point to cardiac edema and cardiac looping defects.

Knockdown of pparγ does not block ciglitazone-induced toxicity at 24 hpf

Although ciglitazone exposure from 4 to 6 hpf did not impact epiboly at 6 hpf (Figure 7A), initiation of ciglitazone exposure at 4 hpf resulted in a concentration-dependent effect on survival and dorsoventral patterning by 24 hpf (Figures 7B and 7C). Embryos injected with water, nc-MOs, or pparγ-MOs, and then exposed to vehicle (0.2% DMSO) from 4 to 24 hpf, exhibited mild effects on survival and dorsoventral patterning (Figures 8A and 8B). However, pparγ knockdown did not block dorsoventral patterning defects following exposure to ciglitazone from 4 to 24 hpf (Figures 8A and 8B).

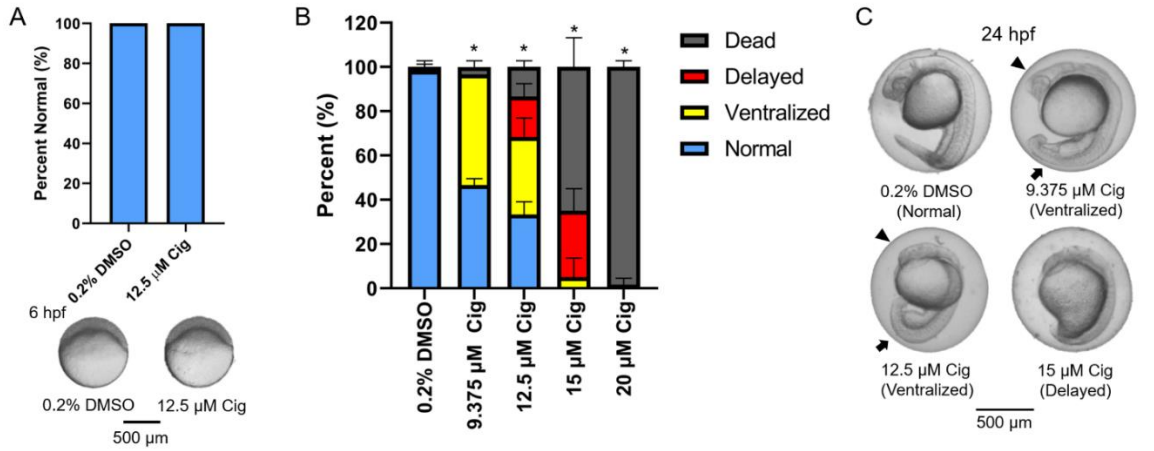

Figure 7: Initiation of ciglitazone (Cig) exposure at 4 hpf does not result in delayed epiboly by 6 hpf (N = 60 embryos per treatment) (A). Mean (± standard deviation) percent of normal, ventralized, dorsalized, or dead embryos following exposure to increasing concentrations of Cig from 4 to 24 hpf (N = 60 embryos per treatment) (B). Asterisk (*) denotes a significant difference (p<0.05) in the percent of normal embryos relative to vehicle controls (0.2% DMSO). Representative images of 1) a normal embryo exposed to vehicle (0.2% DMSO); 2) ventralized embryos exposed to 9.375 and 12.5 µM Cig; and 3) a delayed embryo exposed to 15 µM Cig (C). Arrows point to swollen yolk sac extensions, whereas arrowheads point to underdeveloped heads.

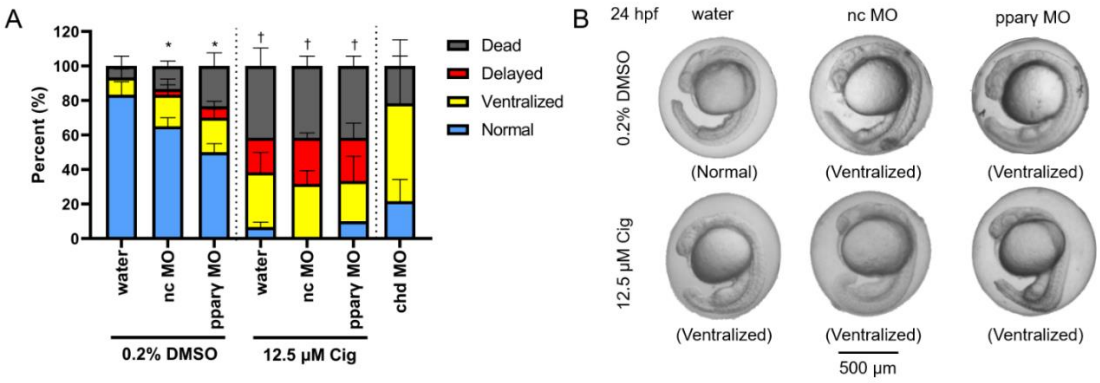

Figure 8: Mean (± standard deviation) percent of normal, ventralized, delayed, or dead embryos following injection of nc-MOs or pparγ-MOs at 0.75 hpf and exposure from 4 to 24 hpf to vehicle (0.2% DMSO) or 12.5 µM ciglitazone (Cig) (N = 60 embryos per treatment). Asterisk (*) denotes a significant difference ($p<0.05$) in the percent of normal embryos relative to within-treatment water-injected controls ($p<0.05$). Cross (†) denotes a significant difference ($p<0.05$) in the percent of normal embryos relative to within-MO vehicle (0.2% DMSO) controls. chd-MO was used as a positive control for ventralization (A). Representative images of nc-MO- and pparγ-MO-injected embryos exposed to either vehicle (0.2% DMSO) or 12.5 µM Cig at 24 hpf (B).

DMP reverses the ventralizing effects of ciglitazone

While exposure to 12.5 µM ciglitazone resulted in ventralized and delayed embryos, the majority of embryos following co-exposure with 12.5 µM ciglitazone + 0.078 µM DMP were dorsalized (Figures 9A and 9B). Although exposure to 0.625 µM DMP (a positive control) disrupted BMP signaling as expected (Figure 9C), exposure to 12.5 µM ciglitazone, 0.078 µM DMP, or 12.5 µM ciglitazone + 0.078 µM DMP did not result in disruption of BMP signaling at 8 hpf (Figure 9C).

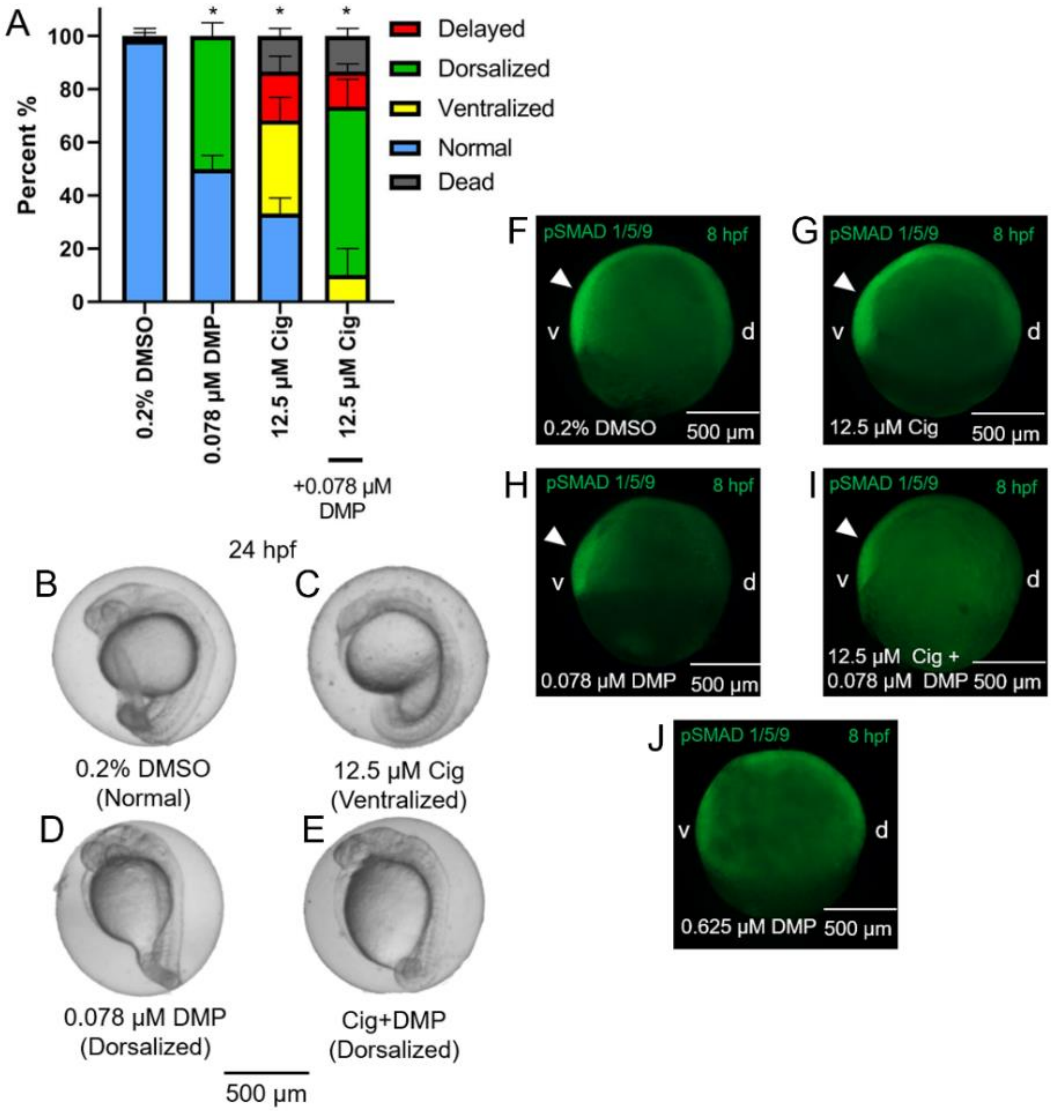

Figure 9: Mean (± standard deviation) percent of normal, ventralized, dorsalized, delayed, or dead embryos following exposure to vehicle (0.2% DMSO), 0.078 µM DMP, 12.5 µM ciglitazone (Cig), or 0.078 µM DMP + 12.5 µM Cig (N = 60 embryos per treatment) (A). Asterisk (*) denotes a significant difference ($p < 0.05$) in the percent of normal embryos relative to vehicle (0.2% DMSO) controls. Representative images of embryos following exposure to vehicle (0.2% DMSO), 0.078 µM DMP, 12.5 µM ciglitazone, or 0.078 µM DMP + 12.5 µM Cig (B). Immunostaining with anti-phosphoSMAD-1/5/9 within 8-hpf embryos following exposure to vehicle (0.2% DMSO), 0.078 µM DMP, 12.5 µM Cig,or 0.078 µM DMP + 12.5 µM Cig; embryos exposed to 0.625 µM DMP were included as a positive control for disruption of BMP signaling gradients. Arrowheads point to elevated pSMAD 1/5/9 staining on the ventral side of the embryo (C).

Ciglitazone exposure impacts cholesterol- and lipid-related biological processes by 24 hpf

Exposure to 12.5 μM ciglitazone, 0.078 μM DMP, or 12.5 μM ciglitazone + 0.078 μM DMP resulted in a significant change in the abundance of 1,641, 1,031, and 1,924 transcripts, respectively, relative to vehicle controls (Figures 10A-10C; Tables S2-S4). Although the magnitude of affected transcripts was similar across all three treatment groups, there was a total of 580, 289, and 724 significantly affected transcripts that were unique to embryos exposed to 12.5 μM ciglitazone, 0.078 μM DMP, or 12.5 μM ciglitazone + 0.078 μM DMP, respectively (Figure 10D). Interestingly, the most significantly altered DAVID-based biological process across all treatment groups was translation (Figure 11A; Tables S5-S7). While all three treatment groups shared certain biological processes that were affected (Figures 11B and 12), exposure to ciglitazone alone primarily affected cholesterol- and lipid-related biological processes (Figure 11C) – an effect that was driven by transcripts specific to apolipoprotein A-IV a (apoa4a), A-IV b (apoa4b.2), A-Ia (apoa1a), A-Ib (apoa1b), Eb (apoeb), antifreeze protein type IV (afp4), and an unnamed transcript (zgc: 162608) (Table S8).

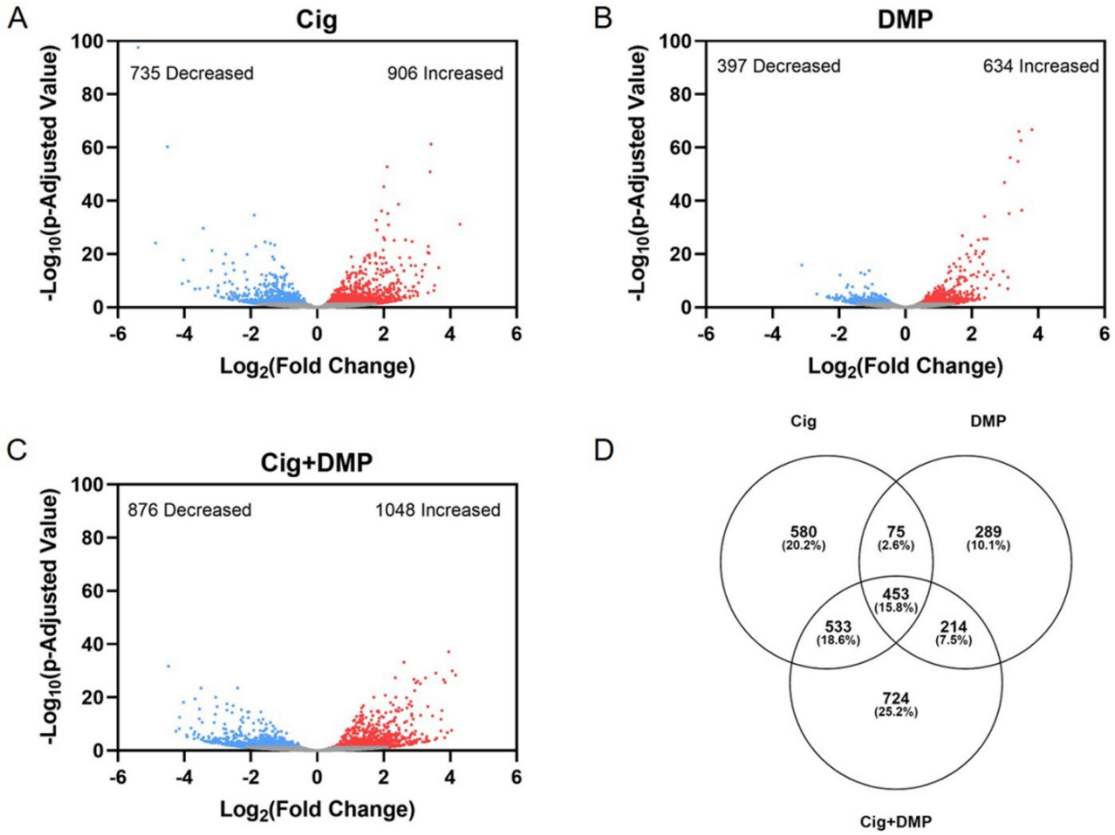

Figure 10: Volcano plots showing the number of significantly different transcripts following exposure to 12.5 µM ciglitazone (Cig) (A), 0.078 µM DMP (B), or 0.078 µM DMP + 12.5 µM Cig (C). All data are relative to vehicle (0.2% DMSO) controls. Log_2 transformed fold change is plotted on the x-axis and log_{10} transformed *p*-adjusted value is plotted on the y-axis. Venn diagram showing the number and percent of significantly different overlapping transcripts among treatment groups; percentage values are relative to the total number of significantly different transcripts across all treatment groups (D).

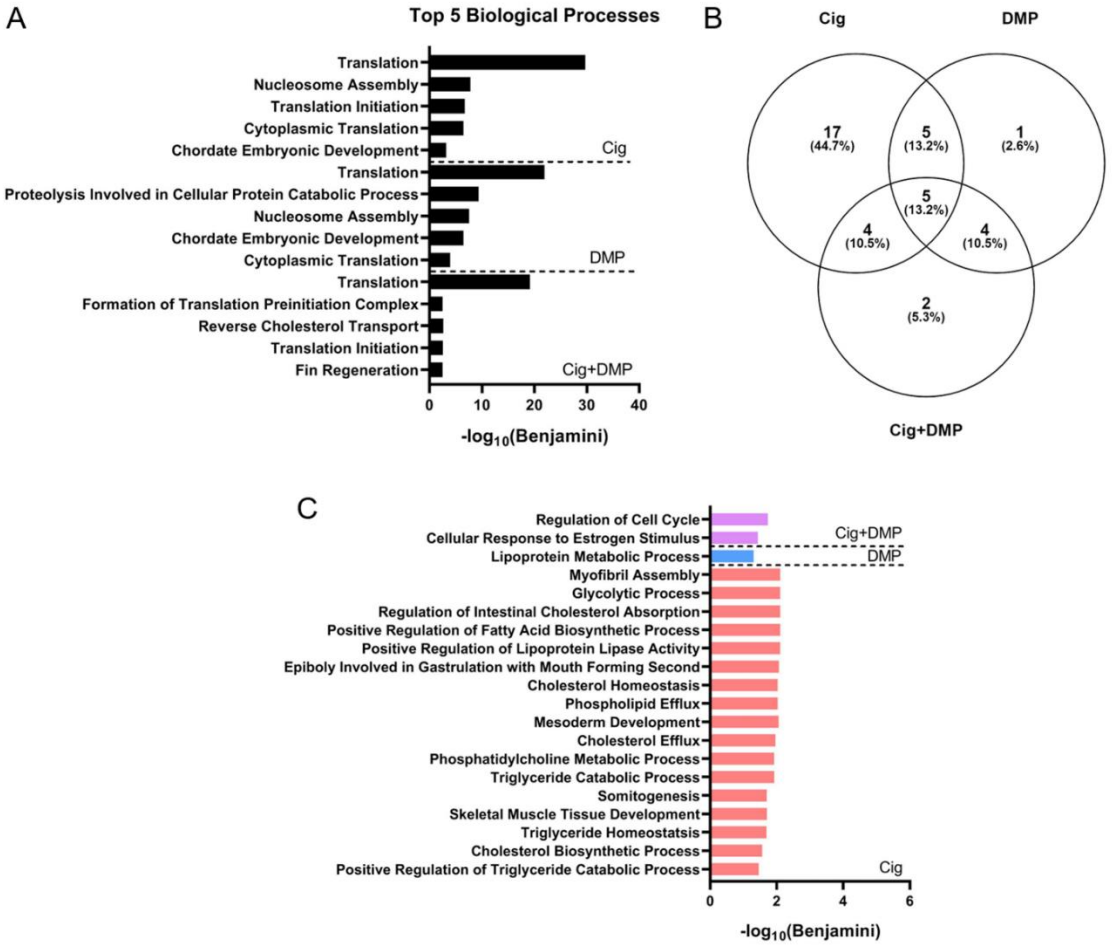

Figure 11: Top 5 DAVID-identified biological processes (based on significantly different transcripts) following exposure to 12.5 µM ciglitazone, 0.078 µM DMP, or 0.078 µM DMP + 12.5 µM ciglitazone (A). Venn diagram showing the number and percent of significantly altered biological processes among treatment groups (B). Significant (Benjamini < 0.05) biological processes unique to each treatment group (C).

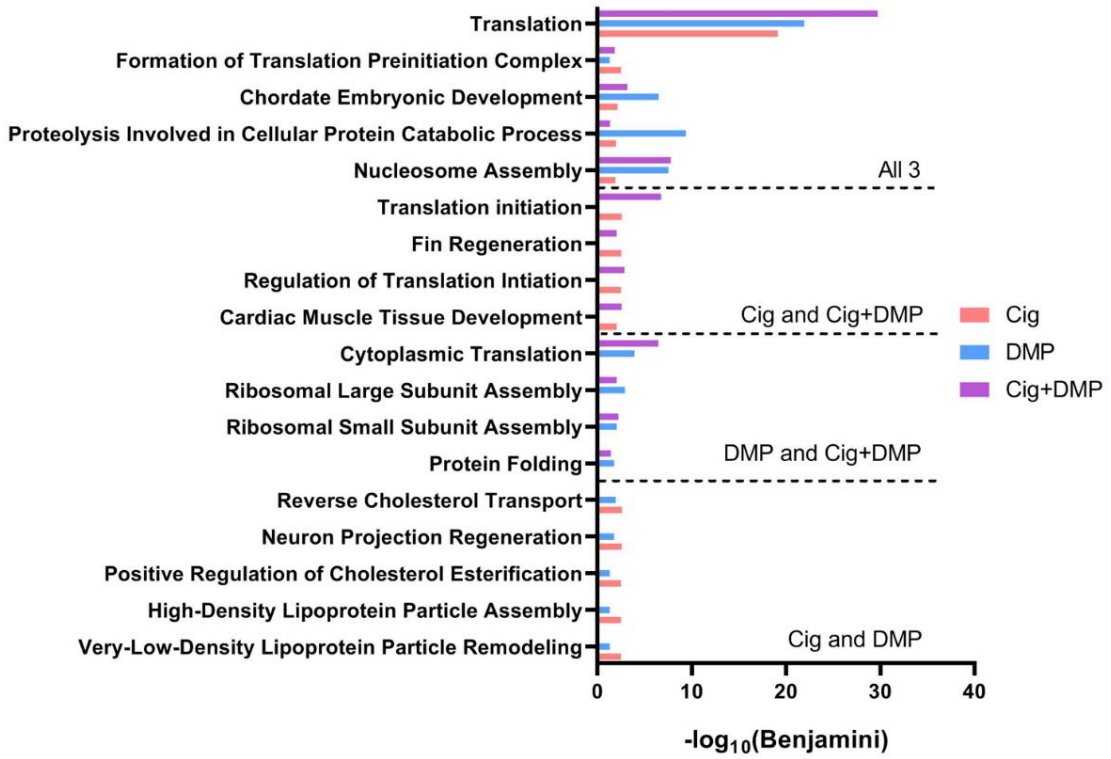

Figure 12: Significant (Benjamini p-value < 0.05) biological processes shared between or among treatment groups.

2.4 Discussion

Based on pairwise amino acid sequence alignments, zebrafish and mammalian PPARγ are strongly conserved, with the highest degree of homology located within the DBD and LBD. When comparing across PPARs, within-isoform homology was higher across species relative to within-species homology across isoforms. However, even with ~80% similarity in the LBD between human and zebrafish PPARγ, it is possible that deleted or altered amino acid residues in the thiazolidinedione binding pocket may affect the binding affinity or selectivity of ciglitazone to zebrafish PPARγ. Indeed, based on *in vitro* reporter assays comparing transactivation of human vs. zebrafish PPARγ, ciglitazone is unable to activate the LBD of zebrafish PPARγ within stably transfected reporter cell lines (HG5LN-GAL4-zfPPARγ) – a finding that is consistent with other thiazolidinediones (rosiglitazone, pioglitazone, and troziglitazone) (Riu et al., 2014). Despite

similar functions in both humans and zebrafish, humans contain two functional isoforms of PPARγ (Li et al., 2016), a species-specific difference that may also account for potential differences in ciglitazone binding and activation of PPARγ within zebrafish.

Injecting embryos with nc-MO or pparγ-MO resulted in mild dorsoventral patterning defects compared to water-injected controls – a finding that may be due to off-target effects of both MOs. However, more severe effects from pparγ knockdown starting at 72 hpf – i.e., cardiac looping defects and pericardial edema – suggest that pparγ is necessary for later stages of embryonic development. Interestingly, these defects resulting from pparγ knockdown coincided with an increase in zygotic transcription of pparγ, suggesting that the delay in abnormalities within pparγ morphants was likely driven by zygotically-derived, unspliced pparγ pre-mRNAs. However, as we were unable to knockdown maternally-loaded pparγ transcripts (since we relied on a splice-blocking MO instead of a translational-blocking MO), it is unclear what role maternal pparγ mRNA may play within the first 5-6 h of development.

Ciglitazone was the first thiazolidinedione developed in the 1980s and was designed to be a potent and selective PPARγ agonist. Within *in vivo* studies, ciglitazone functions as an anti-hyperglycemic agent, inhibits human umbilical vein endothelial cell proliferation and angiogenesis, stimulates adipogenesis in preadipocytes, and decreases osteoblastogenesis in murine mesenchymal stem cells (Kawamatsu et al., 1980; Jozkowicz et al., 2002; Stephens et al., 1999; Lin et al., 2007). Based on dorosoventral patterning defects observed in this study, our findings suggest that, within developing embryos, ciglitazone may interact with other targets. Indeed, other thiazolidinedione compounds (i.e., pioglitazone and rosiglitazone) used to treat type 2 diabetes mellitus have also recently been withdrawn from the market due to off-target side effects such as fluid retention, increased risk of heart failure, and increased risk of bladder cancer

(Nesto et al., 2003; Nissen and Wolski, 2007; Lewis et al., 2011). Therefore, it is possible that thiazolidinediones may have other mechanisms of action in addition to PPARγ activation.

Expression of BMP factors determine ventral cell fates within developing zebrafish embryos (Nikaido et al., 1997), whereas BMP antagonists (e.g., *noggin*, *follistatin*, and *chordin*) determine dorsal cell fates drive a gradient of BMP signaling (Smith and Harland, 1992; Hemmati-Brivanlou, Kelly, and Melton, 1994; Sasai et al., 1994). In order to determine whether ciglitazone-induced dorsoventral patterning defects were mediated by BMP signaling, embryos were co-exposed to both ciglitazone and DMP (a BMP antagonist). We found that DMP reversed the ventralizing effects of ciglitazone, as embryos co-exposed to ciglitazone and DMP were primarily dorsalized. Moreover, in all treatment groups, pSMAD 1/5/9 localization was not disrupted relative to controls, indicating that ciglitazone-induced dorsoventral patterning defects were likely not due to a disruption in BMP signaling. This was further supported by our mRNA-seq data, as neither bmp2 nor psmad1/5/9 transcripts were significantly altered after exposure to 12.5 μM ciglitazone, 0.078 μM DMP, or 12.5 μM ciglitazone + 0.078 μM DMP. Similarly, exposure to tris(1,3-dichloro-2-propyl) phosphate (TDCIPP) – a high-production volume organohalogen flame retardant – induced dorsoventral patterning defects in the absence of effects on BMP signaling within developing zebrafish embryos (Dasgupta et al., 2018).

Our mRNA-seq data also demonstrated that exposure to ciglitazone resulted in significant alterations to lipid- and cholesterol-related biological processes. While it is unlikely that ciglitazone activates zebrafish PPARγ within the first 24 hpf (since pparγ knockdown did not rescue ciglitazone-induced defects at 24 hpf), pparδb may be a potential target of ciglitazone within developing zebrafish, as pparδb is ubiquitously expressed in all tissue types (Bertrand et al., 2007). Unlike other PPARs present in zebrafish, transcription of zygotic pparδb occurs during early stages of zebrafish development and zygotically-derived pparδb transcripts are elevated at

24 hpf. Within mouse and cell models, pparδb regulates fatty acid uptake, transport, and oxidation (Poirier et al., 2001; Holst et al., 2003) – biological processes that were significantly affected following exposure of zebrafish embryos to ciglitazone. In addition, based on pparδb-null mice, knockout of pparδb results in impaired growth and reduced gonadal adipose stores (Peters et al., 2000), showing that pparδb is necessary for proper development.

Overall, we found that exposure of zebrafish embryos to ciglitazone resulted in dorsoventral patterning defects that are likely independent of PPARγ activation or disruption of BMP signaling. While PPARγ is required for normal embryonic development, the precise role of maternally-loaded PPARγ during early embryogenesis, as well as how zygotically-transcribed PPARγ may be mediating later developmental processes, remains unclear. Based on our findings to date, future studies should focus on determining whether 1) knockdown of maternally-loaded PPARγ impacts the first 24 h of development; 2) developmental abnormalities within zebrafish are driven by ciglitazone interaction with other targets or PPARs (such as PPARδb); and 3) ciglitazone exposure results in developmental abnormalities within mammalian models more relevant to human embryos.

Chapter 3: Utilizing Systems Biology to Reveal Cellular Responses to Peroxisome Proliferator-Activated Receptor γ Ligand Exposure

3.0 Abstract

Peroxisome proliferator-activated receptor γ (PPARγ) is a nuclear receptor that, upon activation by ligands, heterodimerizes with retinoid X receptor (RXR), binds to PPAR response elements (PPREs), and activates transcription of downstream genes. As PPARγ plays a central role in adipogenesis, fatty acid storage, and glucose metabolism, PPARγ-specific pharmaceuticals (e.g., thiazolidinediones) have been developed to treat Type II diabetes and obesity within human populations. However, to our knowledge, no prior studies have concurrently assessed the effects of PPARγ ligand exposure on genome-wide PPARγ binding as well as effects on the transcriptome and lipidome within human cells at biologically active, non-cytotoxic concentrations. In addition to quantifying concentration-dependent effects of ciglitazone (a reference PPARγ agonist) and GW 9662 (a reference PPARγ antagonist) on human hepatocarcinoma (HepG2) cell viability, PPARγ abundance *in situ*, and neutral lipids, HepG2 cells were exposed to either vehicle (0.1% DMSO), ciglitazone, or GW 9662 for up to 24 h, and then harvested for 1) chromatin immunoprecipitation-sequencing (ChIP-seq) to identify PPARγ-bound regions across the entire genome, 2) mRNA-sequencing (mRNA-seq) to identify potential impacts on the transcriptome, and 3) lipidomics to identify potential alterations in lipid profiles. Following exposure to ciglitazone and GW 9662, we found that PPARγ levels were not significantly different after 2-8 h of exposure. While ciglitazone and GW 9662 resulted in a concentration-dependent increase in neutral lipids, the magnitude and localization of PPARγ-bound regions across the genome (as identified by ChIP-seq) did not vary by treatment. However, mRNA-seq and lipidomics revealed that exposure of HepG2 cells to ciglitazone and GW 9662 resulted in significant, treatment-specific effects on the transcriptome and lipidome. Overall, our

findings suggest that exposure of human cells to PPARγ ligands at biologically active, non-cytotoxic concentrations results in toxicity that may be driven by a combination of both PPARγ-dependent and PPARγ-independent mechanisms.

3.1 Introduction

Peroxisome proliferator-activated receptor γ (PPARγ) is a nuclear receptor and transcription factor that is activated by both endogenous and exogenous ligands (Issemann and Green, 1990; Tontonoz et al., 1994; Martin et al., 1998). Upon activation by ligand binding, PPARγ heterodimerizes with retinoid X receptor (RXR) and then binds to PPAR response elements (PPREs) as PPARγ:RXR heterodimers across the genome, resulting in transcription of genes involved in lipid/glucose metabolism and adipogenesis (Tontonoz et al., 1994; Martin et al., 1998; Chawla et al., 2004). Polyunsaturated fatty acids are endogenous, low-affinity PPARγ ligands and include prostaglandin PGJ2, linolenic acid, eicosapentaeonic acid, docosahexaenoic acid, and arachidonic acids (Forman et al., 1995; Kliewer et al., 1995; Nagy et al., 1998). Based on structural studies, the PPARγ binding site accommodates lipophilic carboxylic acids and other acidic ligands that can bind to polar residues, consistent with its proposed physiological role as a fatty acid sensor (Velkov, 2013). Exogenous PPARγ ligands include pharmaceuticals (e.g., thiazolidinediones) developed to treat Type II diabetes and obesity within human populations as well as environmental chemicals that have the ability to bind and activate PPARγ (Nolan et al., 1994; Lehmann et al., 1995; Hurst and Waxman, 2003; Riu et al., 2011; Wang et al., 2016).

Activation of PPARγ results in transcription of downstream genes that vary by tissue and cell type. Within liver and adipose tissue, genes transcribed are involved in lipid metabolism and adipogenesis. For example, liver tissue from PPARγ knockout mice are deficient in lipid transport-related transcripts such as fatty acid translocase (CD36) and low-density lipoprotein receptor (LDLR) (Gavrilova et al., 2003). Within adipose tissue, PPARγ induces expression of

cytosolic glycerol 3-phosphate dehydrogenase (cGPDH), which converts glucose into glycerol 3-phosphate that is incorporated into triglycerides (Patsouris et al., 2004). Human meibomian gland epithelial cells exposed to rosiglitazone (a thiazolidinedione-based PPARγ agonist) results in an increase in lipid transport and biosynthesis-related transcripts including angiopoietin-related protein 4 (ANGPTL4), perilipin-2 (PLIN2), CD36, CCAAT/enhancer-binding protein alpha (CEBPA), elongation of very long chain fatty acids protein 4 (ELOVL4), and ELOVL7 (Kim et al., 2019).

As many PPARγ endogenous ligands are derived from dietary sources and PPARγ plays a role in maintaining lipid homeostasis, prior studies have utilized lipidomics to identify changes in lipid profiles upon activation in different tissue types and disease states. While PPARγ is mainly expressed in adipose tissue and regulates adipogenesis, it is also expressed in liver tissue, with elevated levels found in steatotic liver (Pettinelli and Videla, 2011). Lipidome analysis in patients with nonalcoholic fatty liver or nonalcoholic steatohepatitis revealed a significant increase in diacylglycerol and triacylglycerol content relative to healthy patients without liver disease (Puri et al., 2007). Within liver-specific PPARγ knockout mice, hepatic PPARγ was shown to play a major role in fatty acid uptake and monoacylglycerol pathway-mediated fatty acid esterification (Greenstein et al., 2016). Based on these results and other studies in the literature, one of the primary physiological roles for PPARγ within adipocytes and liver tissue includes lipid storage in the form of fatty acids and triglycerides (Wang et al., 2013).

While animal models (e.g., mice and rats) are critical tools for understanding the effects of exogenous PPARγ ligands within physiologically intact systems, the complementary use of human cell-based models provide direct translational relevance and enhance our understanding of PPARγ signaling at the cellular-level. Previous studies have investigated the role of PPARγ as a transcription factor and its effects on transcription and cell physiology. However, to our

knowledge no prior studies have systematically used a systems-level approach to simultaneously assess the effects of PPARγ ligand exposure on genome-wide PPARγ binding and downstream effects on the transcriptome and lipidome within human cell-based models – an approach that is needed for determining whether genome-wide PPARγ binding has the potential to predict systems-level effects at higher levels of biological organization. Therefore, using ciglitazone and GW 9662 as a reference PPARγ agonist and antagonist, respectively, the overall objective of this study was to determine whether exposure of human cells to biologically active, non-cytotoxic concentrations of PPARγ ligands results in systems-level effects on PPARγ binding (using ChIP-seq), transcription (using mRNA-seq), and lipid composition (using lipidomics) that are consistent with the known mechanism of action for both compounds. Our overall hypothesis was that ciglitazone- and GW 9662-induced effects on cell viability and lipid homeostasis were strongly associated with PPARγ-mediated alterations to the cellular transcriptome. Specifically, we hypothesized that ciglitazone (a PPARγ agonist) and GW 9662 (a PPARγ antagonist) would increase and decrease the magnitude and extent of genome-wide PPARγ binding, respectively, relative to vehicle control-treated cells, leading to opposing effects on cellular transcription and physiology.

For this study, we relied on hepatocellular carcinoma (HepG2) cells, as these cells express baseline levels of PPARγ and are widely used as models to understand DNA damage (Yang et al., 1999), regulation of drug metabolizing enzymes (Wilkening et al., 2003), and lipoprotein metabolism (Meex et al., 2011). By analyzing data generated at the genomic-, transcriptomic-, and lipidomic-level under the same conditions and within the same model system, we can begin to understand the relationship and potential association of alterations at each of these levels of biological organization following exposure to reference PPARγ ligands. Moreover, through careful identification of biologically active concentrations in the absence of

cytotoxicity, this study enabled us to eliminate the potential for false negative findings resulting from limited to no chemical uptake while, at the same, providing the foundation for exploring whether systems-level effects induced by exposure to ciglitazone and GW 9662 may be driven by a combination of both PPARγ-dependent and PPARγ-independent mechanisms.

3.2 Materials and Methods

Chemicals

Ciglitazone (>99.4% purity) was purchased from Tocris Biosciences (Bristol, UK) and GW 9662 (>98% purity) was purchased from Enzo Life Sciences (Farmingdale, NY USA). For both chemicals, stock solutions were prepared in high-performance liquid chromatography (HPLC)-grade dimethyl sulfoxide (DMSO) and stored in 2-mL amber glass vials with polytetrafluoroethylene-lined caps. Working solutions were prepared by spiking stock solutions into sterile cell culture media immediately prior to each experiment, resulting in 0.1% DMSO within all treatment groups.

PPARγ ligand exposures and cell viability assays

HepG2 cells were purchased from American Type Culture Collection (Manassas, VA, USA) and grown within T75 cell culture flasks (Millipore Sigma, St. Louis, MO, USA) containing 15 mL of Eagle's Minimum Essential Medium supplemented with 10% fetal bovine serum (FBS) (ATCC, Manassas, VA, USA) at 37ºC and 5% CO_2. Media was changed within each flask every other day and cells were split every four days using 0.25% Trypsin/0.53 mM EDTA (ATCC, Manassas, VA, USA) after reaching ~70-90% confluency.

HepG2 cells were plated at a concentration of $2x10^4$ cells per well in a clear, polystyrene 96-well plate (ThermoFisher, Waltham, MA, USA) and allowed to adhere overnight. Media was removed and replaced with 200 µL media spiked with either vehicle (0.1% DMSO), ciglitazone (52, 65, 82, 102, 128, 160, or 200 µM), or GW 9662 (41, 51, 64, 80, or 100 µM) and incubated at

37ºC and 5% CO_2 for 24 h (4 replicate wells per treatment). At the end of the exposure duration, treatment solution was removed and replaced with 100 µL of clean cell culture media and 20 µL of CellTiter-Blue (Promega, Madison, WI, USA), and then allowed to incubate for 2 h at 37ºC and 5% CO_2. Fluorescence was then quantified using a GloMax Multi+ Detection System (Promega, Madison, WI, USA).

PPARγ immunohistochemistry

To confirm the presence of PPARγ protein *in situ* across treatments, cells were exposed to either vehicle (0.1% DMSO), ciglitazone, or GW 9662 as described above for either 2, 4, 6, 8, or 24 h. At exposure termination, cells were fixed with 4% formaldehyde at room temperature for 10 min. Cells were then rinsed three times with 1X phosphate-buffered saline (PBS) and incubated in blocking buffer [1X PBS + 0.1% Tween-20 (PBST), 2 mg/mL bovine serum albumin, and 2% sheep serum] at room temperature for 1 h by shaking gently. Blocking buffer was then replaced with a 1:100 dilution of a human PPARγ-specific antibody (E-8, sc-7273; Santa Cruz Biotechnology, Dallas, TX USA) diluted in blocking buffer and allowed to incubate overnight at 4°C. Cells were then incubated with a 1:500 dilution of Alexa Fluor 488-conjugated goat anti-mouse IgG_1 antibody (ThermoFisher Scientific, Waltman, MA USA) overnight at 4°C. Cells were then counterstained with a 1:3 solution of DAPI Fluoromount-G (Southern Biotechnology, GA) for 5 min, rinsed with 1X PBS three times, and then imaged (at 10X magnification) and analyzed using our ImageXpress Micro XLS Widefield High-Content Screening System (Molecular Devices, Sunnyvale, CA USA).

Oil Red O staining

To determine whether exposure to ciglitazone or GW 9662 affected neutral lipid abundance, HepG2 cells were stained for neutral lipids using Oil Red O (ORO) (Sigma-Aldrich, St. Louis, MO, USA) following exposure to vehicle (0.1% DMSO), ciglitazone, or GW 9662 as

described above. Briefly, cells were fixed using 4% paraformaldehyde for 20 min at room temperature. Cells were then rinsed with 60% isopropanol and stained with ORO working solution (1.8 mg ORO per 1 mL 60% isopropanol) for 10 min at room temperature. Cells were then rinsed four times with molecular biology-grade water for 5 min at room temperature. After the final wash, cells were counterstained with a 1:3 solution of DAPI Fluoromount-G (Southern Biotech) for 5 min at room temperature. Cells were washed three more times with molecular biology-grade water and imaged (at 10X magnification) and analyzed using our ImageXpress Micro XLS Widefield High-Content Screening System (Molecular Devices, Sunnyvale, CA USA).

Chromatin immunoprecipitation-sequencing (ChIP-seq)

HepG2 cells were plated and exposed for 8 h to either vehicle (0.1% DMSO), 128 μM ciglitazone, or 100 μM GW 9662 (32 wells pooled per replicate; 3 replicates per treatment). Cells were fixed and lysed using the truChIP Chromatin Shearing Kit with Formaldehyde (Covaris, Woburn, MA USA), and chromatin was then sheared using a Covaris S220 Focused-Ultrasonicator (Peak Incident Power: 175 W, Duty Factor: 10%, Cycles per Burst: 200, Time: 500 s, Temperature: 3-6°C). An aliquot of sheared chromatin was treated with 10 mg/mL RNase A and 10 mg/mL Proteinase K to reverse crosslinks, confirm shearing efficiency, and confirm DNA quantity and quality using a Qubit 4.0 Fluorometer and 2100 Bioanalyzer system, respectively. After confirming that chromatin was sheared to the optimal size range (150-700 bp), sheared chromatin was processed for immunoprecipitation using an Imprint Chromatin Immunoprecipitation Kit (Sigma-Aldrich) and ChIP-grade, human PPARγ-specific antibody (sc-7273X) (Santa Cruz Biotechnology, Dallas, TX USA).

An EpiNext ChIP-Seq High Sensitivity Kit (Epigentek, Farmingdale, NY USA) was then used to prepare sequencing libraries per the manufacturers' instructions; treatment replicates were

indexed using EpiNext NGS Barcodes (Epigentek, Farmingdale, NY USA). Library quantity and quality were confirmed using a Qubit 4.0 Fluorometer and Bioanalyzer 2100 system, respectively. Libraries (9 total) were then pooled, diluted to a concentration of 1.3 pM (with 1% PhiX control) and paired-end (2X150) sequenced on our Illumina MiniSeq Sequencing System (San Diego, California, USA) using a 300-cycle High-Output Reagent Kit. Raw Illumina (fastq.qz) sequencing files (9 total) are available via NCBI's BioProject database under BioProject ID PRJNA681430, and a summary of sequencing run metrics are provided in Table S9.

After completion of the sequencing run, reads passing filter were aligned to the human genome (GRCh37/hg19) using a BWA Aligner application within Illumina's BaseSpace to generate BAM files for each treatment replicate. BAM files were downloaded from BaseSpace and then uploaded into Galaxy (usegalaxy.com). Within Galaxy, MACS2 callpeak was run on pooled treatments to identify significant narrow peaks (i.e., transcription factor binding sites) and to generate BED files. All defaults were used for each MACS2 callpeak run, including a q-value = 0.05 as a cutoff for peak detection. BED files were then used to run ChIPseeker within Galaxy to annotate identified peaks using GRCh37/hg19 as a reference genome, and TFmotifView (http://bardet.u-strasbg.fr/tfmotifview/) (Leporcq et al., 2020) was used to identify PPARG-RXRA-specific motifs (i.e., PPREs) within ChIP-seq peaks.

mRNA-sequencing

HepG2 cells were plated and exposed as described above to either vehicle (0.1% DMSO), 128 μM ciglitazone, or 100 μM GW 9662 (2 wells pooled per replicate; 3 replicates per treatment). After 24 h, total RNA from each replicate was isolated using a Promega SV Total RNA Isolation System (Promega, Madison, WI, USA) following the manufacturer's protocol. RNA quantity and quality were confirmed using a Qubit 4.0 Fluorometer and Bioanalyzer 2100

system, respectively. Based on sample-specific Bioanalyzer traces, the RNA Integrity Number (RIN) was >9 for all RNA samples used for library preparations.

Library preps were performed using a QuantSeq 3' mRNA-Seq Library Prep Kit FWD for Illumina (Lexogen, Vienna, Austria) and indexed by treatment replicate per manufacturer's instructions. Library quantity and quality were confirmed using a Qubit 4.0 Fluorometer and 2100 BioAnalyzer system, respectively. Raw Illumina (fastq.qz) sequencing files (9 total) are available via NCBI's BioProject database under BioProject ID PRJNA681430, and a summary of sequencing run metrics are provided in Table S10. All nine raw and indexed Illumina (fastq.gz) sequencing files were downloaded from Illumina's BaseSpace and uploaded to Bluebee's genomics analysis platform (www.bluebee.com) to align reads against the human genome (GRCh38/hg38). After combining treatment replicate files, a DESeq2 application within Bluebee (Lexogen Quantseq DE1.2) was used to identify significant treatment-related effects on transcript abundance (relative to vehicle) based on a false discovery rate (FDR) *p*-adjusted value ≤ 0.05. Significantly affected transcripts were imported into the Database for Annotation, Visualization, and Integrated Discovery (DAVID) v6.8 for Gene Ontology (GO) enrichment analysis. Individual transcripts from significant GO terms (Benjamini score ≤ 0.05) were consolidated into a list of unique transcripts.

Lipidomics

Cells were plated and exposed as described above. Cells were exposed to either vehicle (0.1% DMSO), 128 μM ciglitazone, or 100 μM GW 9662 (6 wells pooled per replicate; 4 replicates per treatment). After 24 h, the exposure solution was removed, cells were rinsed with Hank's Balance Salt Solution warmed to 37°C, replaced with 50 μL of 100% methanol, and incubated at -80°C for 60 min. LC-MS-based lipidomics analysis was performed as described previously with minor modifications (Reddam et al., 2019). Briefly, analysis was performed on a

G2-XS quadrupole time-of-flight mass spectrometer (Waters Corp., Milford, MA USA) coupled to an H-class UPLC system (Waters Corp., Milford, MA USA). Separations were carried out on a CSH C18 column (2.1 x 100 mm, 1.7 µM) (Waters Corp., Milford, MA USA). The mobile phases were (A) 60:40 acetonitrile:water with 10 mM ammonium formate and 0.1% formic acid and (B) 90:10 isopropanol:acetonitrile with 10 mM ammonium formate and 0.1% formic acid. The flow rate was 400 µL/min and the column was held at 65°C. The injection volume was 4 µL. The gradient was as follows: 0 min, 15% B; 2 min, 30% B; 3 min, 50% B; 10 min, 55% B; 14 min, 80% B; 16 min, 100% B; 20 min 100% B; 20.5 min, 15% B.

The MS was operated in positive ion mode (50 to 1600 m/z) with a 100-ms scan time. Source and desolvation temperatures were 150°C and 600°C, respectively. MS/MS was acquired in a data-dependent fashion. Desolvation gas was set to 1100 L/h and cone gas to 150 L/h. All gases were nitrogen except the collision gas, which was argon. Capillary voltage was 1 kV. A quality control sample, generated by pooling equal aliquots of each sample, was analyzed every 4-5 injections to monitor system stability and performance. Samples were analyzed in random order. Leucine enkephalin was infused and used for mass correction.

Untargeted data processing (peak picking, alignment, deconvolution, integration, normalization, and spectral matching) was performed in Progenesis Qi software (Nonlinear Dynamics). Data were normalized to total ion abundance. Features with a CV greater than 30% were removed. To aid in the identification of features that belong to the same metabolite, features were assigned a cluster ID using RAMClust (Broeckling et al., 2014). An extension of the metabolomics standard initiative guidelines was used to assign annotation level confidence (Sumner et al., 2007; Schymanski et al., 2014). Annotation level 1 indicates an MS and MS/MS match or MS and retention time match to an in-house database generated with authentic standards. Level 2a indicates an MS and MS/MS match to an external database. Level 2b

indicates an MS and MS/MS match to the Lipiblast in-silico database (Kind et al., 2013) or an MS match and diagnostic evidence, such as the dominant presence of an m/z 85 fragment ion for acylcarnitines. Level 3 indicates an MS match, though some additional evidence is required, such as adducts were detected to sufficiently deduce the neutral mass or the retention time is in the expected region. Several mass spectral metabolite databases were searched against including Metlin, Mass Bank of North America, and an in-house database.

Statistical analyses

For cell viability, ORO staining, and immunohistochemistry data, a general linear model (GLM) analysis of variance (ANOVA) ($\alpha = 0.05$) was performed using SPSS Statistics 27 (IBM, Armonk, NY USA), as data did not meet the equal variance assumption for non-GLM ANOVAs. Treatment groups were compared with vehicle controls using pair-wise Tukey based multiple comparisons of least square means to identify significant treatment-specific differences.

3.3 Results

Ciglitazone decreases HepG2 cell viability at concentrations >128 µM while GW 9662 had no effect on cell viability up to the limit of solubility

Relative to HepG2 cells exposed to vehicle (0.1% DMSO) for 24 h, HepG2 cells exposed to 128 µM ciglitazone for 24 h resulted in a slight (albeit non-significant) decrease in fluorescence as measured by CellTiter Blue Assay (~70% cell viability), whereas exposure to ciglitazone above 128 µM resulted in a significant increase in cell death (Figure 13). HepG2 cells exposed to GW 9662 for 24 h did not result in decreased fluorescence up to its limit of solubility (100 µM) (Figure 13). Based on cell viability data, the maximum tolerated concentrations (MTCs) for ciglitazone and GW 9662 were 128 µM and 100 µM, respectively. Therefore, samples for ChIP-seq, mRNA-seq, and lipidomics were generated following exposure to these MTCs.

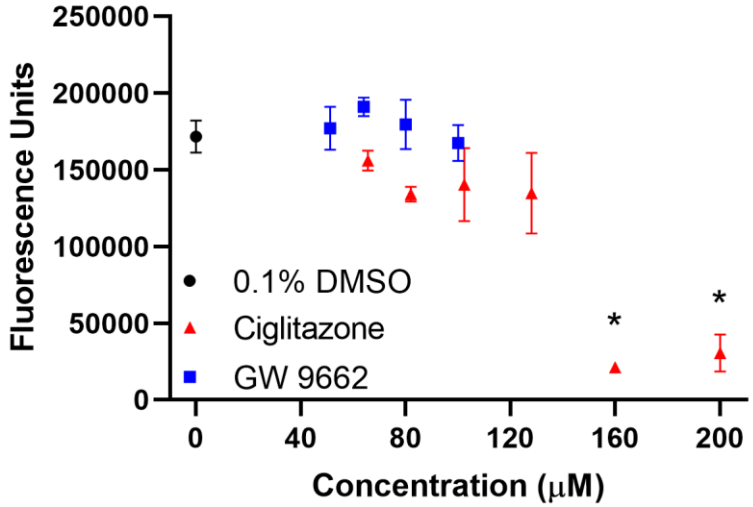

Figure 13. Mean (± standard deviation) of fluorescence of HepG2 cells exposed to vehicle (0.1% DMSO) (black circle), 50-200 μM ciglitazone (red triangles), or 41-100 μM GW 9662 (blue squares) for 24 h as measured by a CellTiter Blue assay. Asterisk (*) indicates a significant difference ($p<0.05$) in cell viability relative to vehicle-exposed cells.

PPARγ levels in situ are not affected after 8 h of exposure to ciglitazone and GW 9662

A human PPARγ-specific antibody was used to quantify PPARγ protein levels within exposed cells. Exposure to ciglitazone (52-128 μM) or GW 9662 (41-80 μM) for 24 h did not affect PPARγ levels detected *in situ* relative to vehicle-exposed cells (Figure 14A). However, exposure to 100 μM GW 9662 for 24 h resulted in a statistically significant decrease in PPARγ levels (Figure 14A). PPARγ levels were also measured at 2, 4, 6, and 8 h after exposure to either 128 μM ciglitazone or 100 μM GW 9662. For both treatment groups, PPARγ levels were not significantly different from 2-8 h following initiation of exposure (Figure 14B).

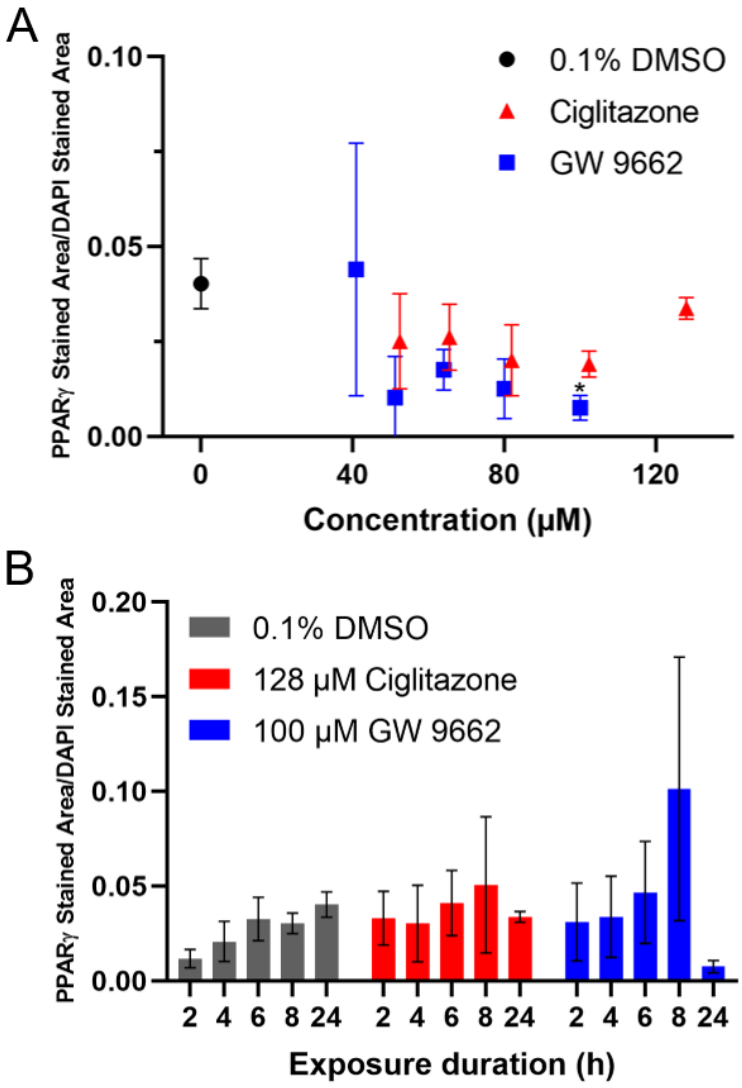

Figure 14. Mean (± standard deviation) of PPARγ immunofluorescence area divided by DAPI stained area of HepG2 cells exposed to vehicle (0.1% DMSO), 52-128 μM ciglitazone, or 41-100 μM GW 9662(A) for 24 h. Mean (± standard deviation) of PPARγ immunofluorescence area divided by DAPI stained area of HepG2 cells exposed to vehicle, 128 μM ciglitazone, or 100 μM GW 9662 for 2, 4, 6, 8, or 24 h (B).

Ciglitazone and GW 9662 increases neutral lipids in a concentration-dependent manner

ORO staining revealed a statistically significant increase in neutral lipids in HepG2 cells exposed to 128 µM ciglitazone relative to vehicle-exposed cells (Figure 15A). In order to account for differences in neutral lipid staining as a function of differences in cell number, ORO staining was normalized to DAPI staining within each well. While there was a slight concentration-dependent increase in DAPI-normalized ORO staining in cells exposed to GW 9662, these results were not statistically significant up to the highest GW 9662 concentration tested. While concentrations of ciglitazone and GW 9662 were not cytotoxic, fixation of cells for ORO staining also revealed that exposed cells were more spherical in shape as opposed to a normal, epithelial-like shape observed following exposure to vehicle (Figure 15B-15G).

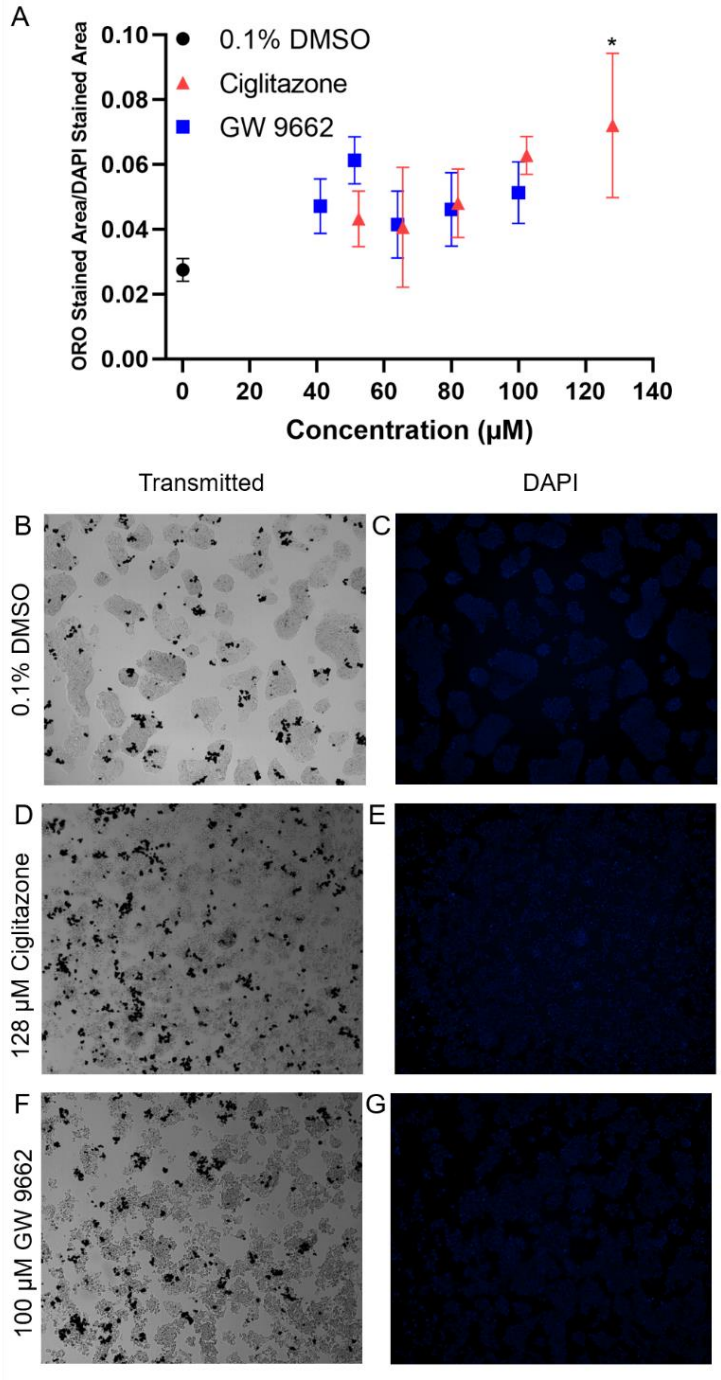

Figure 15. Mean (± standard deviation) of HepG2 cells stained with Oil Red O neutral lipid stain and normalized to DAPI staining after exposure to vehicle (0.1% DMSO), 52-128 µM ciglitazone, or 41-100 µM GW 9662 (A). Representative images taken under transmitted light for vehicle (0.1% DMSO) (B), 128 µM ciglitazone (D), or 100 µM GW 9662 (F), and under DAPI filter for vehicle (C), 128 µM ciglitazone (E), or 100 µM GW 9662 (G).

PPARγ binding occurs genome-wide and the majority of PPARγ-bound PPARG:RXRA motifs are found within distal intergenic or intron regions

Cells were only exposed for 8 h since we hypothesized that binding of PPARγ to PPREs would precede effects on the transcriptome and lipidome at 24 h. Using MACS2 analysis, there were a total of 125, 145, and 89 ChIP peaks identified across the genome within HepG2 cells exposed for 8 h to vehicle (0.1% DMSO), ciglitazone, or GW 9662, respectively (Figure 16A; Tables S11-S13). Each ChIP peak represented a region where reads were significantly abundant (or stacked) relative to a reference genome, indicating that these reads were derived from genomic DNA fragments pulled down following immunoprecipitation. Within MACS2-identified ChIP peaks, TFmotifView then revealed that 29, 39, and 25 PPARG-RXRA (PPRE) motifs were identified across the genome within HepG2 cells exposed for 24 h to vehicle (0.1% DMSO), ciglitazone, or GW 9662, respectively (Figures 16B and 16C; Tables S14-S16). While PPARG-RXRA (PPRE) motifs were distributed among distal intergenic regions, introns, and promoter regions (Figure 16D; Tables S14-S16), the majority of PPARγ-bound PPARG:RXRA motifs were found within distal intergenic or intron regions.

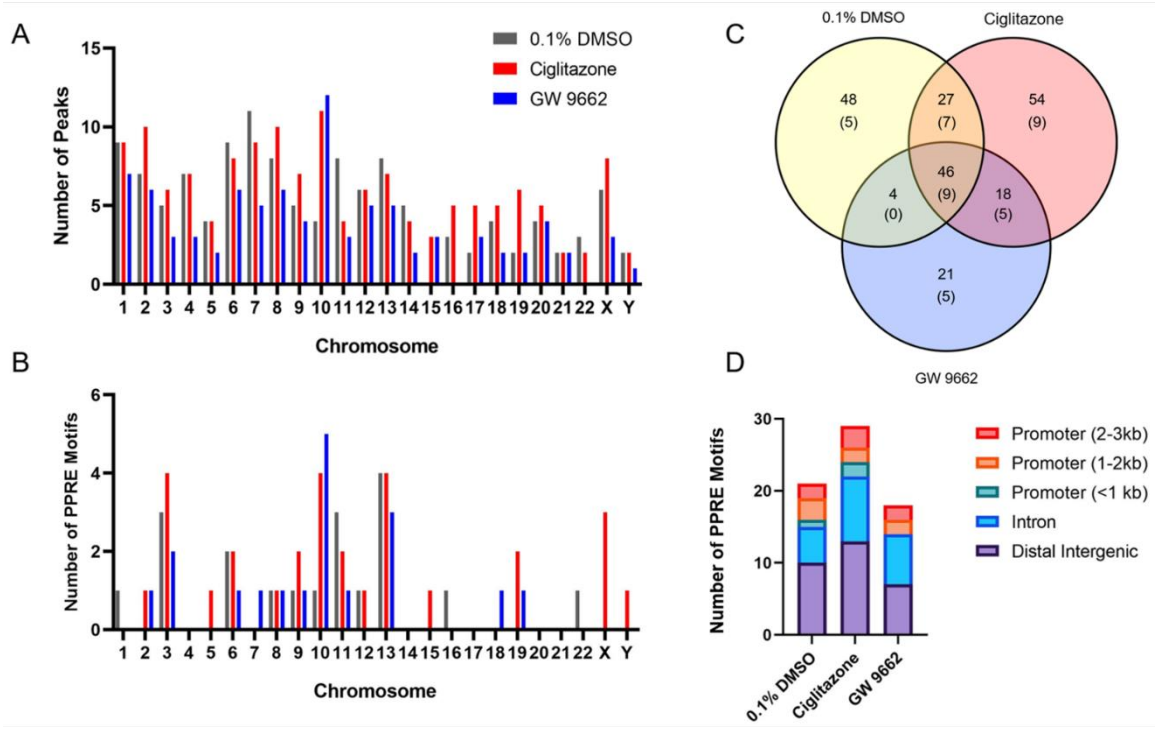

Figure 16. Number of ChIP peaks by chromosome number identified from ChIP-Seq MACS analysis (A). Number of ChIP peaks by chromosome number containing PPARG-RXRA (PPRE) motifs after analysis by TFmotifView (B). Venn diagram showing overlap of ChIP peaks between vehicle (0.1% DMSO), 128 µM ciglitazone, and 100 µM GW 9662 treatment (C). Bolded text indicates the number of peaks identified through MACS analysis. Text within parentheses indicate the number of PPARG-RXRA (PPRE) motifs within each treatment group. Distribution of annotated motif locations by treatment group (D).

Transcripts involved in cholesterol biosynthesis are oppositely affected by ciglitazone and GW 9662 exposure

Exposure of HepG2 cells to 128 µM ciglitazone resulted in significant effects on the abundance of 4,146 transcripts (Figure 17A; Table S17), while exposure to 100 µM GW 9662 resulted in significant effects on the abundance of 3,704 transcripts (Figure 17B; Table S18). Interestingly, a heat map based on significantly affected transcripts revealed that the transcriptome within ciglitazone- and GW 9662-exposed cells were similar, with only a subset of transcripts that were oppositely affected by ciglitazone vs. GW 9662 (Figure 17C). To determine which biological processes were significantly affected due to ciglitazone or GW 9662 exposure, differentially affected transcripts relative to vehicle-exposed cells were analyzed using DAVID to identify top biological processes. To identify biological processes that were oppositely affected by ciglitazone and GW 9662 exposure, significantly affected transcripts were sorted by fold-change for each treatment and then compared to identify transcripts that were either 1) decreased by ciglitazone exposure and increased by GW 9662 exposure (Figure 17D) or 2) increased by ciglitazone exposure and decreased by GW 9662 exposure (Figure 17E). DAVID gene ontology analysis identified nine transcripts involved in cholesterol biosynthesis that were decreased by ciglitazone exposure and increased by GW9662 exposure (Figures 17F and 17G; Table S19-S20).

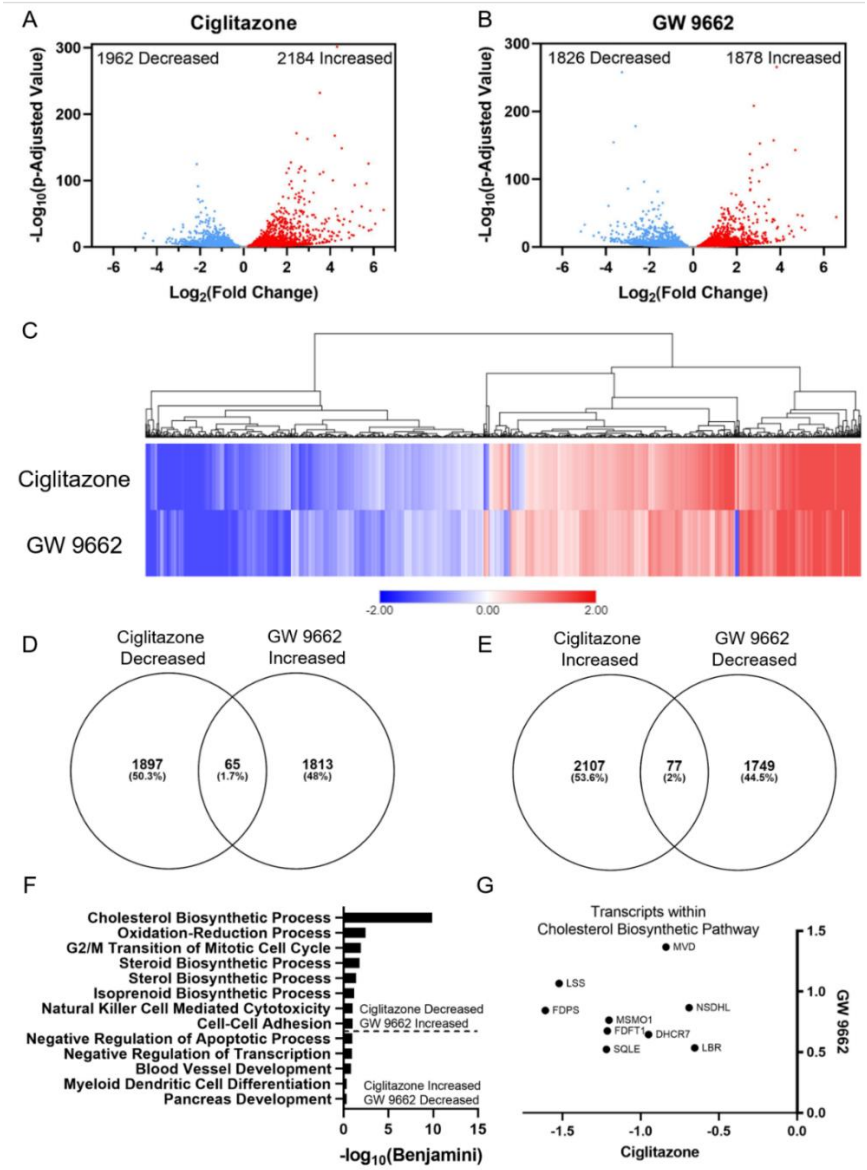

Figure 17. Volcano plots indicating number of significantly affected transcripts for ciglitazone (A) or GW 9662 (B) relative to vehicle-exposed cells. Heat map of significantly affected transcripts organized by hierarchical clustering using Euclidean distance and complete linkage method (C). Venn diagrams showing overlap in transcripts between ciglitazone and GW 9662 (D, E). Gene ontology analysis of biological processes identified by DAVID based on decreased transcripts following ciglitazone exposure and increased transcripts following GW 9662 exposure or increased transcripts following ciglitazone exposure and decreased transcripts following GW 9662 exposure (E). Transcripts within cholesterol biosynthetic process plotted by $\log_2$(fold change) in GW 9662-exposed cells along the Y-axis, and $\log_2$(fold change) in ciglitazone-exposed cells along the x-axis (F). MVD: Mevalonate Diphosphate Decarboxylase, NSDHL: Sterol-4-alpha-caroxylate 3-dehydrogenase (NAD(P) dependent steroid dehydrogenase-like), LBR: Lamin B receptor, DHCR7: 7-Dehydrocholesterol Reductase, MSMO1: Methylsterol Monooxygenase 1, FDFT1: Farnesyl-Diphosphate Farnesyltransferase 1, SQLE: Squalene Epoxidase, LSS: Lanosterol synthase, FDPS: Farnesyl pyrophosphate synthase.

Ciglitazone alters lipid composition across several lipid classes while the lipid profile of GW 9662-exposed cells was more similar to vehicle-exposed cells

Lipid profile analysis revealed that, relative to vehicle-exposed cells, 1,075 lipids were significantly altered after 24 h of exposure to ciglitazone whereas 498 lipids were significantly altered after exposure to GW 9662 (Figure 18A; Table S21). The total abundance of lipids in ciglitazone- or GW 9662-exposed cells were not significantly altered compared to vehicle-exposed cells (Figure 18C; Table S21). However, the relative composition of lipids within exposed cells were different relative to vehicle-exposed cells (Figure 18B; Table S21). Within ciglitazone-exposed cells, there was a significant increase in lipids from the acylcarnitine, ceramide, lyso phosphatidylcholine (PC), spermidine, sterol, sterol ester, and triglyceride classes, and a significant decrease in lipids from the choline, lyso phosphatidylethanolamine (PE), PC, PE, and sphingomyelin (SM) classes. Although the lipid profile of GW 9662-exposed cells was more similar to vehicle-exposed cells (Figure 18A), there was a significant increase in lyso PE lipids and significant decrease in SM and spermidine lipid classes. Cholesterol and two different sterol esters (16.0 and 16.3) were significantly increased following exposure to ciglitazone, whereas sterol ester (16.0) was significantly increased following exposure to GW 9662 (Figure 18D).

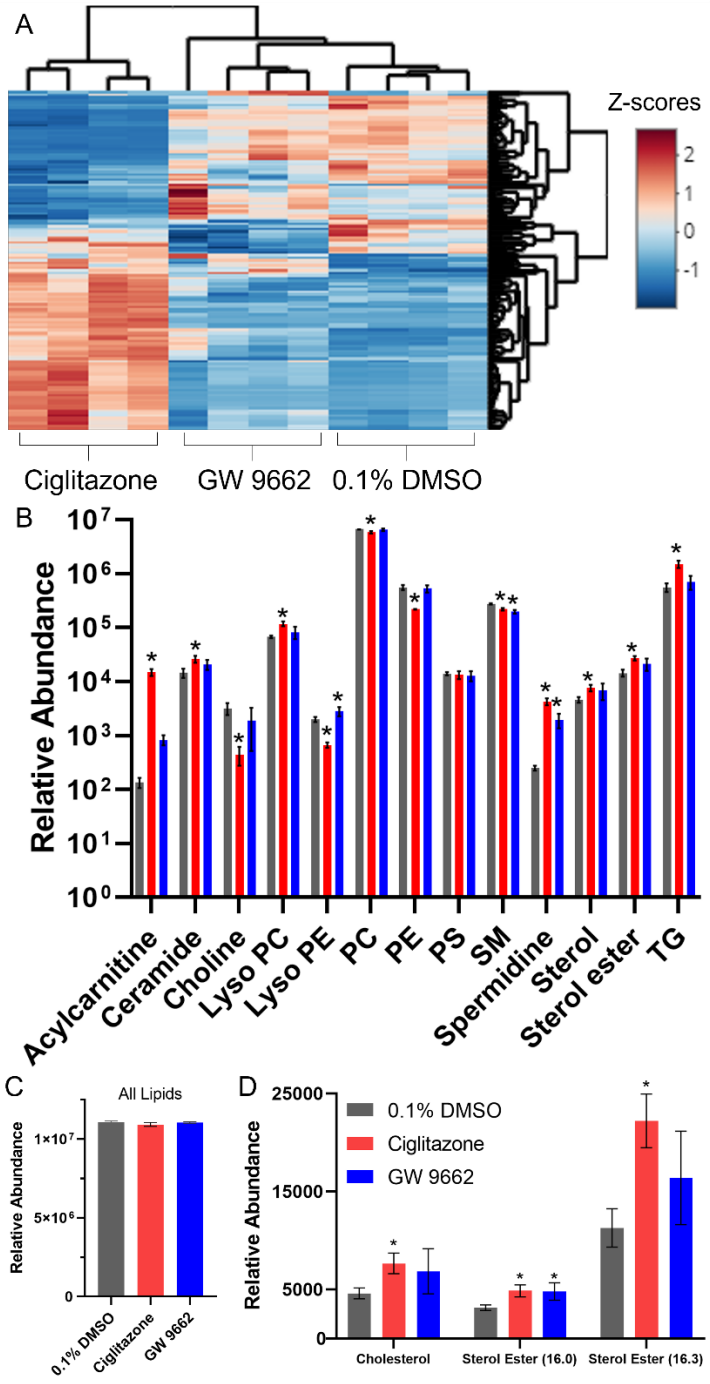

Figure 18. Heat map of significantly altered lipids (data shown as z-scores) following exposure to 128 µM ciglitazone or 100 µM GW 9662 relative to vehicle-exposed cells (A). Relative lipid abundance divided into lipid class and treatment (B). Asterisk (*) indicates a significant difference ($p<0.05$) in lipid abundance relative to vehicle. Sum of relative lipid abundance by treatment (C). Relative abundance of cholesterol and sterol esters following exposure to vehicle (0.1% DMSO), 128 µM ciglitazone, or 100 µM GW 9662 (D). PC: Phosphatidylcholine, PE: Phosphatidylethanolamine, PS: Phosphatidylserine, SM: Sphingomyelin, TG: Triacylglyceride

3.4 Discussion

A prior study that exposed HepG2 cells to ciglitazone estimated an IC_{50} value of 46 µM based on a 16-h exposure and cell viability as an endpoint using a 3-(4, 5-dimethyl-2-thiazolyl)-2, 5-diphenyl-2H-tetrazolium bromide (MTT) assay (Guo et al., 2006), whereas our study identified 128 µM ciglitazone as the MTC following a 24-h exposure – differences that may be attributable to the type of assay (CellTiter-Blue vs. MTT) used to quantify cell viability. Within the same study, the IC_{50} value of ciglitazone relative to other thiazolidinedione compounds was the second lowest (Guo et al., 2006), indicating that higher nominal concentrations required within our study were not driven by a lack of potency of ciglitazone. To our knowledge, no studies have been conducted to determine the IC_{50} or MTC for GW 9662 within HepG2 cells. Within other human cell-based models, the IC_{50} for ciglitazone and GW 9662 based on cell viability as an endpoint ranged from 12-230 µM and 20-30 µM, respectively (Eibl et al., 2001; Strakova et al., 2004; Strakova et al., 2005; Vignati et al., 2006; Seargent et al., 2004).

While HepG2 cells express PPARγ, expression within liver tissue is lower relative to adipocytes (Elbrecht et al., 1996), suggesting that lower expression may account for the lower sensitivity of HepG2 cells to PPARγ ligands. As there are studies showing that PPARγ regulates adipogenesis in 3T3-L1 cells through a positive feedback loop (Wakabayashi et al., 2009), we wanted to determine if ciglitazone or GW 9662 also regulated the accumulation of neutral lipids in this manner within HepG2 cells. Despite the higher nominal concentrations of ciglitazone and GW 9662 used within our study, there was a concentration-dependent increase in neutral lipids following exposure to either compound – a finding that may be PPARγ-independent since 1) we observed a similar response even though both compounds have opposing mechanisms of action (PPARγ agonist vs. antagonist) and 2) we did not observe a concentration-dependent effect on PPARγ protein levels *in situ*.

While previous PPARγ-specific ChIP-seq studies have been utilized to map PPARγ binding during adipogenesis (Nielsen et al., 2008) or understand differences in cell-specific PPARγ binding (Lefterova et al., 2010), to our knowledge our study was the first to utilize ChIP-seq to correlate phenotypic changes after PPARγ agonist exposure to genome binding within human cell-based models. As expected, PPARγ-bound DNA fragments sequenced after ChIP revealed binding of PPARγ across the genome. While we expected a strong increase in ChIP peaks following exposure to ciglitazone (a PPARγ agonist), the number of ChIP peaks within ciglitazone-exposed cells were similar relative to vehicle-exposed cells. As GW 9662 is a PPARγ antagonist that irreversibly binds to the ligand binding pocket of PPARγ (Leesnitzer et al., 2002), we expected GW 9662 to result in a decrease in ChIP peaks relative to vehicle-exposed cells. However, contrary to our hypothesis, we detected numerous ChIP peaks across the genome within GW 9662-exposed cells. Indeed, chromosome-specific effects were not detected following exposure to vehicle, ciglitazone, nor GW 9662, as the distribution of ChIP peaks were similar across all three treatment groups. Likewise, there was no clear treatment-dependent pattern of PPARG:RXRA (PPRE) motifs, and the majority of PPARG:RXRA (PPRE) motifs identified were located within intron and distal intergenic regions rather than within promoter regions that regulate transcription, a finding that is consistent with prior PPARγ-specific ChIP-seq studies (Lefterova et al., 2008) and other studies proposing that transcription factor binding to distal regions directs DNA looping as well as recruits coactivators and chromatin remodelers to the transcription start site of target genes (West and Fraser, 2005). Overall, these data suggest that the phenotypic effects of ciglitazone and GW 9662 on HepG2 cells were not associated with PPARγ binding to PPRE motifs within promoter regions across the genome.

Consistent with our finding that genome-wide PPARγ binding was similar following exposure to ciglitazone or GW 9662, both ciglitazone and GW 9662 also induced a similar

magnitude of effect on transcripts that were either increased or decreased. While we expected ciglitazone and GW 9662 to act as a PPARγ agonist and antagonist, respectively, we found that the majority of transcripts were similarly affected by both compounds, suggesting that these overlapping transcriptional responses may be PPARγ-independent. To identify transcriptional responses that may be driven by PPARγ activation or inactivation, we identified transcripts that were oppositely affected by ciglitazone and GW 9662 exposure. Based on this analysis, cholesterol biosynthesis was the most significant pathway identified within the group of transcripts that were decreased and increased by ciglitazone and GW 9662, respectively. To our knowledge, our study was the first to identify cholesterol biosynthesis as a significantly affected process in human cell-based models after ciglitazone or GW 9662 exposure.

Interestingly, lipidomics revealed a unique lipid profile within ciglitazone-exposed cells compared to GW 9662- or vehicle-exposed cells, suggesting that ciglitazone exposure resulted in significant effects on the lipidome. Moreover, while total lipid abundance among all three treatment groups was not different, the abundance of certain lipid-specific classes was altered within ciglitazone- and GW 9662-exposed cells. Based on our mRNA-seq data, we expected to detect a decrease in cholesterol abundance, as cholesterol biosynthesis was predicted to be significantly decreased due to ciglitazone exposure. However, in both ciglitazone- and GW 9662-exposed cells, there was a significant increase in cholesterol and other sterol lipids relative to vehicle-exposed cells – differences that may have been attributable to the timing of chemically-induced effects on the transcriptome vs. lipidome. As samples for mRNA-seq and lipidomics were both derived from cells that were exposed for 24 h, it is possible that effects on the transcriptome observed at 24 h may have been associated with effects on the lipidome before or after 24 h of exposure. To our knowledge, our study was the first to associate transcriptional

responses to lipidomic responses after exposure to a PPARγ agonist or antagonist within human cell-based models.

While ciglitazone and GW 9662 are marketed and used as a PPARγ agonist and antagonist, respectively, it is unclear whether the effects observed within our study were due to direct PPARγ modulation and/or off-target effects. While the mechanisms of PPARγ activation have been well studied and compounds within the thiazolidinedione class have been widely used as reference chemicals for PPARγ activation, previous studies have identified PPARγ-independent mechanisms of ciglitazone such as activation of MAP kinase cascades in human preadipocytes (Lennon et al., 2002) as well as regulation of cell cycle proteins in human prostate cancer cells (Lyles et al., 2009). Although thiazolidinediones have previously been used to treat Type 2 diabetes mellitus, these compounds were subsequently removed from the market due to adverse effects suggesting that other targets may be present (Nesto et al., 2003; Nissen et al., 2007; Lewis et al., 2011). Our study relied on the MTC of ciglitazone based on cell viability, and the maximum concentration of GW 9662 based on its solubility in DMSO. Based on ORO staining, the concentrations of ciglitazone and GW 9662 used resulted in phenotypic effects on neutral lipids and cell morphology – effects which were not detected based on cell viability alone. Gene ontology analysis of mRNA-seq data for ciglitazone identified apoptotic processes, suggesting that ciglitazone may have resulted in systemic toxicity and, as such, PPARγ-driven effects may have been masked by off-target effects of ciglitazone within HepG2 cells.

In conclusion, our study systematically deployed multiple large-scale, high-resolution approaches to enhance our understanding of the effects of PPARγ ligand exposure within human cells at the systems-level. Moreover, our study was the first to 1) utilize ChIP-seq to correlate phenotypic changes after PPARγ agonist exposure to genome binding within human cell-based models; 2) identify cholesterol biosynthesis as a significantly affected process in human cell-

based models after ciglitazone or GW 9662 exposure; and 3) associate transcriptional responses to lipidomic responses after exposure to a PPARγ agonist or antagonist within human cell-based models. Specifically, we found that 1) ciglitazone decreased HepG2 cell viability at concentrations >128 μM while GW 9662 had no effect on cell viability up to its limit of solubility; 2) ciglitazone and GW 9662 increased neutral lipids in a concentration-dependent manner; 3) PPARγ binding occurred genome-wide and the majority of PPARγ-bound PPARG:RXRA motifs were found within distal intergenic or intron regions; 4) transcripts involved in cholesterol biosynthesis were oppositely affected by ciglitazone and GW 9662 exposure; and 5) ciglitazone altered lipid composition across several lipid classes while the lipid profile of GW 9662-exposed cells was more similar to vehicle-exposed cells. Overall, our data suggest that exposure of human cells to PPARγ ligands at biologically active, non-cytotoxic concentrations results in effects on the transcriptome and lipidome that may be driven by a combination of both PPARγ-dependent and PPARγ-independent mechanisms. As such, our findings demonstrate that systems-level responses to PPARγ ligand exposure within human cells are complex and concentration-dependent, providing the foundation for continuing to investigate the specificity of PPARγ ligands within intact cells as well as discover novel mechanisms of action for reference PPARγ ligands such as ciglitazone and GW 9662.

Chapter 4: Halogenated bisphenol A analogues induce PPARγ-independent toxicity within human hepatocellular carcinoma cells

4.0 Abstract

Tetrabromobisphenol A (TBBPA) and tetrachlorobisphenol A (TCBPA) – both halogenated bisphenol (BPA) analogues – are suspected ligands of peroxisome proliferator-activated receptor gamma (PPARγ) based on cell-free, competitive binding assays. PPARγ is a ligand-activated transcription factor that heterodimerizes with retinoid X receptor (RXR) and transcribes genes that regulate lipid homeostasis and fatty acid metabolism. While previous studies have shown that TBBPA and TCBPA activate PPARγ *in vitro*, few studies have assessed whether TBBPA or TCBPA alter levels of neutral lipids and fatty acid synthase (FASN) – an enzyme that catalyzes synthesis of long-chain saturated fatty acids – within intact cells in a PPARγ-dependent manner. Therefore, using human hepatocellular carcinoma (HepG2) cells as a model, the objective of this study was to determine whether TBBPA or TCBPA exposure (either alone or in combination) results in PPARγ-mediated effects on neutral lipid and FASN levels *in situ*. Although exposure to TBBPA and TCBPA alone did not affect cell viability nor neutral lipid and FASN levels in a concentration-dependent manner, exposure to binary mixtures of TBBPA and TCBPA resulted in a concentration-dependent decrease in cell viability in the absence of consistent, concentration-dependent effects on neutral lipid and FASN levels. Interestingly, exposure to TBBPA or TCBPA alone or as a mixture enhanced the effects of a reference PPARγ agonist (ciglitazone) and antagonist (GW 9662) on cell viability (but not neutral lipid levels), suggesting that these two halogenated BPA analogues may interact synergistically with ciglitazone and GW 9662 to induce cytotoxicity. However, overexpression of PPARγ did not mitigate nor enhance the effects of TBBPA – a potent PPARγ ligand predicted by ToxCast's cell-free competitive binding assays – on cell viability, neutral lipid levels, nor the cellular transcriptome. Overall, our findings suggest

that halogenated BPA analogues such as TCBPA and TBBPA induce toxicity within HepG2 cells in a PPARγ-independent manner.

4.1 Introduction

Although bisphenol A (BPA) is mainly used as a plasticizer in polycarbonate and epoxy resins, tetrabromobisphenol A (TBBPA) and tetrachlorobisphenol A (TCBPA) are two halogenated BPA analogs primarily used as flame retardants in electronic devices. As a result, these two halogenated BPA analogues have the potential to migrate into indoor dust (Leisewitz et al., 2001) and expose humans within the built environment, where levels of TBBPA in house dust have been previously found to range from 1 to 3600 ng/g (Wang et al., 2015). TBBPA-sulfate and TBBPA-glucuronide (Schauer et al., 2006) – the primary metabolites of TBBPA – have been found in both serum and urine samples in populations around the world (Nagayama et al., 2000; Thomsen et al., 2001; Jakobsson et al., 2002; Dirtu et al., 2008; Shi et al., 2013; Ho et al., 2017). While BPA is a weak ligand for the estrogen receptor (Gould et al., 1998; Liu et al., 2018), neither TBBPA nor TCBPA activate ER to the same degree as BPA (Lee et al., 2012; Cao et al., 2017). However, TBBPA and TCBPA have both been shown to activate another member of the nuclear receptor family – peroxisome proliferator activated receptor gamma (PPARγ) (Riu et al., 2011; Akiyama et al., 2015; Chappell et al., 2018).

PPARγ is a transcription factor (Issemann and Green, 1990; Tontonoz et al., 1994; Martin et al., 1998) that can be activated by both endogenous ligands such as prostaglandin PGJ2 and eicosapentaeonic acid (Forman et al., 1995; Kliewer et al., 1995; Nagy et al., 1998) or exogenous ligands such as pharmaceutical compounds (e.g., thiazolidinediones) (Nolan et al., 1994; Lehmann et al., 1995). Upon activation by ligand binding, PPARγ heterodimerizes with retinoid X receptor (RXR) and then binds to PPAR response elements (PPREs), resulting in transcription of genes involved in lipid/glucose metabolism and adipogenesis (Tontonoz et al., 1994; Martin et

al., 1998; Chawla et al., 2004). While several thiazolidinediones have been developed to treat Type II diabetes and obesity within human populations, many of these compounds have severe side effects and have been discontinued from use (Nesto et al., 2003; Nissen and Wolski, 2007; Lewis et al., 2011). As several environmental chemicals have been shown to bind and activate PPARγ, there is concern about human exposure to xenobiotic PPARγ ligands and potential downstream effects (Hurst and Waxman, 2003; Riu et al., 2011; Wang et al., 2016).

Although TBBPA and TCBPA have nearly identical chemical structures (TBBPA is brominated whereas TCBPA is chlorinated), TBBPA binds to the ligand binding domain of PPARγ with greater affinity than TCBPA (Riu et al., 2011). For example, TBBPA induces neurotoxic effects within mouse primary neuronal cells that is partially PPARγ-dependent (Wojtowicz et al., 2014). While previous studies have investigated the ability of TBBPA and TCBPA to bind to PPARγ within reporter and ligand binding assays, to our knowledge no prior studies have linked TBBPA or TCBPA exposure to PPARγ activation and subsequent downstream effects within a human liver cell model. Therefore, the overall objective of this study was to determine whether exposure of human liver cells to non-cytotoxic concentrations of TBBPA or TCBPA results in effects on transcription and other endpoints that are consistent with the known mechanism of action for PPARγ activation, such as neutral lipid staining (Wakabayashi et al., 2009). We also utilized immunohistochemical staining of fatty acid synthase (FASN) protein *in situ,* as FASN catalyzes synthesis of long-chain saturated fatty acids and is correlated with PPARγ expression in adipocytes (Zhao et al., 2011).

For this study, we relied on human hepatocellular carcinoma (HepG2) cells as a model since these liver cells express basal levels of PPARγ and have previously been used to study lipoprotein metabolism (Meex et al., 2011) and regulation of drug metabolizing enzymes (Wilkening et al., 2003). Since PPARγ levels within HepG2 cells are lower compared to

adipocytes (Elbrecht et al., 1996), we also utilized a human PPARγ expression plasmid to overexpress PPARγ and determine whether the effects of halogenated BPA analogues were mitigated or enhanced in the presence of increased PPARγ levels. Our overall hypothesis was that TBBPA- and TCBPA-induced effects on cell viability, lipid homeostasis, and FASN protein levels were associated with PPARγ-mediated alterations to the cellular transcriptome. In addition, we reasoned that our findings will help us further understand the mechanisms of action of TBBPA and TCBPA within the context of human exposure.

4.2 Materials and Methods

Chemicals

TBBPA (>97% purity) and TCBPA (>98% purity) were purchased from Millipore Sigma (St. Louis, MO, USA). Ciglitazone (>99.4% purity) was purchased from Tocris Biosciences (Bristol, UK) and GW 9662 (>98% purity) was purchased from Enzo Life Sciences (Farmingdale, NY, USA). For all chemicals, stock solutions were prepared in high-performance liquid chromatography (HPLC)-grade dimethyl sulfoxide (DMSO) and stored in 2-mL amber glass vials with polytetrafluoroethylene-lined caps. Working solutions were prepared by spiking stock solutions into sterile cell culture media immediately prior to each experiment, resulting in 0.1% DMSO (single chemical exposures) or 0.2% DMSO (binary mixture exposures) within all treatment groups.

PPARγ ligand exposures and cell viability assays

HepG2 cells were purchased from American Type Culture Collection (ATCC) (Manassas, VA, USA) and grown within T75 cell culture flasks (MilliporeSigma, St. Louis, MO, USA) containing 15 mL of Eagle's Minimum Essential Medium supplemented with 10% fetal bovine serum (FBS) (ATCC, Manassas, VA, USA) at 37ºC and 5% CO_2. Media was changed

within each flask every other day and cells were split every four days using 0.25% Trypsin/0.53 mM EDTA (ATCC, Manassas, VA, USA) after reaching ~70-90% confluency.

HepG2 cells were plated at a concentration of $0.5x10^4$ cells per well in a clear, polystyrene 96-well plate (Thermo Fisher Scientific, Waltham, MA, USA) and allowed to adhere overnight. Media was removed and replaced with 200 µL media spiked with either vehicle (0.1% DMSO), TBBPA (10-100 µM), or TCBPA (10-100 µM) and incubated at 37ºC and 5% CO_2 for 24 h (4 replicate wells per treatment). To assess whether TBBPA and TCBPA resulted in additive or synergistic effects on cell viability and FASN levels, cells were also exposed to either vehicle (0.2% DMSO), 60 or 80 µM TBBPA alone, 60 or 80 µM TCBPA alone, or binary mixtures of 30-100 µM TBBPA and 30-100 µM TCBPA and then incubated at 37ºC and 5% CO_2 for 24 h. At the end of the exposure duration, treatment solution was removed and replaced with 100 µL of clean cell culture media and 20 µL of CellTiter-Blue (Promega, Madison, WI, USA), and then allowed to incubate for 2 h at 37ºC and 5% CO_2. Fluorescence was then quantified using a GloMax Multi+ Detection System (Promega, Madison, WI, USA).

Oil Red O staining

To determine whether exposure to TBBPA or TCBPA affected neutral lipid abundance, HepG2 cells were exposed to vehicle (0.1% DMSO), TBBPA, or TCBPA as described above and then stained for neutral lipids using Oil Red O (ORO) (MilliporeSigma, St. Louis, MO, USA) as previously described (Cheng et al., 2021). Briefly, cells were fixed using 4% paraformaldehyde for 20 min at room temperature. Cells were then rinsed with 60% isopropanol and stained with ORO working solution (1.8 mg ORO per 1 mL 60% isopropanol) for 10 min at room temperature. Cells were then rinsed four times with molecular biology-grade water for 5 min at room temperature. After the final wash, cells were counterstained with a 1:4 solution of DAPI Fluoromount-G (SouthernBiotech, Birmingham, AL, USA) for 5 min at room temperature. Cells

were washed three more times with molecular biology-grade water and then imaged (at 10X magnification) and analyzed using our ImageXpress Micro XLS Widefield High-Content Screening System (Molecular Devices, Sunnyvale, CA, USA).

FASN immunohistochemistry

To quantify FASN protein levels *in situ*, cells were exposed to either vehicle (0.1% DMSO), TBBPA, or TCBPA as described above for 24 h. At exposure termination, cells were fixed with 4% formaldehyde at room temperature for 10 min. Cells were then rinsed three times with 1X phosphate-buffered saline (PBS) and incubated in blocking buffer [1X PBS + 0.1% Tween-20 (PBST), 2 mg/mL bovine serum albumin, and 2% sheep serum] at room temperature for 1 h by shaking gently. Blocking buffer was then replaced with a 1:500 dilution of a human FASN-specific antibody (G-11, sc-48357; Santa Cruz Biotechnology, Dallas, TX, USA) in blocking buffer and allowed to incubate overnight at 4°C. Cells were then incubated with a 1:500 dilution of Alexa Fluor 488-conjugated goat anti-mouse IgG_1 antibody (Thermo Fisher Scientific, Waltman, MA, USA) overnight at 4°C. Cells were then counterstained with a 1:4 solution of DAPI Fluoromount-G (SouthernBiotech, Birmingham, AL, USA) for 5 min, rinsed with 1X PBS three times, and then imaged (at 10X magnification) and analyzed using our ImageXpress Micro XLS Widefield High-Content Screening System (Molecular Devices, Sunnyvale, CA, USA).

Pretreatment with reference PPARγ ligands

To determine whether TBBPA- or TCBPA-induced effects were mitigated or enhanced by a reference PPARγ agonist (ciglitazone) or antagonist (GW 9662), HepG2 cells were plated in 96-well plates as described above. As shown in our prior study (Cheng et al., 2021), exposure to GW 9662 resulted in decreased PPARγ protein levels after 24 h; therefore, we relied on a 24-h pretreatment with either ciglitazone or GW 9662. Following pretreatment with either vehicle (0.1% DMSO), 30-100 µM ciglitazone, or 10-100 µM GW 9662, cells were then exposed to

either vehicle (0.2% DMSO), 30 µM TBBPA, 60 µM TCBPA, or 30 µM TBBPA + 60 µM TCBPA for 24 h and collected for cell viability, neutral lipid staining, and FASN protein IHC as described above.

ToxCast data mining

ToxCast assay endpoint data for TBBPA and TCBPA were downloaded from the U.S. Environmental Protection Agency's website (http://www.epa.gov/ncct/toxcast/data/html). Half-maximal activity concentrations (AC_{50}) for TBBPA and TCBPA were used to calculate assay hit rates and develop overall summary statistics. Since the number of assay endpoints for TBBPA and TCBPA were not identical, the percent assay hit rate for each chemical was defined as the number of assay endpoints with an AC_{50} of <1000 µM – the maximal concentration tested and the basis for an "inactive" activity call – relative to the total number of assay endpoints per chemical. Assays were then sorted by "Intended_Target_Family" for "Nuclear Receptor" to determine the hit rate for nuclear receptor assays. Finally, "Gene_Name" was sorted by "PPARγ" to determine the hit rate for PPARγ-specific assay endpoints.

Overexpression of PPARγ within HepG2 cells

To determine whether overexpression of PPARγ modified the effects of TBBPA (a potent PPARγ ligand based on ToxCast data), HepG2 cells were plated and transfected with either a negative control (NC) cloning plasmid (pCMV6-XL4, OriGene, Rockville, MD, USA) or an expression plasmid containing human untagged PPARγ clone (SC124177, OriGene, Rockville, MD, USA) following the manufacturer's protocol. Briefly, 100 ng/well of either NC plasmid or PPARγ expression plasmid were diluted in Opti-MEM reduced serum media (Thermo Fisher Scientific, Waltman, MA, USA). Turbofectin 8.0 (OriGene, Rockville, MD USA) (0.3 µL/well) was added to plasmids diluted in Opti-MEM and incubated for 15 minutes at room temperature to form complexes. Following incubation, plasmid:Turbofectin 8.0 complexes were added to each

well and gently shaken to distribute evenly. Transfected HepG2 cells were then allowed to incubate for 48 h followed by exposure to either vehicle (0.1% DMSO) or 30 μM TBBPA for 24 h as described above. PPARγ protein levels *in situ* across transfections and treatments were then quantified using a 1:150 dilution of a human PPARγ-specific antibody (E-8, sc-7273; Santa Cruz Biotechnology, Dallas, TX, USA) following previously described protocols (Cheng et al., 2021). Transfected cells were also collected for cell viability, ORO neutral lipid staining, and FASN IHC as described above.

mRNA-sequencing

HepG2 cells were plated, transfected with either NC plasmid or PPARγ expression plasmid, and exposed to either vehicle (0.1% DMSO) or 30 μM TBBPA (3 wells pooled per replicate; 3 replicates per treatment) as described above. After 24 h, total RNA from each replicate was isolated using a Promega SV Total RNA Isolation System (Promega, Madison, WI, USA) following the manufacturer's protocol. RNA quantity and quality were confirmed using a Qubit 4.0 Fluorometer and Bioanalyzer 2100 system, respectively. Based on sample-specific Bioanalyzer traces, the RNA Integrity Number (RIN) was >8.5 for all RNA samples used for library preparations.

Library preps were performed using a QuantSeq 3' mRNA-Seq Library Prep Kit FWD for Illumina (Lexogen, Vienna, Austria) and indexed by treatment replicate per manufacturer's instructions. Library quantity and quality were confirmed using a Qubit 4.0 Fluorometer and 2100 BioAnalyzer system, respectively. Raw Illumina (fastq.qz) sequencing files (12 total) are available via NCBI's BioProject database under BioProject ID PRJNA752134, and a summary of sequencing run metrics are provided in Table S22. All 12 raw and indexed Illumina (fastq.gz) sequencing files were downloaded from Illumina's BaseSpace and uploaded to Bluebee's genomics analysis platform (www.bluebee.com) to align reads against the human genome

(GRCh38/hg38). After combining treatment replicate files, a DESeq2 application within Bluebee (Lexogen Quantseq DE1.4) was used to identify significant treatment-related effects on transcript abundance (relative to vehicle) based on a false discovery rate (FDR) *p*-adjusted value ≤ 0.05. To determine whether differentially expressed genes contained PPREs, we searched for PPRE consensus sequences (AGGTCA) up to 5000 bases upstream of the transcription start site (TSS) using the sequence text view tool within NCBI (https://www.ncbi.nlm.nih.gov).

Statistical analyses

For cell viability, ORO staining, and immunohistochemistry data, a general linear model (GLM) analysis of variance (ANOVA) ($\alpha = 0.05$) was performed using SPSS Statistics 27 (IBM, Armonk, NY, USA), as data did not meet the equal variance assumption for non-GLM ANOVAs. Treatment groups were compared with vehicle controls using pair-wise Tukey based multiple comparisons of least square means to identify significant treatment-specific differences.

4.3 Results

Exposure to TBBPA and TCBPA alone or as binary mixtures decreases cell viability in the absence of effects on neutral lipid and FASN levels

Relative to cells exposed to vehicle (0.1% DMSO) for 24 h, cells exposed to 100 µM TBBPA for 24 h resulted in a significant decrease in cell viability (Figure 19A), whereas exposure to concentrations of TBBPA and TCBPA between 40-100 µM resulted in a slight (albeit non-significant) increase in neutral lipid staining (Figure 19B) and decrease in FASN protein levels (Figure 19C). Following exposure to binary mixtures of TBBPA and TCBPA, cell viability decreased in a concentration-dependent manner (based on the total sum concentration of TBBPA and TCBPA), with significant decreases in cell viability occurring at 90 µM and higher (Figure 20A). However, effects on cell viability occurred in the absence of consistent, concentration-dependent effects on neutral lipid (Figure 20B) and FASN levels (Figure 20C). Since neutral

lipid staining has previously been used as a readout for PPARγ activation (Wakabayashi et al., 2009), ORO was used in subsequent experiments. However, since FASN is not a downstream PPARγ-activated protein, FASN was not used as an endpoint for subsequent experiments.

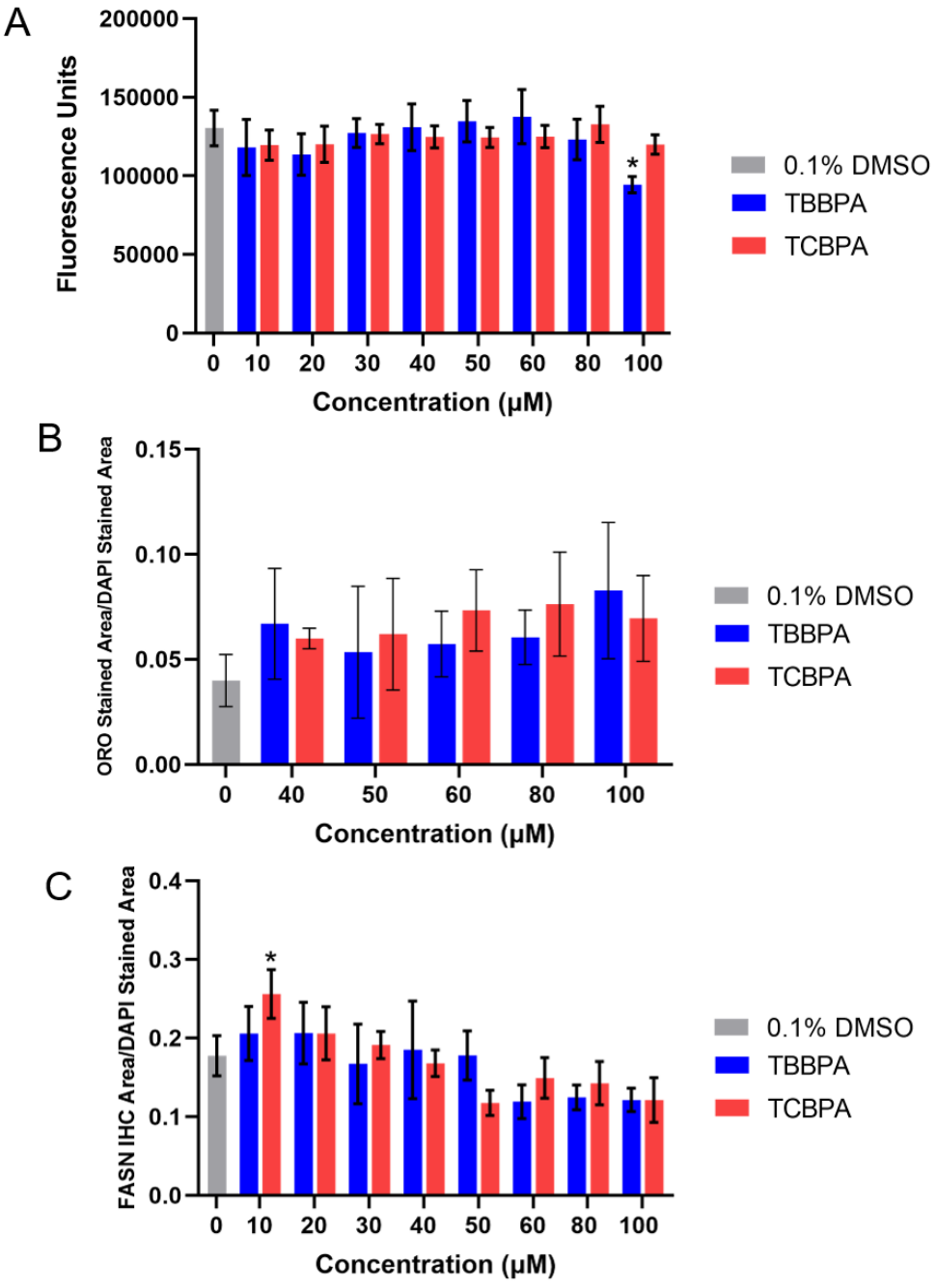

Figure 19. Mean (± standard deviation) fluorescence (cell viability) (A), neutral lipid staining normalized to DAPI staining (B), and fatty acid synthase protein levels normalized to DAPI staining (C) of HepG2 cells exposed to vehicle (0.1% DMSO), 10-100 µM TBBPA, or 10-100 µM TCBPA for 24 h. Asterisk (*) denotes a significant difference ($p<0.05$) relative to vehicle-exposed cells.

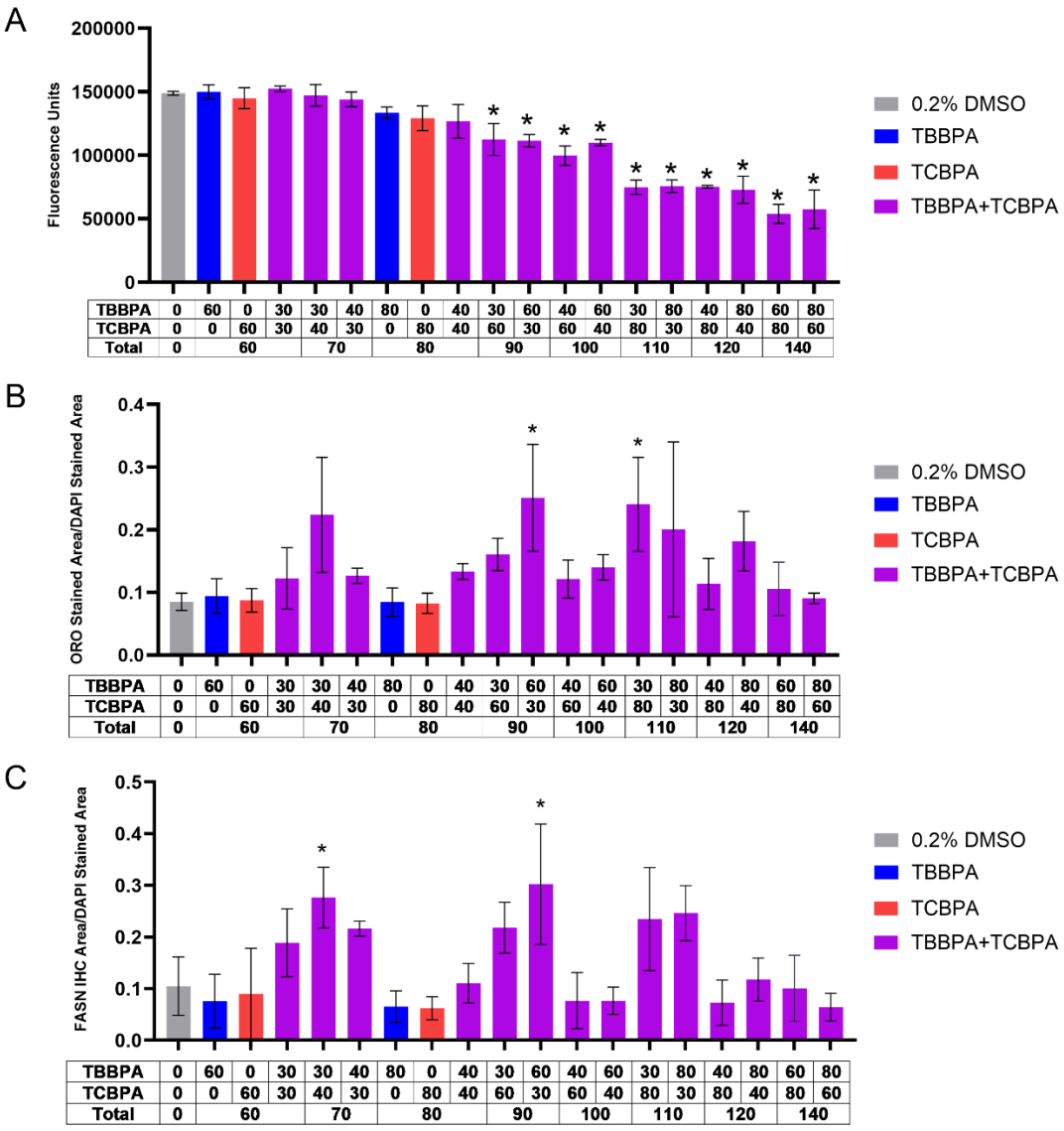

Figure 20. Mean (± standard deviation) fluorescence (cell viability) (A), Oil Red O neutral lipid-stained area divided by DAPI stained area (B), or FASN immunofluorescence area divided by DAPI stained area of HepG2 cells exposed to vehicle (0.2% DMSO) or TBBPA and/or TCBPA for 24 h. Asterisk (*) denotes a significant difference ($p<0.05$) in cell viability, neutral lipid staining, or FASN immunofluorescence relative to vehicle-exposed cells.

Exposure to TBBPA or TCBPA alone or as a mixture enhances the toxic effects of reference PPARγ ligands on cell viability

Pretreatment with ciglitazone alone at 80 µM or higher resulted in a significant decrease in cell viability within all treatment groups. Following pretreatment with 100 µM ciglitazone, exposure to 60 µM TCBPA or 30 µM TBBPA + 60 µM TCBPA resulted in a significant decrease in cell viability relative to vehicle (0.2% DMSO) and 100 µM ciglitazone alone even though exposure to 60 µM TCBPA or 30 µM TBBPA + 60 µM TCBPA alone did not affect cell viability relative to vehicle-treated cells (Figure 21A). Moreover, exposure to 30 µM TBBPA or 30 µM TCBPA resulted in a significant decrease in cell viability relative to vehicle (0.2% DMSO) and GW 9662 alone even though GW 9662 alone did not affect cell viability at all concentrations tested (Figure 21B). However, pretreatment with ciglitazone or GW 9662 did not consistently enhance nor mitigate the effects on neutral lipid levels after TBBPA or TCBPA exposure (Figure 21C and 21D).

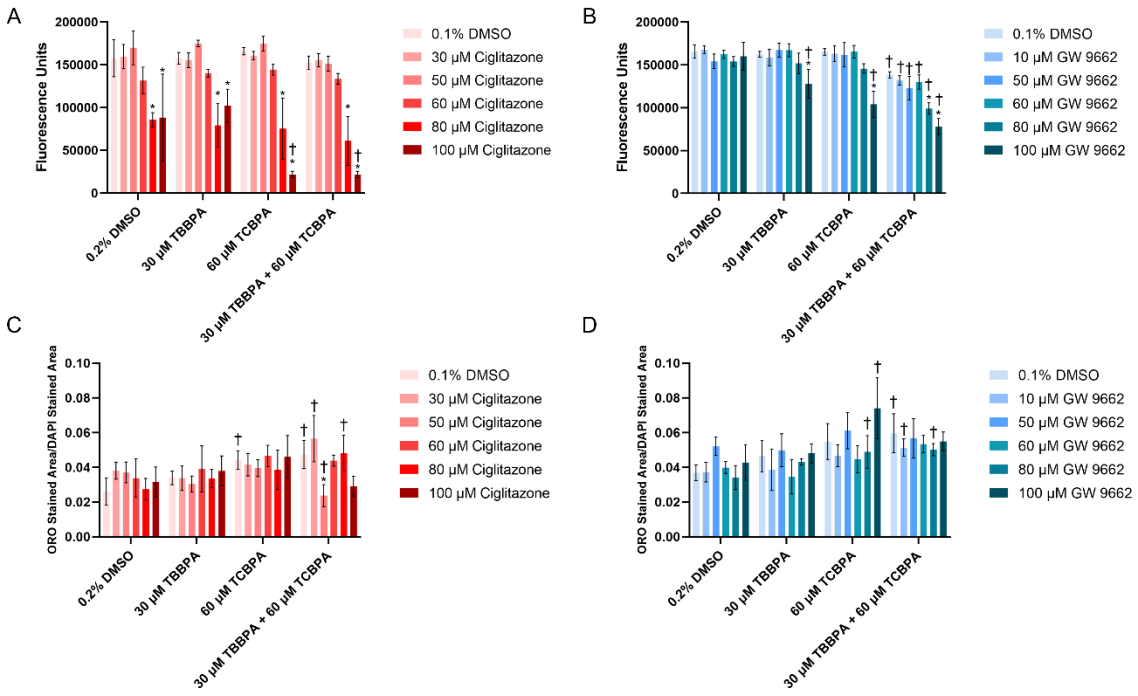

Figure 21. Mean (± standard deviation) fluorescence (cell viability) (A, B) or Oil Red O neutral lipid staining normalized to DAPI stained area (C, D) of HepG2 cells after 24 h pretreatment with ciglitazone or GW 9662 followed by exposure to vehicle (0.2% DMSO), 30 µM TBBPA, 60 µM TCBPA, or 30 µM TBBPA+60 µM TCBPA for 24 h. Asterisk (*) denotes a significant PPARγ ligand-driven difference ($p<0.05$) in cell viability or neutral lipid staining relative to vehicle (0.1% DMSO)-pretreated cells. Cross (†) denotes a significant TBBPA- and/or TCBPA-driven difference ($p<0.05$) in cell viability or neutral lipid staining relative to vehicle (0.2% DMSO)-exposed cells pretreated with the same PPARγ ligand concentration.

Relative to TCBPA, TBBPA is a more potent PPARγ agonist based on cell-free, competitive binding assays

When comparing available ToxCast assays for TBBPA and TCBPA, both compounds had similar hit rates (active assay endpoint divided by total available assays) within the global, nuclear receptor, and PPARγ data sets (Figure 22A). When comparing the range of AC_{50} values across active assays, TBBPA and TCBPA also had very similar distributions (Figure 22B). Of all ToxCast assays, TBBPA was the most potent (AC_{50} = 0.002 µM) within a cell-free, human-specific PPARγ ligand binding assay (NVS_NR_hPPARg), whereas the AC_{50} for TCBPA was

1.83 µM based on the same assay. AC_{50} values for all other available PPARγ assays were similar between TBBPA and TCBPA (Figure 22C).

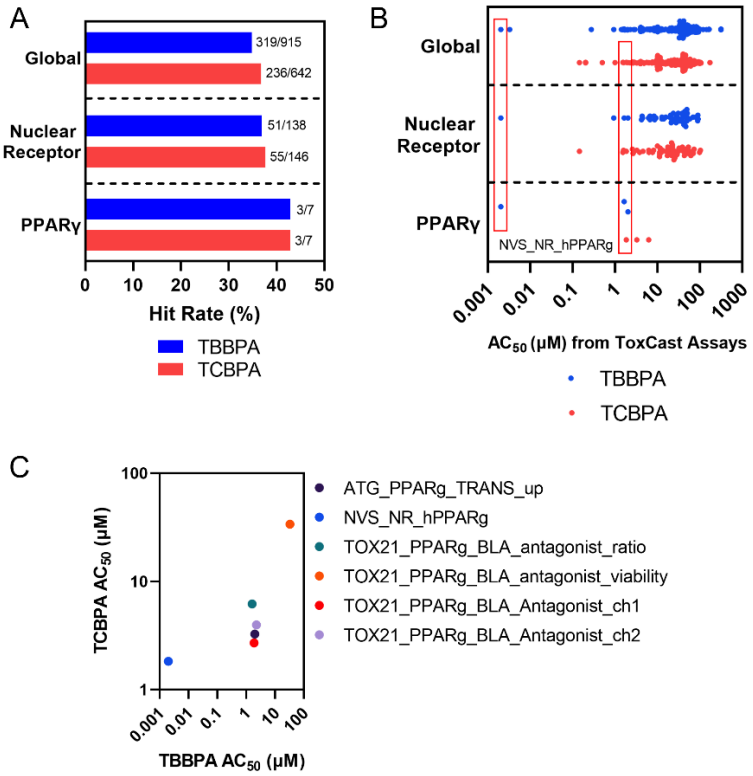

Figure 22. Hit rate (A) and summary statistics (B) based on AC_{50} values for TBBPA and TCBPA screened within ToxCast. AC_{50} values based on the "NVS_NR_PPARg" assay are boxed in red for both TBBPA and TCBPA. Correlation plot mapping AC_{50} values for TBBPA vs. TCBPA based on active hits within PPARγ-related ToxCast assays (C).

Transfection with a PPARγ expression plasmid increases PPARγ protein levels in situ

As a ToxCast-based human-specific PPARγ ligand binding assay predicted TBBPA to be ~900X more potent relative to TCBPA, we focused on the potential effects of PPARγ overexpression on TBBPA-induced toxicity. A human PPARγ-specific antibody was used to determine whether cells transfected with a PPARγ expression plasmid increased PPARγ protein *in situ* within HepG2 cells. Relative to cells transfected to NC plasmid, PPARγ levels were approximately doubled within PPARγ-transfected cells exposed to either vehicle (0.1% DMSO) or 30 µM TBBPA (Figure 23A). While transfection with Turbofectin 8.0 alone decreased cell

viability, the viability of cells transfected with either NC and PPARγ expression plasmid was not affected across all treatment groups. As expected, exposure to 100 μM TBBPA resulted in significant decrease in cell viability across all transfection groups (Figure 23B). Interestingly, within the vehicle (0.1% DMSO) or 100 μM TBBPA treatment groups, cells transfected with PPARγ expression plasmid slightly increased neutral lipid levels relative to non-transfected cells; however, this effect was not observed following exposure 30 nor 60 μM TBBPA (Figure 23C).

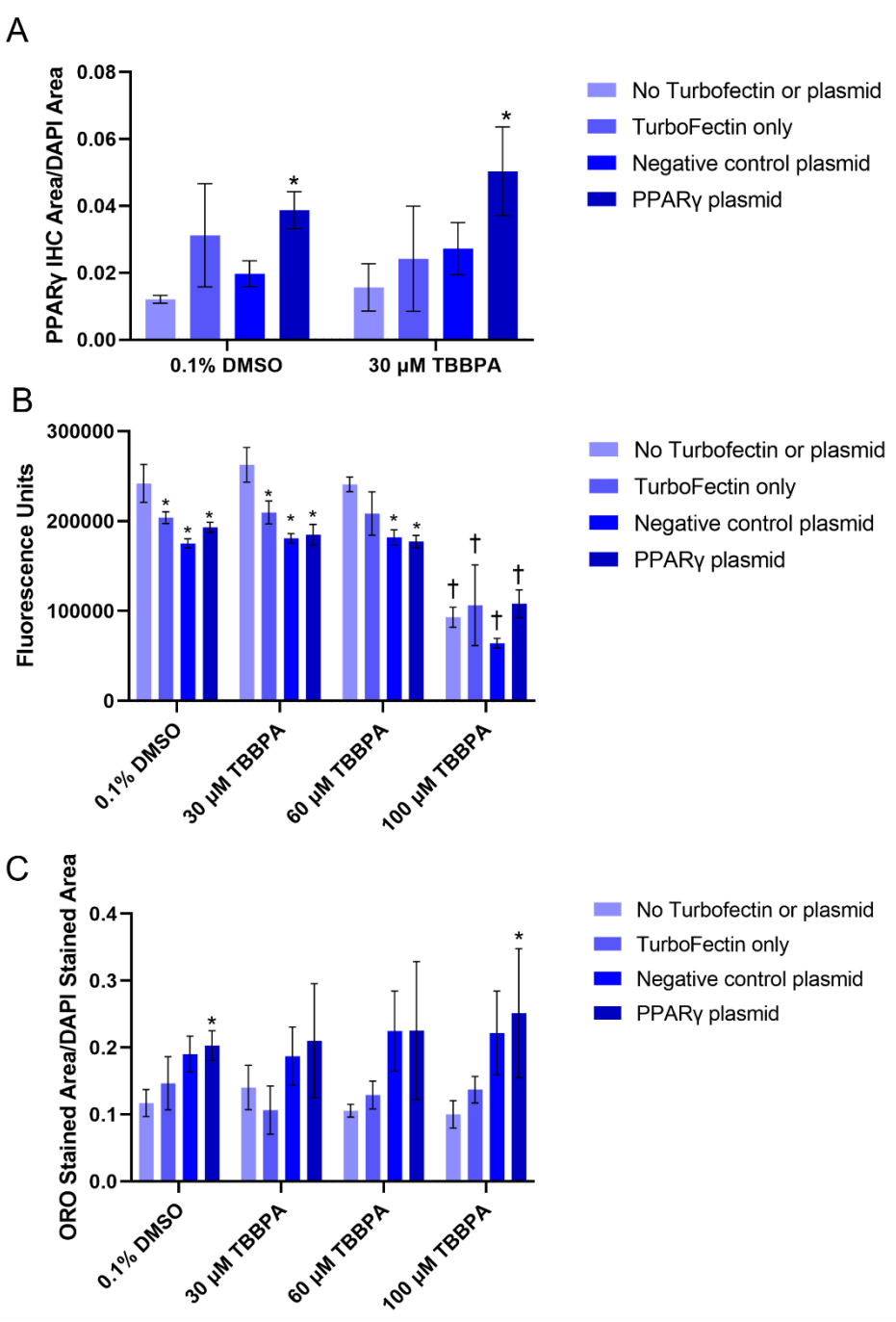

Figure 23. Mean (± standard deviation) of PPARγ immunofluorescence area divided by DAPI stained area (A), fluorescence (B), and Oil Red O neutral lipid staining divided by DAPI stained area (C) of HepG2 cells transfected with either no Turbofection 8.0 or plasmid, Turbofectin 8.0 only, negative control plasmid, or PPARγ expression plasmid and then exposed to either vehicle (0.1% DMSO), 30, 60, or 100 µM TBBPA for 24 h. Asterisk (*) denotes a significant difference ($p<0.05$) in cell viability or neutral lipid staining relative to no Turbofection or plasmid-transfected cells. Cross (†) denotes a significant difference ($p<0.05$) in cell viability or neutral lipid staining relative to vehicle-exposed cells.

TBBPA does not significantly alter the number of differentially expressed genes in cells transfected with PPARγ expression plasmid

Relative to cells transfected with NC plasmid, exposure of cells transfected with PPARγ expression plasmid to vehicle (0.1% DMSO) or 30 μM TBBPA resulted in significant effects on the abundance of four and two transcripts, respectively. Interestingly, growth hormone 1 (GH1) and PPARγ were significantly decreased and increased, respectively, in both groups (Figures 24A and 24B; Table S23 and S24). Relative to vehicle-treated cells, exposure of cells transfected with NC plasmid to 30 μM TBBPA – a concentration that did not affect cell viability – resulted in a significant increase in the abundance of three transcripts (MT-CO1, MT-RNR2, and MT-ATP8), all of which were mitochondrially encoded genes (Figure 24C; Table S25). Relative to vehicle-treated cells, exposure of cells transfected with PPARγ expression plasmid to 30 μM TBBPA resulted in significant effects on the abundance of five transcripts – HNRNPA0, DHRS2, GDF15, FGA, and PTMA (Figure 24D; Table S26). Of the transcripts that were significantly affected across all four comparisons, there were 1-4 PPRE consensus sequences within 5000 bases upstream of the respective TSS within corresponding genes, whereas mitochondrially encoded genes did not have any PPREs within 5000 bases upstream of the respective TSS (Table 1).

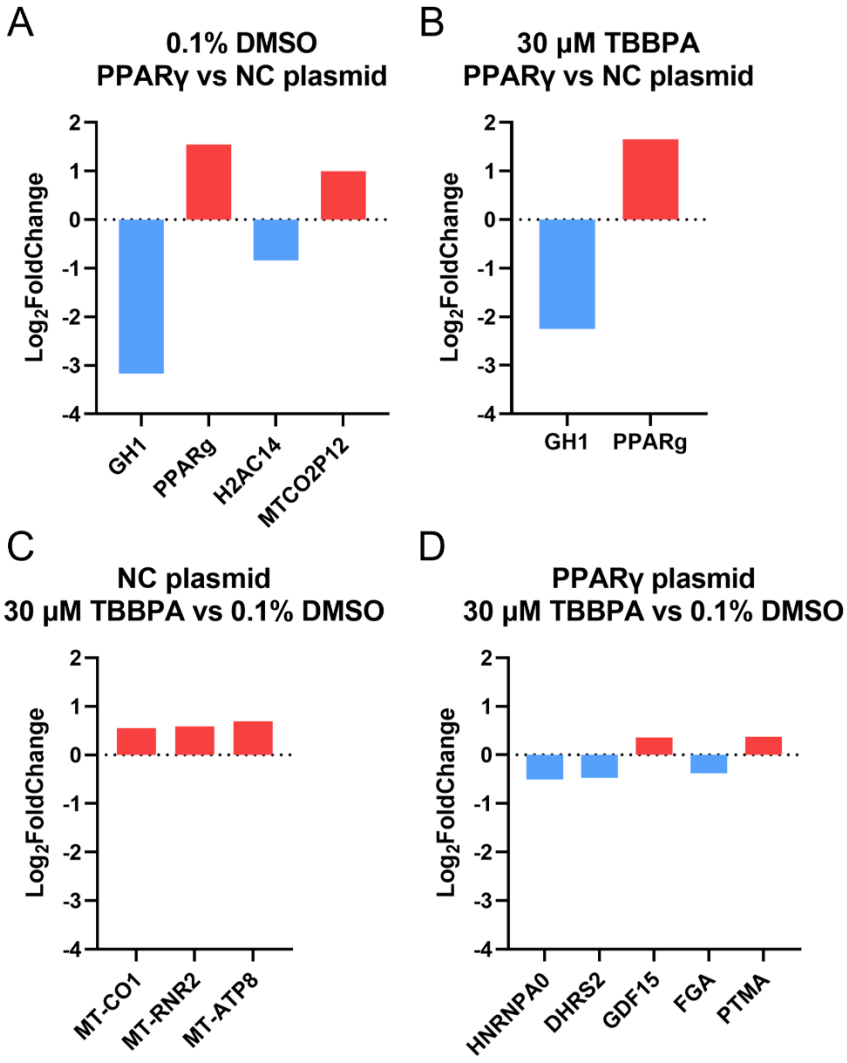

Figure 24. Significantly affected transcripts for cells transfected with negative control (NC) plasmid transfected cells or PPARγ plasmid transfected cells and then exposed to vehicle (0.1% DMSO) or 30 µM TBBPA. Panels A and B are based on within-treatment group comparisons relative to NC plasmid, whereas Panels C and D are based on within-transfection group comparisons relative to vehicle-exposed cells.

Table 1. Number of PPREs within 5000 base pairs upstream of the transcription start site for differentially expressed genes.

Gene Name	Gene Symbol	Number of PPREs
Mitochondrially encoded cytochrome c oxidase 1	MT-CO1	0
Mitochondrially encoded 16s rRNA	MT-RNR2	0
Mitochondrially encoded ATP synthase membrane subunit 8	MT-ATP8	0
Heterogeneous nuclear ribonucleoprotein A0	HNRNPA0	4
Dehydrogenase reductase 2	DHRS2	4
Growth differentiation factor 15	GDF15	3
Fibrinogen alpha chain	FGA	1
Prothymosin alpha	PTMA	2
Growth hormone 1	GH1	1
Peroxisome Proliferator activated Receptor Gamma	PPARγ	2
H2A clustered histone 14	H2AC14	1
MT-CO2 pseudogene 12	MTCO2P12	0

4.4 Discussion

Cell-based studies using TBBPA have previously identified cytotoxic (LC_{50}) concentrations ranging from 21 µM in mouse TM4 Sertoli cells (Ogunbayo et al., 2008) to 200 µM in Cal-62 human thyroid cells (Strack et al., 2007). Likewise, following a 24-h exposure, TBBPA and TCBPA are cytotoxic in mouse embryonic stem cells at 150 and 200 µM, respectively (Yin et al., 2018). Within this study, we found that TBBPA and TCBPA (either alone or as binary mixtures) induce cytotoxicity within HepG2 cells within a similar range of concentrations. When cells were exposed to binary mixtures of TBBPA and TCBPA, cell viability decreased in a concentration-dependent manner based on the total sum concentration of TBBPA and TCBPA, suggesting that these effects were driven by simple additive toxicity. Interestingly, based on pretreatment experiments with reference PPARγ ligands (ciglitazone and GW 9662), we found that TCBPA enhanced the cytotoxic effects of ciglitazone whereas exposure

to GW 9662 and TBBPA or TCBPA resulted in synergistic toxicity (based on cell viability) relative to cells exposed to GW 9662, TBBPA or TCBPA alone. However, overexpression of PPARγ did not alter TBBPA-induced cytotoxicity, suggesting that the cytotoxic effects of halogenated BPA analogues within HepG2 cells may be PPARγ-independent.

To determine whether TBBPA or TCBPA exposure resulted in effects on lipid homeostasis, ORO neutral lipid staining was used to quantify potential changes in neutral lipid abundance. Neutral lipid staining by ORO has previously been linked to PPARγ activation and activity during 3T3-L1 adipocyte differentiation (Wakabayashi et al., 2009). While reliable and reproducible within adipocytes that express greater levels of PPARγ relative to hepatocytes (Elbrecht et al., 1996), neutral lipid staining by ORO appears to lack sensitivity in HepG2 cells, as PPARγ reference ligands (ciglitazone and GW 9662) only alter neutral lipid abundance at higher concentrations (>100 μM) (Cheng et al., 2021). As a result, pretreatment with ciglitazone and GW 9662 did not enhance nor mitigate TBBPA- or TCBPA-induced effects on neutral lipid abundance. However, we found that overexpression of PPARγ within HepG2 cells increased neutral lipid staining, suggesting that PPARγ transfection in combination with ORO staining may enable HepG2 cells to be a more sensitive model system for PPARγ activation using neutral lipid abundance as a readout.

While FASN activity has been shown to be strongly correlated to PPARγ mRNA levels in adipocytes (Schmid et al., 2005), exposure to TBBPA and TCBPA (either alone or as binary mixtures) did not increase FASN protein levels in a concentration-dependent manner within HepG2 cells. Additionally, TBBPA did not result in differential expression of the FASN transcript based on our mRNA-seq data, further confirming that FASN transcription was not affected by exposure to TBBPA and TCBPA. Since FASN inhibitors are able to reduce PPARγ mRNA levels (Schmid et al., 2005), this suggests that FASN activity is upstream of PPARγ and

may explain the lack of response of TBBPA and TCBPA within HepG2 cells, as we would expect downstream (rather than upstream) responses to be altered following PPARγ ligand activation.

While TBBPA has been shown in several ToxCast assays to activate PPARγ with relatively strong potency, we found no evidence of PPARγ activation at the transcriptional-level following TBBPA exposure. Despite using a lower concentration of TBBPA to minimize possible off-target effects, we were unable to detect significant PPARγ-related transcriptional effects even after overexpression of PPARγ. Instead, we found that TBBPA may target mitochondria pathways since mitochondrially encoded genes were the only significantly altered transcripts within TBBPA- vs. vehicle-exposed cells transfected with the NC plasmid. These findings are consistent with previous studies that have shown that TBBPA exposure to L02 human hepatocytes increased reactive oxygen species, induced mitochondrial apoptosis, and altered transcripts related to oxidative stress within the Nrf2 pathway (Zhang et al., 2019). Within cells transfected with PPARγ expression plasmid, exposure to TBBPA resulted in significant effects on the abundance of five transcripts (HNRNPA0, DHRS2, GDF15, FGA, and PTMA), all of which have at least at least one PPRE consensus sequence within 5000 bases upstream of the TSS. Of these transcripts, DHRS2 is part of the short-chain dehydrogenase reductase enzyme family involved in the metabolism of steroids, prostaglandins, lipids, and xenobiotics (Gabrielli et al., 1995). However, no studies have found any of these transcripts to be directly regulated by PPARγ.

Overall, our study found that, while TBBPA and TCBPA affected cell viability to a similar degree and in an additive manner, TBBPA and TCBPA did not significantly affect FASN protein levels or neutral lipid abundance in a PPARγ-dependent manner. Moreover, TBBPA and TCBPA enhanced the toxic effects of reference PPARγ ligands on cell viability, but neither compound had effects on downstream neutral lipid abundance after reference PPARγ ligand

pretreatment. Although ToxCast assays identified PPARγ as a target for TBBPA and previous studies have confirmed TBBPA binding within *in vitro* studies, we were unable to link TBBPA-induced effects on the transcriptome to PPARγ-dependent downstream effects even after overexpression of PPARγ. Therefore, further studies are needed to identify other targets or mechanisms of action for TBBPA and TCBPA within intact cells.

Chapter 5: Summary and Conclusions

5.1 Summary

As the use of chemicals continues to increase, there is a need to identify their mechanisms of action quickly and efficiently to determine potential health effects and risks associated with exposure to these chemicals. By understanding the changes that are occurring at the molecular and cellular levels, we can further prioritize these compounds for more in-depth analysis of their toxicity and assess their risk to public and environmental health. Nuclear receptors, which are important regulators of gene transcription and subsequent downstream protein expression, are common targets for xenobiotics and have the potential to alter cellular and tissue function within organisms. As PPARγ is known to regulate lipid homeostasis and fatty acid metabolism, it is important to understand the alterations to the lipid profile of a cell under xenobiotic stress. Therefore, while several studies have already elucidated some of the effects of PPARγ activation, more information is needed to understand the role of PPARγ during early stages of development and the more detailed steps between PPARγ binding to DNA and corresponding alterations to lipid levels within cellular systems.

The findings and data presented in this dissertation 1) demonstrates off-target developmental effects of a human PPARγ target compound, 2) identifies systems-level alterations after treatment with PPARγ reference compounds, and 3) tests halogenated bisphenol A analogues for their potential to alter downstream effects of PPARγ activation. With regards to PPARγ effects during development, the data presented in Chapter 2 demonstrates that ciglitazone induces dorsoventral patterning defects in zebrafish embryos independently of PPARγ. Regarding systems-level effects of reference PPARγ chemicals, ciglitazone and GW 9662, in Chapter 3, we identify changes at various levels of organization, and found that alterations at one level of organization were not predictive of changes at other levels. Finally, in Chapter 4, we

demonstrated that TBBPA and TCBPA did not impact downstream endpoints of PPARγ. Overall, these data highlight the developmental effects and systems-level effects of a PPARγ agonist, as well as the effects of two xenobiotics on PPARγ.

5.2 The role of PPARγ during Embryonic Development

During early stages of development, zebrafish embryos rely on a lipid-rich yolk sac as their main source of energy and nutrients to support this rapid period of growth. As PPARγ is responsible for regulating lipid homeostasis, in Chapter 2, we aimed to understand the role of PPARγ during early stages of development using ciglitazone as a reference PPARγ agonist and a PPARγ morpholino to knock down PPARγ expression. We found that zebrafish embryo exposure to ciglitazone during early developmental stages resulted in dorsoventral patterning defects, namely ventralization of embryos, by 24 hpf. Dorsomorphin, a BMP signaling inhibitor, was able to mitigate phenotypic dorsoventral patterning defects induced by ciglitazone, but phosphoSMAD staining revealed that ciglitazone did not impact BMP signaling. The dorsoventral patterning effects of ciglitazone persisted despite knock down of PPARγ, suggesting that these effects are independent of PPARγ. By utilizing mRNA-sequencing, we identified several lipid- and cholesterol-related transcripts and pathways that were significantly impacted by ciglitazone exposure. This suggests that ciglitazone may be impacting other targets responsible for lipid homeostasis during early stages of development. Future studies are needed to 1) identify other targets of ciglitazone within zebrafish and 2) further understand the role PPARγ may play during early developmental stages.

5.3 Cellular Systems-Levels Alterations of PPARγ

As PPARγ is a nuclear receptor that regulates the transcription of genes involved in lipid metabolism and homeostasis, we hypothesized that agonism or antagonism of PPARγ by ciglitazone and GW 9662, respectively, would result in downstream alterations to target gene

expression and subsequent lipid substrates. Therefore, within Chapter 3, our aim was to simultaneously characterize changes to PPARγ binding to the genome, transcriptome, and lipidome within a human cell-based model. As PPARγ is expressed in liver tissue, we relied on human hepatocellular carcinoma, HepG2, cells to accomplish this aim. Our research demonstrated that PPARγ activation or inactivation at the maximum tolerated concentrations of ciglitazone and GW 9662 did not significantly alter PPARγ binding to response elements within the genome. We identified the majority of PPARγ binding sites within intron and distal intergenic regions, instead of promoter regions, suggesting that PPARγ may have additional roles aside from its well-studied role as a nuclear receptor.

At the transcriptomic level, despite having opposing effects on PPARγ activity, we found that ciglitazone and GW 9662 altered a similar magnitude of transcripts in a similar manner (i.e. transcripts that were increased by ciglitazone were also increased by GW 9662). By comparing transcripts that were oppositely affected by ciglitazone and GW 9662, transcripts within the cholesterol biosynthetic pathway were altered, suggesting that cholesterol biosynthesis may be regulated by PPARγ within HepG2 cells. At the lipidomic level, ciglitazone altered the abundance of several lipid classes, while GW 9662 altered the abundance of only two classes. As we would predict that cholesterol and other sterol esters levels would be lowered based on decreased cholesterol-related transcripts, we found that they were increased, suggesting that other mechanisms, aside from transcriptomic changes, may be regulating lipid levels within the cell.

While we were able to identify changes at the genomic, transcriptomic, and lipidomic levels after exposure to ciglitazone and GW 9662, we were not able use the results at one level of organization to predict changes to other levels. These findings suggest that there may be other regulatory mechanisms involved between PPARγ activation and binding to the genome, transcription of genes, translation of proteins, and protein activity on lipid substrates to explain

the discrepancies found within the data presented in Chapter 3. Furthermore, as we were limited in our ability to test multiple time points, changes in genomic, transcriptomic, or lipidomic results may be due to time delays between PPARγ activation and downstream results. Based on the findings and limitations of our results, further studies are needed to 1) identify other potential roles of PPARγ, 2) understand additional layers of regulation that may be occurring between nuclear receptor binding to DNA and protein activity on lipid substrates, and 3) determine delays between PPARγ activation and downstream systems-level effects.

5.4 TBBPA and TCBPA as xenobiotic PPARγ agonists

Tetrabromobisphenol A (TBBPA) and tetrachlorobisphenol A (TCBPA), two halogenated bisphenol A analogues, are used as flame retardants and have been shown to bind to PPARγ within *in vitro*, cell free studies. In Chapter 4, we aimed to determine whether TBBPA or TCBPA exposure to HepG2 cells resulted in alterations to downstream PPARγ endpoints. While TBBPA and TCBPA decreased cell viability in an additive manner, neither chemical significantly impacted neutral lipid staining levels or fatty acid synthase (FASN) protein levels. Based on results in Chapter 3 which revealed that GW 9662 decreased PPARγ protein levels within the cells, we used ciglitazone and GW 9662 to pretreat HepG2 cells prior to exposure to TBBPA or TCBPA and found that TBBPA and TCBPA exposure enhanced the toxicity of either reference compound but did not significantly alter neutral lipid levels.

As PPARγ levels within liver cells are lower compared to adipocytes, we transfected cells with a PPARγ expression plasmid to increase the levels of PPARγ within HepG2 cells. Transcript analysis and PPARγ immunostaining confirmed that PPARγ levels were elevated at both the transcript and protein levels after transfection. However, exposure to TBBPA did not result in significant alterations to the number of differentially expressed genes and resulted in increased neutral lipid levels at only the highest concentration of TBBPA tested. Taken together, this data

suggests that TBBPA and TCBPA effects are likely PPARγ-independent. Further studies are needed to identify other targets and mechanisms of action of TBBPA and TCBPA within intact cellular systems.

5.5 PPARγ: Further Directions and Considerations

To address growing concerns over animal testing and to bridge species differences between rodents and humans, human cell lines are utilized to identify xenobiotic mechanisms of action. Unlike *in vitro*, cell-free assays, intact cells allow for identification of downstream effects after exposure to xenobiotics. While primary cell lines may better represent cellular processes, running multiple assays and experiments with these cells can become costly. Instead, immortalized human cell lines provide a cost-effective option to understand mechanisms of action. Results from these assays can contribute to the prioritization of chemical testing. However, as expression of proteins and nuclear receptors vary between cell types, it is useful to understand these differences and utilize the most relevant cell models, as not all cells respond similarly to chemical exposure.

As PPARγ is a common target for various xenobiotics and the use of these xenobiotics continues to increase, there is a need to characterize the effects of PPARγ activation. The research conducted within Chapter 2 utilized zebrafish embryos to understand whole organism effects of PPARγ during early stages of development. While we were able to identify dorsoventral patterning defects as a result of PPARγ ligand exposure, future work is needed to understand the role of PPARγ during earlier stages of development as well as other potential targets of ciglitazone within zebrafish embryos. The research conducted in Chapter 3 leveraged a human cell-based model to identify genomic, transcriptomic, and lipidomic changes of PPARγ alterations. While we found alterations at each level of organization, future studies are needed to understand other layers of regulation between nuclear receptor binding to DNA and protein

activity on lipid substrates. Additionally, future work is needed to understand the temporal relationships between nuclear receptor activation, mRNA levels, protein levels, and lipid alterations. Finally, the research conducted in Chapter 4 determined potential xenobiotic effects on PPARγ activation. Although several *in vitro*, cell-free assays identified PPARγ as a target for TBBPA and TCBPA, we did not observe alterations to downstream PPARγ endpoints within HepG2 cells. As a result, future studies are needed to identify other mechanisms of action of TBBPA and TCBPA within intact cellular systems. Taken together, this work contributes to our understanding of the potential role of PPARγ in mediating chemically-induced toxicity.

References

Adams, M., Reginato, M.J., Shao, D., Lazar, M.A., Chatterjee, V.K., 1997. Transcriptional activation by peroxisome proliferator-activated receptor gamma is inhibited by phosphorylation at a consensus mitogen-activated protein kinase site. J. Biol. Chem. 272, 5128–5132. https://doi.org/10.1074/jbc.272.8.5128

Agrawal, R., 2014. The First Approved Agent in the Glitazar's Class: Saroglitazar [WWW Document]. Curr. Drug Targets. URL https://www.eurekaselect.com/113860/article (accessed 8.16.20).

Akiyama, E., Kakutani, H., Nakao, T., Motomura, Y., Takano, Y., Sorakubo, R., Mizuno, A., Aozasa, O., Tachibana, K., Doi, T., Ohta, S., 2015. Facilitation of adipocyte differentiation of 3T3-L1 cells by debrominated tetrabromobisphenol A compounds detected in Japanese breast milk. Environmental Research 140, 157–164. https://doi.org/10.1016/j.envres.2015.03.035

Aoyama, T., Peters, J.M., Iritani, N., Nakajima, T., Furihata, K., Hashimoto, T., Gonzalez, F.J., 1998. Altered Constitutive Expression of Fatty Acid-metabolizing Enzymes in Mice Lacking the Peroxisome Proliferator-activated Receptor α (PPARα). J. Biol. Chem. 273, 5678–5684. https://doi.org/10.1074/jbc.273.10.5678

Auboeuf, D., Rieusset, J., Fajas, L., Vallier, P., Frering, V., Riou, J.P., Staels, B., Auwerx, J., Laville, M., Vidal, H., 1997. Tissue distribution and quantification of the expression of mRNAs of peroxisome proliferator-activated receptors and liver X receptor-alpha in humans: no alteration in adipose tissue of obese and NIDDM patients. Diabetes 46, 1319–1327. https://doi.org/10.2337/diab.46.8.1319

Barak, Y., Nelson, M.C., Ong, E.S., Jones, Y.Z., Ruiz-Lozano, P., Chien, K.R., Koder, A., Evans, R.M., 1999. PPARγ Is Required for Placental, Cardiac, and Adipose Tissue Development. Mol. Cell 4, 585–595. https://doi.org/10.1016/S1097-2765(00)80209-9

Bertrand, S., Thisse, B., Tavares, R., Sachs, L., Chaumot, A., Bardet, P.-L., Escrivà, H., Duffraisse, M., Marchand, O., Safi, R., Thisse, C., Laudet, V., 2007. Unexpected Novel Relational Links Uncovered by Extensive Developmental Profiling of Nuclear Receptor Expression. PLoS Genet. 3. https://doi.org/10.1371/journal.pgen.0030188

Bility, M.T., Thompson, J.T., McKee, R.H., David, R.M., Butala, J.H., Vanden Heuvel, J.P., Peters, J.M., 2004. Activation of mouse and human peroxisome proliferator-activated receptors (PPARs) by phthalate monoesters. Toxicol. Sci. 82, 170–182. https://doi.org/10.1093/toxsci/kfh253

Blitek, A., Szymanska, M., 2019. Expression and role of peroxisome proliferator–activated receptors in the porcine early placenta trophoblast. Domest. Anim. Endocrinol. 67, 42–53. https://doi.org/10.1016/j.domaniend.2018.12.001

Blount, B.C., Silva, M.J., Caudill, S.P., Needham, L.L., Pirkle, J.L., Sampson, E.J., Lucier, G.W., Jackson, R.J., Brock, J.W., 2000. Levels of seven urinary phthalate metabolites in a human reference population. Environ. Health Perspect. 108, 979–982. https://doi.org/10.1289/ehp.00108979

Blumberg, B., Sabbagh, W., Juguilon, H., Bolado, J., van Meter, C.M., Ong, E.S., Evans, R.M., 1998. SXR, a novel steroid and xenobioticsensing nuclear receptor. Genes Dev. 12, 3195–3205.

Braissant, O., Foufelle, F., Scotto, C., Dauça, M., Wahli, W., 1996. Differential expression of peroxisome proliferator-activated receptors (PPARs): tissue distribution of PPAR-alpha, -beta, and -gamma in the adult rat. Endocrinology 137, 354–366. https://doi.org/10.1210/endo.137.1.8536636

Broeckling, C.D., Afsar, F.A., Neumann, S., Ben-Hur, A., Prenni, J.E., 2014. RAMClust: A Novel Feature Clustering Method Enables Spectral-Matching-Based Annotation for Metabolomics Data. Anal. Chem. 86, 6812–6817. https://doi.org/10.1021/ac501530d

Brooks, K.E., Burns, G.W., Spencer, T.E., 2015. Peroxisome Proliferator Activator Receptor Gamma (PPARG) Regulates Conceptus Elongation in Sheep. Biol. Reprod. 92. https://doi.org/10.1095/biolreprod.114.123877

Cano-Sancho, G., Smith, A., La Merrill, M.A., 2017. Triphenyl phosphate enhances adipogenic differentiation, glucose uptake and lipolysis via endocrine and noradrenergic mechanisms. Toxicol. In Vitro 40, 280–288. https://doi.org/10.1016/j.tiv.2017.01.021

Cao, H., Wang, F., Liang, Y., Wang, H., Zhang, A., Song, M., 2017. Experimental and computational insights on the recognition mechanism between the estrogen receptor α with bisphenol compounds. Arch Toxicol 91, 3897–3912. https://doi.org/10.1007/s00204-017-2011-0

Cha, B.S., Ciaraldi, T.P., Carter, L., Nikoulina, S.E., Mudaliar, S., Mukherjee, R., Paterniti, J.R., Henry, R.R., 2001. Peroxisome proliferator-activated receptor (PPAR) gamma and retinoid X receptor (RXR) agonists have complementary effects on glucose and lipid metabolism in human skeletal muscle. Diabetologia 44, 444–452. https://doi.org/10.1007/s001250051642

Chandra, V., Huang, P., Hamuro, Y., Raghuram, S., Wang, Y., Burris, T.P., Rastinejad, F., 2008. Structure of the intact PPAR-γ–RXR-α nuclear receptor complex on DNA. Nature 456, 350–356. https://doi.org/10.1038/nature07413

Chappell, V.A., Janesick, A., Blumberg, B., Fenton, S.E., 2018. Tetrabromobisphenol-A Promotes Early Adipogenesis and Lipogenesis in 3T3-L1 Cells. Toxicological Sciences 166, 332–344. https://doi.org/10.1093/toxsci/kfy209

Chawla, A., Boisvert, W.A., Lee, C.-H., Laffitte, B.A., Barak, Y., Joseph, S.B., Liao, D., Nagy, L., Edwards, P.A., Curtiss, L.K., Evans, R.M., Tontonoz, P., 2001. A PPARγ-LXR-ABCA1 Pathway in Macrophages Is Involved in Cholesterol Efflux and Atherogenesis. Molecular Cell 7, 161–171. https://doi.org/10.1016/S1097-2765(01)00164-2

Chawla, A., Schwarz, E.J., Dimaculangan, D.D., Lazar, M.A., 1994. Peroxisome proliferator-activated receptor (PPAR) gamma: adipose-predominant expression and induction early in adipocyte differentiation. Endocrinology 135, 798–800. https://doi.org/10.1210/en.135.2.798

Chazaud, C., Bouillet, P., Oulad-Abdelghani, M., Dollé, P., 1996. Restricted expression of a novel retinoic acid responsive gene during limb bud dorsoventral patterning and endochondral ossification. Dev. Genet. 19, 66–73. https://doi.org/10.1002/(SICI)1520-6408(1996)19:1<66::AID-DVG7>3.0.CO;2-Z

Cheng, V., Reddam, A., Bhatia, A., Hur, M., Kirkwood, J.S., Volz, D.C., 2021. Utilizing systems biology to reveal cellular responses to peroxisome proliferator-activated receptor γ ligand exposure. Current Research in Toxicology 2, 169–178. https://doi.org/10.1016/j.crtox.2021.03.003

Chiang, C., Litingtung, Y., Lee, E., Young, K.E., Corden, J.L., Westphal, H., Beachy, P.A., 1996. Cyclopia and defective axial patterning in mice lacking Sonic hedgehog gene function. Nature 383, 407. https://doi.org/10.1038/383407a0

Chung, J.-E., Park, J.-H., Yun, J.-W., Kang, Y.-H., Park, B.-W., Hwang, S.-C., Cho, Y.-C., Sung, I.-Y., Woo, D.K., Byun, J.-H., 2016. Cultured Human Periosteum-Derived Cells Can Differentiate into Osteoblasts in a Perioxisome Proliferator-Activated Receptor Gamma-Mediated Fashion via Bone Morphogenetic Protein signaling. Int. J. Med. Sci. 13, 806–818. https://doi.org/10.7150/ijms.16484

Dasgupta, S., Cheng, V., Vliet, S.M.F., Mitchell, C.A., Volz, D.C., 2018. Tris(1,3-dichloro-2-propyl) Phosphate Exposure During the Early-Blastula Stage Alters the Normal Trajectory of Zebrafish Embryogenesis. Environ. Sci. Technol. 52, 10820–10828. https://doi.org/10.1021/acs.est.8b03730

Dasgupta, S., Vliet, S.M., Kupsco, A., Leet, J.K., Altomare, D., Volz, D.C., 2017. Tris(1,3-dichloro-2-propyl) phosphate disrupts dorsoventral patterning in zebrafish embryos. PeerJ 5, e4156. https://doi.org/10.7717/peerj.4156

Dick, A., Hild, M., Bauer, H., Imai, Y., Maifeld, H., Schier, A.F., Talbot, W.S., Bouwmeester, T., Hammerschmidt, M., 2000. Essential role of Bmp7 (snailhouse) and its prodomain in dorsoventral patterning of the zebrafish embryo. Development 127, 343–354.

Dietz, M., Mohr, P., Kuhn, B., Maerki, H.P., Hartman, P., Ruf, A., Benz, J., Grether, U., Wright, M.B., 2012. Comparative Molecular Profiling of the PPARα/γ Activator Aleglitazar: PPAR Selectivity, Activity and Interaction with Cofactors. Chemmedchem 7, 1101–1111. https://doi.org/10.1002/cmdc.201100598

Dirtu, A.C., Roosens, L., Geens, T., Gheorghe, A., Neels, H., Covaci, A., 2008. Simultaneous determination of bisphenol A, triclosan, and tetrabromobisphenol A in human serum using solid-

phase extraction and gas chromatography-electron capture negative-ionization mass spectrometry. Anal Bioanal Chem 391, 1175–1181. https://doi.org/10.1007/s00216-007-1807-9

Dunnick, J.K., Sanders, J.M., Kissling, G.E., Johnson, C., Boyle, M.H., Elmore, S.A., 2015. Environmental chemical exposure may contribute to uterine cancer development: studies with tetrabromobisphenol A. Toxicol. Pathol. 43, 464–473. https://doi.org/10.1177/0192623314557335

Eibl, G., Wente, M.N., Reber, H.A., Hines, O.J., 2001. Peroxisome Proliferator-Activated Receptor γ Induces Pancreatic Cancer Cell Apoptosis. Biochemical and Biophysical Research Communications 287, 522–529. https://doi.org/10.1006/bbrc.2001.5619

El Dairi, R., Huuskonen, P., Pasanen, M., Rysä, J., 2018. Peroxisome proliferator activated receptor gamma (PPAR-γ) ligand pioglitazone regulated gene networks in term human primary trophoblast cells. Reprod. Toxicol. 81, 99–107. https://doi.org/10.1016/j.reprotox.2018.07.077

Elbrecht, A., Chen, Y., Cullinan, C.A., Hayes, N., Leibowitz, M.D., Moller, D.E., Berger, J., 1996. Molecular Cloning, Expression and Characterization of Human Peroxisome Proliferator Activated Receptors γ1 and γ2. Biochemical and Biophysical Research Communications 224, 431–437. https://doi.org/10.1006/bbrc.1996.1044

EPA, 2012. Phthalates ActionPlan - 2012-03-14 16.

Fajas, L., Auboeuf, D., Raspé, E., Schoonjans, K., Lefebvre, A.M., Saladin, R., Najib, J., Laville, M., Fruchart, J.C., Deeb, S., Vidal-Puig, A., Flier, J., Briggs, M.R., Staels, B., Vidal, H., Auwerx, J., 1997. The organization, promoter analysis, and expression of the human PPARgamma gene. J. Biol. Chem. 272, 18779–18789. https://doi.org/10.1074/jbc.272.30.18779

Fernandes-Santos, C., Carneiro, R.E., de Souza Mendonca, L., Aguila, M.B., Mandarim-de-Lacerda, C.A., 2009. Pan-PPAR agonist beneficial effects in overweight mice fed a high-fat high-sucrose diet. Nutrition, 818–827. https://doi.org/10.1016/j.nut.2008.12.010

Forman, B.M., Chen, J., Evans, R.M., 1997. Hypolipidemic drugs, polyunsaturated fatty acids, and eicosanoids are ligands for peroxisome proliferator-activated receptors α and δ. Proc. Natl. Acad. Sci. 94, 4312–4317. https://doi.org/10.1073/pnas.94.9.4312

Forman, B.M., Tontonoz, P., Chen, J., Brun, R.P., Spiegelman, B.M., Evans, R.M., 1995. 15-Deoxy-delta 12, 14-prostaglandin J2 is a ligand for the adipocyte determination factor PPAR gamma. Cell 83, 803–812. https://doi.org/10.1016/0092-8674(95)90193-0

Fürthauer, M., Celst, J.V., Thisse, C., Thisse, B., 2004. Fgf signalling controls the dorsoventral patterning of the zebrafish embryo. Development 131, 2853–2864. https://doi.org/10.1242/dev.01156

Furthauer, M., Thisse, C., Thisse, B., 1997. A role for FGF-8 in the dorsoventral patterning of the zebrafish gastrula. Development 124, 4253–4264. https://doi.org/10.1242/dev.124.21.4253

Gabrielli, F., Donadel, G., Bensi, G., Heguy, A., Melli, M., 1995. A Nuclear Protein, Synthesized in Growth-Arrested Human Hepatoblastoma Cells, is a Novel Member of the Short-Chain Alcohol Dehydrogenase Family. European Journal of Biochemistry 232, 473–477. https://doi.org/10.1111/j.1432-1033.1995.473zz.x

Gavrilova, O., Haluzik, M., Matsusue, K., Cutson, J.J., Johnson, L., Dietz, K.R., Nicol, C.J., Vinson, C., Gonzalez, F.J., Reitman, M.L., 2003. Liver Peroxisome Proliferator-activated Receptor γ Contributes to Hepatic Steatosis, Triglyceride Clearance, and Regulation of Body Fat Mass. J. Biol. Chem. 278, 34268–34276. https://doi.org/10.1074/jbc.M300043200

Ge, K., Guermah, M., Yuan, C.-X., Ito, M., Wallberg, A.E., Spiegelman, B.M., Roeder, R.G., 2002. Transcription coactivator TRAP220 is required for PPAR gamma 2-stimulated adipogenesis. Nature 417, 563–567. https://doi.org/10.1038/417563a

Gilroy, D.W., Colville-Nash, P.R., Willis, D., Chivers, J., Paul-Clark, M.J., Willoughby, D.A., 1999. Inducible cyclooxygenase may have anti-inflammatory properties. Nat. Med. 5, 698–701. https://doi.org/10.1038/9550

Gould, J.C., Leonard, L.S., Maness, S.C., Wagner, B.L., Conner, K., Zacharewski, T., Safe, S., McDonnell, D.P., Gaido, K.W., 1998. Bisphenol A interacts with the estrogen receptor α in a distinct manner from estradiol. Molecular and Cellular Endocrinology 142, 203–214. https://doi.org/10.1016/S0303-7207(98)00084-7

Green, A.J., Graham, J.L., Gonzalez, E.A., La Frano, M.R., Petropoulou, S.-S.E., Park, J.-S., Newman, J.W., Stanhope, K.L., Havel, P.J., La Merrill, M.A., 2017. Perinatal triphenyl phosphate exposure accelerates type 2 diabetes onset and increases adipose accumulation in UCD-type 2 diabetes mellitus rats. Reprod. Toxicol. 68, 119–129. https://doi.org/10.1016/j.reprotox.2016.07.009

Greenstein, A.W., Majumdar, N., Yang, P., Subbaiah, P.V., Kineman, R.D., Cordoba-Chacon, J., 2017. Hepatocyte-specific, PPARγ-regulated mechanisms to promote steatosis in adult mice. J Endocrinol 232, 107–121. https://doi.org/10.1530/JOE-16-0447

Guo, L., Zhang, L., Sun, Y., Muskhelishvili, L., Blann, E., Dial, S., Shi, L., Schroth, G., Dragan, Y.P., 2006. Differences in hepatotoxicity and gene expression profiles by anti-diabetic PPAR γ agonists on rat primary hepatocytes and human HepG2 cells. Mol Divers 10, 349–360. https://doi.org/10.1007/s11030-006-9038-0

Gupta, R.A., Tan, J., Krause, W.F., Geraci, M.W., Willson, T.M., Dey, S.K., DuBois, R.N., 2000. Prostacyclin-mediated activation of peroxisome proliferator-activated receptor δ in colorectal cancer. Proc. Natl. Acad. Sci. 97, 13275–13280. https://doi.org/10.1073/pnas.97.24.13275

Gurnell, M., Savage, D.B., Chatterjee, V.K.K., O'Rahilly, S., 2003. The Metabolic Syndrome: Peroxisome Proliferator-Activated Receptor γ and Its Therapeutic Modulation. J. Clin. Endocrinol. Metab. 88, 2412–2421. https://doi.org/10.1210/jc.2003-030435

Han, L., Zhou, R., Niu, J., McNutt, M.A., Wang, P., Tong, T., 2010. SIRT1 is regulated by a PPAR{γ}-SIRT1 negative feedback loop associated with senescence. Nucleic Acids Res. 38, 7458–7471. https://doi.org/10.1093/nar/gkq609

Hao, C., Cheng, X., Guo, J., Xia, H., Ma, X., 2013. Perinatal exposure to diethyl-hexyl-phthalate induces obesity in mice. Front. Biosci. Elite 5, 725–733. https://doi.org/10.2741/e653

He, W., Barak, Y., Hevener, A., Olson, P., Liao, D., Le, J., Nelson, M., Ong, E., Olefsky, J.M., Evans, R.M., 2003. Adipose-specific peroxisome proliferator-activated receptor knockout causes insulin resistance in fat and liver but not in muscle. Proc. Natl. Acad. Sci. 100, 15712–15717. https://doi.org/10.1073/pnas.2536828100

Hemmati-Brivanlou, A., Kelly, O.G., Melton, D.A., 1994. Follistatin, an antagonist of activin, is expressed in the Spemann organizer and displays direct neuralizing activity. Cell 77, 283–295. https://doi.org/10.1016/0092-8674(94)90320-4

Heyman, R.A., Mangelsdorf, D.J., Dyck, J.A., Stein, R.B., Eichele, G., Evans, R.M., Thaller, C., 1992. 9-cis retinoic acid is a high affinity ligand for the retinoid X receptor. Cell 68, 397–406. https://doi.org/10.1016/0092-8674(92)90479-V

Ho, K.-L., Yuen, K.-K., Yau, M.-S., Murphy, M.B., Wan, Y., Fong, B.M.-W., Tam, S., Giesy, J.P., Leung, K.S.-Y., Lam, M.H.-W., 2017. Glucuronide and sulfate conjugates of tetrabromobisphenol A (TBBPA): Chemical synthesis and correlation between their urinary levels and plasma TBBPA content in voluntary human donors. Environment International 98, 46–53. https://doi.org/10.1016/j.envint.2016.09.018

Högberg, J., Hanberg, A., Berglund, M., Skerfving, S., Remberger, M., Calafat, A.M., Filipsson, A.F., Jansson, B., Johansson, N., Appelgren, M., Håkansson, H., 2008. Phthalate diesters and their metabolites in human breast milk, blood or serum, and urine as biomarkers of exposure in vulnerable populations. Environ. Health Perspect. 116, 334–339. https://doi.org/10.1289/ehp.10788

Holst, D., Luquet, S., Nogueira, V., Kristiansen, K., Leverve, X., Grimaldi, P.A., 2003. Nutritional regulation and role of peroxisome proliferator-activated receptor δ in fatty acid catabolism in skeletal muscle. Biochim. Biophys. Acta BBA - Mol. Cell Biol. Lipids 1633, 43–50. https://doi.org/10.1016/S1388-1981(03)00071-4

Honkakoski, P., Zelko, I., Sueyoshi, T., Negishi, M., 1998. The nuclear orphan receptor CAR-retinoid X receptor heterodimer activates the phenobarbital-responsive enhancer module of the CYP2B gene. Mol. Cell. Biol. 18, 5652–5658. https://doi.org/10.1128/mcb.18.10.5652

Hu, E., Kim, J.B., Sarraf, P., Spiegelman, B.M., 1996. Inhibition of adipogenesis through MAP kinase-mediated phosphorylation of PPARgamma. Science 274, 2100–2103. https://doi.org/10.1126/science.274.5295.2100

Hurst, C.H., Waxman, D.J., 2003. Activation of PPARα and PPARγ by Environmental Phthalate Monoesters. Toxicol Sci 74, 297–308. https://doi.org/10.1093/toxsci/kfg145

IJpenberg, A., Jeannin, E., Wahli, W., Desvergne, B., 1997. Polarity and Specific Sequence Requirements of Peroxisome Proliferator-activated Receptor (PPAR)/Retinoid X Receptor Heterodimer Binding to DNA: A Functional Analysis of the Malic Enzyme Gene PPAR Response Element. J. Biol. Chem. 272, 20108–20117. https://doi.org/10.1074/jbc.272.32.20108

Issemann, I., Green, S., 1990. Activation of a member of the steroid hormone receptor superfamily by peroxisome proliferators. Nature 347, 645–650. https://doi.org/10.1038/347645a0

Jackevicius, C.A., Tu, J.V., Ross, J.S., Ko, D.T., Carreon, D., Krumholz, H.M., 2011. Use of Fibrates in the United States and Canada. JAMA 305, 1217–1224. https://doi.org/10.1001/jama.2011.353

Jakobsson, K., Thuresson, K., Rylander, L., Sjödin, A., Hagmar, L., Bergman, Å., 2002. Exposure to polybrominated diphenyl ethers and tetrabromobisphenol A among computer technicians. Chemosphere 46, 709–716. https://doi.org/10.1016/S0045-6535(01)00235-1

Jiang, X., Ye, X., Guo, W., Lu, H., Gao, Z., 2014. Inhibition of HDAC3 promotes ligand-independent PPARγ activation by protein acetylation. J. Mol. Endocrinol. 53, 191–200. https://doi.org/10.1530/JME-14-0066

Jozkowicz, A., Dulak, J., Nigisch, A., Weigel, G., Sporn, E., Fügl, A., Huk, I., 2002. Ciglitazone, ligand of peroxisome proliferator-activated receptor-γ, inhibits vascular endothelial growth factor activity. Eur. Surg. 34, 127–130. https://doi.org/10.1046/j.1563-2563.2002.02024.x

Kato, K., Silva, M.J., Reidy, J.A., Hurtz, D., Malek, N.A., Needham, L.L., Nakazawa, H., Barr, D.B., Calafat, A.M., 2004. Mono(2-ethyl-5-hydroxyhexyl) phthalate and mono-(2-ethyl-5-oxohexyl) phthalate as biomarkers for human exposure assessment to di-(2-ethylhexyl) phthalate. Environ. Health Perspect. 112, 327–330.

Kawamatsu, Y., Asakawa, H., Saraie, T., Imamiya, E., Nishikawa, K., Hamuro, Y., 1980. Studies on antihyperlipidemic agents. II. Synthesis and biological activities of 2-chloro-3-arylpropionic acids. Arzneimittelforschung. 30, 585–589.

Kim, S.W., Brown, D.J., Jester, J.V., 2019. Transcriptome analysis after PPARγ activation in human meibomian gland epithelial cells (hMGEC). Ocul Surf 17, 809–816. https://doi.org/10.1016/j.jtos.2019.02.003

Kimmel, C.B., Ballard, W.W., Kimmel, S.R., Ullmann, B., Schilling, T.F., 1995. Stages of embryonic development of the zebrafish. Dev. Dyn. 203, 253–310. https://doi.org/10.1002/aja.1002030302

Kind, T., Liu, K.-H., Yup Lee, D., DeFelice, B., Meissen, J.K., Fiehn, O., 2013. LipidBlast - in-silico tandem mass spectrometry database for lipid identification. Nat Methods 10, 755–758. https://doi.org/10.1038/nmeth.2551

Kishimoto, Y., Lee, K.-H., Zon, L., Hammerschmidt, M., Schulte-Merker, S., 1997. The molecular nature of zebrafish swirl: BMP2 function is essential during early dorsoventral patterning. Development 124, 4457-4466. https://doi.org/10.1242/dev.124.22.4457

Kliewer, S.A., Forman, B.M., Blumberg, B., Ong, E.S., Borgmeyer, U., Mangelsdorf, D.J., Umesono, K., Evans, R.M., 1994. Differential expression and activation of a family of murine peroxisome proliferator-activated receptors. Proc. Natl. Acad. Sci. 91, 7355–7359. https://doi.org/10.1073/pnas.91.15.7355

Kliewer, S.A., Lenhard, J.M., Willson, T.M., Patel, I., Morris, D.C., Lehmann, J.M., 1995. A prostaglandin J2 metabolite binds peroxisome proliferator-activated receptor gamma and promotes adipocyte differentiation. Cell 83, 813–819. https://doi.org/10.1016/0092-8674(95)90194-9

Kliewer, S.A., Sundseth, S.S., Jones, S.A., Brown, P.J., Wisely, G.B., Koble, C.S., Devchand, P., Wahli, W., Willson, T.M., Lenhard, J.M., Lehmann, J.M., 1997. Fatty acids and eicosanoids regulate gene expression through direct interactions with peroxisome proliferator-activated receptors and. Proc. Natl. Acad. Sci. 94, 4318–4323. https://doi.org/10.1073/pnas.94.9.4318

Kliewer, S.A., Umesono, K., Noonan, D.J., Heyman, R.A., Evans, R.M., 1992. Convergence of 9-cis retinoic acid and peroxisome proliferator signalling pathways through heterodimer formation of their receptors. Nature 358, 771–774. https://doi.org/10.1038/358771a0

Kliewer, S.A., Xu, H.E., Lambert, M.H., and Willson, T.M., 2001. Peroxisome Proliferator-Activated Receptors: From Genes to Physiology. Recent Pro. Horm. Res. 56, 239–265. https://doi.org/10.1210/rp.56.1.239

Kubota, N., Terauchi, Y., Miki, H., Tamemoto, H., Yamauchi, T., Komeda, K., Satoh, S., Nakano, R., Ishii, C., Sugiyama, T., Eto, K., Tsubamoto, Y., Okuno, A., Murakami, K., Sekihara, H., Hasegawa, G., Naito, M., Toyoshima, Y., Tanaka, S., Shiota, K., Kitamura, T., Fujita, T., Ezaki, O., Aizawa, S., Kadowaki, T., 1999. PPAR gamma mediates high-fat diet-induced adipocyte hypertrophy and insulin resistance. Mol. Cell 4, 597–609. https://doi.org/10.1016/s1097-2765(00)80210-5

Kumar, S., Boulton, A.J., Beck-Nielsen, H., Berthezene, F., Muggeo, M., Persson, B., Spinas, G.A., Donoghue, S., Lettis, S., Stewart-Long, P., 1996. Troglitazone, an insulin action enhancer,

improves metabolic control in NIDDM patients. Troglitazone Study Group. Diabetologia 39, 701–709. https://doi.org/10.1007/BF00418542

Lalwani, N.D., Kumudavalli Reddy, M., Qureshi, S.A., Sirtori, C.R., Abiko, Y., Reddy, J.K., 1983. Evaluation of Selected Hypolipidemic Agents for the Induction of Peroxisomal Enzymes and Peroxisome Proliferation in the Rat Liver. Hum. Toxicol. 2, 27–48. https://doi.org/10.1177/096032718300200103

Lee, C.-H., Olson, P., Hevener, A., Mehl, I., Chong, L.-W., Olefsky, J.M., Gonzalez, F.J., Ham, J., Kang, H., Peters, J.M., Evans, R.M., 2006. PPARδ regulates glucose metabolism and insulin sensitivity. Proc. Natl. Acad. Sci. 103, 3444–3449. https://doi.org/10.1073/pnas.0511253103

Lee, H.K., Kim, T.S., Kim, C.Y., Kang, I.H., Kim, M.G., Kyung Jung, K., Kim, H.S., Han, S.Y., Yoon, H.J., Rhee, G.S., 2012. Evaluation of *in vitro* screening system for estrogenicity: comparison of stably transfected human estrogen receptor-α transcriptional activation (OECD TG455) assay and estrogen receptor (ER) binding assay. J. Toxicol. Sci. 37, 431–437. https://doi.org/10.2131/jts.37.431

Lee, Y.J., Ko, E.H., Kim, J.E., Kim, E., Lee, H., Choi, H., Yu, J.H., Kim, H.J., Seong, J.-K., Kim, K.-S., Kim, J., 2012. Nuclear receptor PPARγ-regulated monoacylglycerol O-acyltransferase 1 (MGAT1) expression is responsible for the lipid accumulation in diet-induced hepatic steatosis. Proc. Natl. Acad. Sci. U. S. A. 109, 13656–13661. https://doi.org/10.1073/pnas.1203218109

Leesnitzer, L.M., Parks, D.J., Bledsoe, R.K., Cobb, J.E., Collins, J.L., Consler, T.G., Davis, R.G., Hull-Ryde, E.A., Lenhard, J.M., Patel, L., Plunket, K.D., Shenk, J.L., Stimmel, J.B., Therapontos, C., Willson, T.M., Blanchard, S.G., 2002. Functional Consequences of Cysteine Modification in the Ligand Binding Sites of Peroxisome Proliferator Activated Receptors by GW9662. Biochemistry 41, 6640–6650. https://doi.org/10.1021/bi0159581

Lefterova, M.I., Steger, D.J., Zhuo, D., Qatanani, M., Mullican, S.E., Tuteja, G., Manduchi, E., Grant, G.R., Lazar, M.A., 2010. Cell-specific determinants of peroxisome proliferator-activated receptor gamma function in adipocytes and macrophages. Mol. Cell. Biol. 30, 2078–2089. https://doi.org/10.1128/MCB.01651-09

Lefterova, M.I., Zhang, Y., Steger, D.J., Schupp, M., Schug, J., Cristancho, A., Feng, D., Zhuo, D., Stoeckert, C.J., Liu, X.S., Lazar, M.A., 2008. PPAR and C/EBP factors orchestrate adipocyte biology via adjacent binding on a genome-wide scale. Genes & Development 22, 2941–2952. https://doi.org/10.1101/gad.1709008

Lehmann, J.M., Moore, L.B., Smith-Oliver, T.A., Wilkison, W.O., Willson, T.M., Kliewer, S.A., 1995. An Antidiabetic Thiazolidinedione Is a High Affinity Ligand for Peroxisome Proliferator-activated Receptor γ (PPARγ). J. Biol. Chem. 270, 12953–12956. https://doi.org/10.1074/jbc.270.22.12953

Leisewitz, A., Kruse, H., Schramm, E. 2001. Substituting environmentally relevant flame retardants: Assessment fundamentals. Federal Environmental Agency Umweltbundesamt, Berlin Postfach 33 00 22 14191.

Lennon, A.M., Ramaugé, M., Dessouroux, A., Pierre, M., 2002. MAP Kinase Cascades Are Activated in Astrocytes and Preadipocytes by 15-Deoxy-Δ12–14-prostaglandin J2 and the Thiazolidinedione Ciglitazone through Peroxisome Proliferator Activator Receptor γ-independent Mechanisms Involving Reactive Oxygenated Species*. Journal of Biological Chemistry 277, 29681–29685. https://doi.org/10.1074/jbc.M201517200

Leporcq, C., Spill, Y., Balaramane, D., Toussaint, C., Weber, M., Bardet, A.F., 2020. TFmotifView: a webserver for the visualization of transcription factor motifs in genomic regions. Nucleic Acids Res 48, W208–W217. https://doi.org/10.1093/nar/gkaa252

Lewis, J.D., Ferrara, A., Peng, T., Hedderson, M., Bilker, W.B., Quesenberry, C.P., Vaughn, D.J., Nessel, L., Selby, J., Strom, B.L., 2011. Risk of Bladder Cancer Among Diabetic Patients Treated With Pioglitazone: Interim report of a longitudinal cohort study. Diabetes Care 34, 916–922. https://doi.org/10.2337/dc10-1068

Li, D., Zhang, F., Zhang, X., Xue, C., Namwanje, M., Fan, L., Reilly, M.P., Hu, F., Qiang, L., 2016. Distinct functions of PPARγ isoforms in regulating adipocyte plasticity. Biochem. Biophys. Res. Commun. 481, 132–138. https://doi.org/10.1016/j.bbrc.2016.10.152

Lin, T.-H., Yang, R.-S., Tang, C.-H., Lin, C.-P., Fu, W.-M., 2007. PPARγ inhibits osteogenesis via the down-regulation of the expression of COX-2 and iNOS in rats. Bone 41, 562–574. https://doi.org/10.1016/j.bone.2007.06.017

Liu, Y., Qu, K., Hai, Y., Zhao, C., 2018. Bisphenol A (BPA) binding on full-length architectures of estrogen receptor. Journal of Cellular Biochemistry 119, 6784–6794. https://doi.org/10.1002/jcb.26872

Lyles, B.E., Akinyeke, T.O., Moss, P.E., Stewart, L.V., 2009. Thiazolidinediones regulate expression of cell cycle proteins in human prostate cancer cells via PPARγ-dependent and PPARγ-independent pathways. Cell Cycle 8, 268–277. https://doi.org/10.4161/cc.8.2.7584

Madeira, F., Park, Y.M., Lee, J., Buso, N., Gur, T., Madhusoodanan, N., Basutkar, P., Tivey, A.R.N., Potter, S.C., Finn, R.D., Lopez, R., 2019. The EMBL-EBI search and sequence analysis tools APIs in 2019. Nucleic Acids Res. https://doi.org/10.1093/nar/gkz268

Maloney, E.K., Waxman, D.J., 1999. trans-Activation of PPARalpha and PPARgamma by structurally diverse environmental chemicals. Toxicol. Appl. Pharmacol. 161, 209–218. https://doi.org/10.1006/taap.1999.8809

Martens, F.M.A.C., Visseren, F.L.J., Lemay, J., de Koning, E.J.P., Rabelink, T.J., 2002. Metabolic and Additional Vascular Effects of Thiazolidinediones. Drugs 62, 1463–1480. https://doi.org/10.2165/00003495-200262100-00004

Martin, G., Schoonjans, K., Lefebvre, A.-M., Staels, B., Auwerx, J., 1997. Coordinate Regulation of the Expression of the Fatty Acid Transport Protein and Acyl-CoA Synthetase Genes by

PPARα and PPARγ Activators. J. Biol. Chem. 272, 28210–28217. https://doi.org/10.1074/jbc.272.45.28210

Martin, G., Schoonjans, K., Staels, B., Auwerx, J., 1998. PPARγ activators improve glucose homeostasis by stimulating fatty acid uptake in the adipocytes. Atherosclerosis 137, S75–S80. https://doi.org/10.1016/S0021-9150(97)00315-8

Matsusue, K., Haluzik, M., Lambert, G., Yim, S.-H., Gavrilova, O., Ward, J.M., Brewer, B., Reitman, M.L., Gonzalez, F.J., 2003. Liver-specific disruption of PPARγ in leptin-deficient mice improves fatty liver but aggravates diabetic phenotypes. J. Clin. Invest. 111, 737–747. https://doi.org/10.1172/JCI17223

McGee, S.P., Konstantinov, A., Stapleton, H.M., Volz, D.C., 2013. Aryl Phosphate Esters Within a Major PentaBDE Replacement Product Induce Cardiotoxicity in Developing Zebrafish Embryos: Potential Role of the Aryl Hydrocarbon Receptor. Toxicol. Sci. 133, 144–156. https://doi.org/10.1093/toxsci/kft020

Meex, S.J.R., Andreo, U., Sparks, J.D., Fisher, E.A., 2011. Huh-7 or HepG2 cells: which is the better model for studying human apolipoprotein-B100 assembly and secretion? J. Lipid Res. 52, 152–158. https://doi.org/10.1194/jlr.D008888

Michalik, L., Desvergne, B., Tan, N.S., Basu-Modak, S., Escher, P., Rieusset, J., Peters, J.M., Kaya, G., Gonzalez, F.J., Zakany, J., Metzger, D., Chambon, P., Duboule, D., Wahli, W., 2001. Impaired skin wound healing in peroxisome proliferator–activated receptor (PPAR)α and PPARβ mutant mice. J. Cell Biol. 154, 799–814. https://doi.org/10.1083/jcb.200011148

Mitchell, C.A., Dasgupta, S., Zhang, S., Stapleton, H.M., Volz, D.C., 2018. Disruption of Nuclear Receptor Signaling Alters Triphenyl Phosphate-Induced Cardiotoxicity in Zebrafish Embryos. Toxicol. Sci. 163, 307–318. https://doi.org/10.1093/toxsci/kfy037

Muerhoff, A.S., Griffin, K.J., Johnson, E.F., 1992. The peroxisome proliferator-activated receptor mediates the induction of CYP4A6, a cytochrome P450 fatty acid omega-hydroxylase, by clofibric acid. J. Biol. Chem. 267, 19051–19053.

Nagayama, J., Tsuji, H., Takasuga, T., 2000. Comparison between brominated flame retardants and dioxins or organochlorine compounds in blood levels of Japanese adults. Organohalogen Compd. 48, 27–30.

Nagy, L., Tontonoz, P., Alvarez, J.G., Chen, H., Evans, R.M., 1998. Oxidized LDL regulates macrophage gene expression through ligand activation of PPARgamma. Cell 93, 229–240. https://doi.org/10.1016/s0092-8674(00)81574-3

Narala, V.R., Adapala, R.K., Suresh, M.V., Brock, T.G., Peters-Golden, M., Reddy, R.C., 2010. Leukotriene B4 Is a Physiologically Relevant Endogenous Peroxisome Proliferator-activated Receptor-α Agonist. J. Biol. Chem. 285, 22067–22074. https://doi.org/10.1074/jbc.M109.085118

Nesto R.W., Bell David, Bonow Robert O., Fonseca Vivian, Grundy Scott M., Horton Edward S., Le Winter Martin, Porte Daniel, Semenkovich Clay F., Smith Sidney, Young Lawrence H., Kahn Richard, 2003. Thiazolidinedione Use, Fluid Retention, and Congestive Heart Failure. Circulation 108, 2941–2948. https://doi.org/10.1161/01.CIR.0000103683.99399.7E

Nielsen, R., Pedersen, T.Å., Hagenbeek, D., Moulos, P., Siersbæk, R., Megens, E., Denissov, S., Børgesen, M., Francoijs, K.-J., Mandrup, S., Stunnenberg, H.G., 2008. Genome-wide profiling of PPARγ:RXR and RNA polymerase II occupancy reveals temporal activation of distinct metabolic pathways and changes in RXR dimer composition during adipogenesis. Genes Dev 22, 2953–2967. https://doi.org/10.1101/gad.501108

Nikaido, M., Tada, M., Saji, T., Ueno, N., 1997. Conservation of BMP signaling in zebrafish mesoderm patterning. Mech. Dev. 61, 75–88. https://doi.org/10.1016/S0925-4773(96)00625-9

Nishii, N., Arai, M., Yanai, N., Togari, A., Nakabayashi, T., 2009. Effect of Bone Morphogenetic Protein-2 (BMP-2) or Troglitazone, as an Inducer of Osteogenic Cells or Adipocytes, on Differentiation of a Bone Marrow Mesenchymal Progenitor Cell Line Established from Temperature-Sensitive (ts) Simian Virus (SV) 40 T-Antigen Gene Transgenic Mice. Biol. Pharm. Bull. 32, 10–17. https://doi.org/10.1248/bpb.32.10

Nissen, S.E., Wolski, K., 2007. Effect of Rosiglitazone on the Risk of Myocardial Infarction and Death from Cardiovascular Causes. New England Journal of Medicine 356, 2457–2471. https://doi.org/10.1056/NEJMoa072761

Nolan, J.J., Ludvik, B., Beerdsen, P., Joyce, M., Olefsky, J., 1994. Improvement in Glucose Tolerance and Insulin Resistance in Obese Subjects Treated with Troglitazone. New England Journal of Medicine 331, 1188–1193. https://doi.org/10.1056/NEJM199411033311803

Ogunbayo, O.A., Lai, P.F., Connolly, T.J., Michelangeli, F., 2008. Tetrabromobisphenol A (TBBPA), induces cell death in TM4 Sertoli cells by modulating Ca2+ transport proteins and causing dysregulation of Ca2+ homeostasis. Toxicology in Vitro 22, 943–952. https://doi.org/10.1016/j.tiv.2008.01.015

Ohshima, T., Koga, H., Shimotohno, K., 2004. Transcriptional Activity of Peroxisome Proliferator-activated Receptor γ Is Modulated by SUMO-1 Modification. J. Biol. Chem. 279, 29551–29557. https://doi.org/10.1074/jbc.M403866200

Passeri, M.J., Cinaroglu, A., Gao, C., Sadler, K.C., 2009. Hepatic steatosis in response to acute alcohol exposure in zebrafish requires sterol regulatory element binding protein activation. Hepatology 49, 443–452. https://doi.org/10.1002/hep.22667

Patsouris, D., Mandard, S., Voshol, P.J., Escher, P., Tan, N.S., Havekes, L.M., Koenig, W., März, W., Tafuri, S., Wahli, W., Müller, M., Kersten, S., 2004. PPARα governs glycerol metabolism. J Clin Invest 114, 94–103. https://doi.org/10.1172/JCI20468

Peters, J.M., Lee, S.S.T., Li, W., Ward, J.M., Gavrilova, O., Everett, C., Reitman, M.L., Hudson, L.D., Gonzalez, F.J., 2000. Growth, Adipose, Brain, and Skin Alterations Resulting from Targeted Disruption of the Mouse Peroxisome Proliferator-Activated Receptor β(δ). Mol. Cell. Biol. 20, 5119–5128. https://doi.org/10.1128/MCB.20.14.5119-5128.2000

Pettinelli, P., Videla, L.A., 2011. Up-regulation of PPAR-gamma mRNA expression in the liver of obese patients: an additional reinforcing lipogenic mechanism to SREBP-1c induction. J Clin Endocrinol Metab 96, 1424–1430. https://doi.org/10.1210/jc.2010-2129

Poirier, H., Niot, I., Monnot, M.-C., Braissant, O., Meunier-Durmort, C., Costet, P., Pineau, T., Wahli, W., Willson, T.M., Besnard, P., 2001. Differential involvement of peroxisome-proliferator-activated receptors α and δ in fibrate and fatty-acid-mediated inductions of the gene encoding liver fatty-acid-binding protein in the liver and the small intestine. Biochem. J. 355, 481–488. https://doi.org/10.1042/bj3550481

Puri, P., Baillie, R.A., Wiest, M.M., Mirshahi, F., Choudhury, J., Cheung, O., Sargeant, C., Contos, M.J., Sanyal, A.J., 2007. A lipidomic analysis of nonalcoholic fatty liver disease. Hepatology 46, 1081–1090. https://doi.org/10.1002/hep.21763

Qiang, L., Wang, L., Kon, N., Zhao, W., Lee, S., Zhang, Y., Rosenbaum, M., Zhao, Y., Gu, W., Farmer, S.R., Accili, D., 2012. Brown Remodeling of White Adipose Tissue by SirT1-Dependent Deacetylation of Pparγ. Cell 150, 620–632. https://doi.org/10.1016/j.cell.2012.06.027

Reddam, A., Mitchell, C.A., Dasgupta, S., Kirkwood, J.S., Vollaro, A., Hur, M., Volz, D.C., 2019. mRNA-sequencing identifies liver as a potential target organ for triphenyl phosphate in embryonic zebrafish. Toxicol. Sci. 172(1), 51-62. doi: 10.1093/toxsci/kfz169

Ribeiro, E.S., Greco, L.F., Bisinotto, R.S., Lima, F.S., Thatcher, W.W., Santos, J.E., 2016. Biology of Preimplantation Conceptus at the Onset of Elongation in Dairy Cows. Biol. Reprod. 94, 1-18. https://doi.org/10.1095/biolreprod.115.134908

Ricote, M., Li, A.C., Willson, T.M., Kelly, C.J., Glass, C.K., 1998. The peroxisome proliferator-activated receptor-γ is a negative regulator of macrophage activation. Nature 391, 79–82. https://doi.org/10.1038/34178

Rieusset, J., Seydoux, J., Anghel, S.I., Escher, P., Michalik, L., Soon Tan, N., Metzger, D., Chambon, P., Wahli, W., Desvergne, B., 2004. Altered growth in male peroxisome proliferator-activated receptor gamma (PPARgamma) heterozygous mice: involvement of PPARgamma in a negative feedback regulation of growth hormone action. Mol. Endocrinol. Baltim. Md 18, 2363–2377. https://doi.org/10.1210/me.2003-0325

Riu, A., Grimaldi, M., le Maire, A., Bey, G., Phillips, K., Boulahtouf, A., Perdu, E., Zalko, D., Bourguet, W., Balaguer, P., 2011. Peroxisome proliferator-activated receptor γ is a target for halogenated analogs of bisphenol A. Environ Health Perspect 119, 1227–1232. https://doi.org/10.1289/ehp.1003328

Riu, A., McCollum, C.W., Pinto, C.L., Grimaldi, M., Hillenweck, A., Perdu, E., Zalko, D., Bernard, L., Laudet, V., Balaguer, P., Bondesson, M., Gustafsson, J.-A., 2014. Halogenated Bisphenol-A Analogs Act as Obesogens in Zebrafish Larvae (Danio rerio). Toxicol. Sci. 139, 48–58. https://doi.org/10.1093/toxsci/kfu036

Rosen, E.D., Sarraf, P., Troy, A.E., Bradwin, G., Moore, K., Milstone, D.S., Spiegelman, B.M., Mortensen, R.M., 1999. PPAR gamma is required for the differentiation of adipose tissue in vivo and in vitro. Mol. Cell 4, 611–617. https://doi.org/10.1016/s1097-2765(00)80211-7

Sasai, Y., Lu, B., Steinbeisser, H., Geissert, D., Gont, L.K., De Robertis, E.M., 1994. Xenopus chordin: A novel dorsalizing factor activated by organizer-specific homeobox genes. Cell 79, 779–790. https://doi.org/10.1016/0092-8674(94)90068-X

Schauer, U.M.D., Völkel, W., Dekant, W., 2006. Toxicokinetics of Tetrabromobisphenol A in Humans and Rats after Oral Administration. Toxicological Sciences 91, 49–58. https://doi.org/10.1093/toxsci/kfj132

Schmid, B., Rippmann, J.F., Tadayyon, M., Hamilton, B.S., 2005. Inhibition of fatty acid synthase prevents preadipocyte differentiation. Biochemical and Biophysical Research Communications 328, 1073–1082. https://doi.org/10.1016/j.bbrc.2005.01.067

Schoonjans, K., Watanabe, M., Suzuki, H., Mahfoudi, A., Krey, G., Wahli, W., Grimaldi, P., Staels, B., Yamamoto, T., Auwerx, J., 1995. Induction of the Acyl-Coenzyme A Synthetase Gene by Fibrates and Fatty Acids Is Mediated by a Peroxisome Proliferator Response Element in the C Promoter. J. Biol. Chem. 270, 19269–19276. https://doi.org/10.1074/jbc.270.33.19269

Schymanski, E.L., Jeon, J., Gulde, R., Fenner, K., Ruff, M., Singer, H.P., Hollender, J., 2014. Identifying Small Molecules via High Resolution Mass Spectrometry: Communicating Confidence. Environ. Sci. Technol. 48, 2097–2098. https://doi.org/10.1021/es5002105

Seargent, J.M., Yates, E.A., Gill, J.H., 2004. GW9662, a potent antagonist of PPARγ, inhibits growth of breast tumour cells and promotes the anticancer effects of the PPARγ agonist rosiglitazone, independently of PPARγ activation. Br J Pharmacol 143, 933–937. https://doi.org/10.1038/sj.bjp.0705973

Shen, B., Wei, A., Whittaker, S., Williams, L.A., Tao, H., Ma, D.D.F., Diwan, A.D., 2010. The role of BMP-7 in chondrogenic and osteogenic differentiation of human bone marrow multipotent mesenchymal stromal cells in vitro. J. Cell. Biochem. 109, 406–416. https://doi.org/10.1002/jcb.22412

Sheu, S.-H., Kaya, T., Waxman, D.J., Vajda, S., 2005. Exploring the Binding Site Structure of the PPARγ Ligand-Binding Domain by Computational Solvent Mapping †. Biochemistry 44, 1193–1209. https://doi.org/10.1021/bi048032c

Shi, Z., Jiao, Y., Hu, Y., Sun, Z., Zhou, X., Feng, J., Li, J., Wu, Y., 2013. Levels of tetrabromobisphenol A, hexabromocyclododecanes and polybrominated diphenyl ethers in human

milk from the general population in Beijing, China. Science of The Total Environment 452–453, 10–18. https://doi.org/10.1016/j.scitotenv.2013.02.038

Silva, M.J., Reidy, J.A., Herbert, A.R., Preau, J.L., Needham, L.L., Calafat, A.M., 2004. Detection of phthalate metabolites in human amniotic fluid. Bull. Environ. Contam. Toxicol. 72, 1226–1231. https://doi.org/10.1007/s00128-004-0374-4

Smith, W.C., Harland, R.M., 1992. Expression cloning of noggin, a new dorsalizing factor localized to the Spemann organizer in Xenopus embryos. Cell 70, 829–840. https://doi.org/10.1016/0092-8674(92)90316-5

Sprecher, D.L., Massien, C., Pearce, G., Billin, A.N., Perlstein, I., Willson, T.M., Hassall, D.G., Ancellin, N., Patterson, S.D., Lobe, D.C., Johnson, T.G., 2007. Triglyceride:High-Density Lipoprotein Cholesterol Effects in Healthy Subjects Administered a Peroxisome Proliferator Activated Receptor δ Agonist. Arterioscler. Thromb. Vasc. Biol. 27, 359–365. https://doi.org/10.1161/01.ATV.0000252790.70572.0c

Stapleton, H.M., Klosterhaus, S., Eagle, S., Fuh, J., Meeker, J.D., Blum, A., Webster, T.F., 2009. Detection of organophosphate flame retardants in furniture foam and U.S. house dust. Environ. Sci. Technol. 43, 7490–7495. https://doi.org/10.1021/es9014019

Stechschulte, L.A., Czernik, P.J., Rotter, Z.C., Tausif, F.N., Corzo, C.A., Marciano, D.P., Asteian, A., Zheng, J., Bruning, J.B., Kamenecka, T.M., Rosen, C.J., Griffin, P.R., Lecka-Czernik, B., 2016. PPARG Post-translational Modifications Regulate Bone Formation and Bone Resorption. EBioMedicine 10, 174–184. https://doi.org/10.1016/j.ebiom.2016.06.040

Stephens, J.M., Morrison, R.F., Wu, Z., Farmer, S.R., 1999. PPARγ Ligand-Dependent Induction of STAT1, STAT5A, and STAT5B during Adipogenesis. Biochem. Biophys. Res. Commun. 262, 216–222. https://doi.org/10.1006/bbrc.1999.0889

Storvik, M., Huuskonen, P., Pehkonen, P., Pasanen, M., 2014. The unique characteristics of the placental transcriptome and the hormonal metabolism enzymes in placenta. Reprod. Toxicol. 47, 9–14. https://doi.org/10.1016/j.reprotox.2014.04.010

Strack, S., Detzel, T., Wahl, M., Kuch, B., Krug, H.F., 2007. Cytotoxicity of TBBPA and effects on proliferation, cell cycle and MAPK pathways in mammalian cells. Chemosphere, Halogenated Persistent Organic Pollutants Dioxin 2004 67, S405–S411. https://doi.org/10.1016/j.chemosphere.2006.05.136

Strakova, N., Ehrmann, J., Bartoš, J., Malikova, J., Dolezel, J., Kolar, Z., 2005. Peroxisome proliferator-activated receptor (PPAR) agonists affect cell viability, apoptosis and expression of cell cycle related proteins in cell lines of glial brain tumors. Neoplasma 52, 126–36.

Strakova, N., Ehrmann, J., Dzubak, P., Bouchal, J., Kolar, Z., 2004. The Synthetic Ligand of Peroxisome Proliferator-Activated Receptor-γ Ciglitazone Affects Human Glioblastoma Cell Lines. J Pharmacol Exp Ther 309, 1239–1247. https://doi.org/10.1124/jpet.103.063438

Su, J.-L., Simmons, C.J., Wisely, B., Ellis, B., Winegar, D.A., 1998. Monitoring of PPAR Alpha Protein Expression in Human Tissue by the Use of PPAR Alpha-Specific MAbs. Hybridoma 17, 47–53. https://doi.org/10.1089/hyb.1998.17.47

Sumner, L.W., Amberg, A., Barrett, D., Beale, M.H., Beger, R., Daykin, C.A., Fan, T.W.-M., Fiehn, O., Goodacre, R., Griffin, J.L., Hankemeier, T., Hardy, N., Harnly, J., Higashi, R., Kopka, J., Lane, A.N., Lindon, J.C., Marriott, P., Nicholls, A.W., Reily, M.D., Thaden, J.J., Viant, M.R., 2007. Proposed minimum reporting standards for chemical analysis Chemical Analysis Working Group (CAWG) Metabolomics Standards Initiative (MSI). Metabolomics 3, 211–221. https://doi.org/10.1007/s11306-007-0082-2

Thomsen, C., Lundanes, E., Becher, G., 2001. Brominated flame retardants in plasma samples from three different occupational groups in Norway. Journal of Environmental Monitoring 3, 366–370. https://doi.org/10.1039/B104304H

Tilly-Kiesi, M., Tikkanen, M.J., 1991. Low density lipoprotein density and composition in hypercholesterolaemic men treated with HMG CoA reductase inhibitors and gemfibrozil. J. Intern. Med. 229, 427–434. https://doi.org/10.1111/j.1365-2796.1991.tb00370.x

Tontonoz, P., Hu, E., Graves, R.A., Budavari, A.I., Spiegelman, B.M., 1994. mPPAR gamma 2: tissue-specific regulator of an adipocyte enhancer. Genes Dev. 8, 1224–1234. https://doi.org/10.1101/gad.8.10.1224

Tontonoz, P., Hu, E., Spiegelman, B.M., 1994. Stimulation of adipogenesis in fibroblasts by PPARγ2, a lipid-activated transcription factor. Cell 79, 1147–1156. https://doi.org/10.1016/0092-8674(94)90006-X

Tontonoz, P., Singer, S., Forman, B.M., Sarraf, P., Fletcher, J.A., Fletcher, C.D.M., Brun, R.P., Mueller, E., Altiok, S., Oppenheim, H., Evans, R.M., Spiegelman, B.M., 1997. Terminal differentiation of human liposarcoma cells induced by ligands for peroxisome proliferator-activated receptor γ and the retinoid X receptor. Proc. Natl. Acad. Sci. 94, 237–241. https://doi.org/10.1073/pnas.94.1.237

Velkov, T., 2013. Interactions between Human Liver Fatty Acid Binding Protein and Peroxisome Proliferator Activated Receptor Selective Drugs [WWW Document]. PPAR Research. https://doi.org/10.1155/2013/938401

Vidal-Puig, A., Jimenez-Liñan, M., Lowell, B.B., Hamann, A., Hu, E., Spiegelman, B., Flier, J.S., Moller, D.E., 1996. Regulation of PPAR gamma gene expression by nutrition and obesity in rodents. J. Clin. Invest. 97, 2553–2561. https://doi.org/10.1172/JCI118703

Vignati, S., Albertini, V., Rinaldi, A., Kwee, I., Riva, C., Oldrini, R., Capella, C., Bertoni, F., Carbone, G.M., Catapano, C.V., 2006. Cellular, Molecular Consequences of Peroxisome Proliferator- Activated Receptor-δ Activation in Ovarian Cancer Cells. Neoplasia 8, 851-IN12. https://doi.org/10.1593/neo.06433

Wakabayashi, K., Okamura, M., Tsutsumi, S., Nishikawa, N.S., Tanaka, T., Sakakibara, I., Kitakami, J., Ihara, S., Hashimoto, Y., Hamakubo, T., Kodama, T., Aburatani, H., Sakai, J., 2009. The Peroxisome Proliferator-Activated Receptor γ/Retinoid X Receptor α Heterodimer Targets the Histone Modification Enzyme PR-Set7/Setd8 Gene and Regulates Adipogenesis through a Positive Feedback Loop. Molecular and Cellular Biology 29, 3544–3555. https://doi.org/10.1128/MCB.01856-08

Wang, D., Jiang, X., Lu, A., Tu, M., Huang, W., Huang, P., 2018. BMP14 induces tenogenic differentiation of bone marrow mesenchymal stem cells in vitro. Exp. Ther. Med. 16, 1165–1174. https://doi.org/10.3892/etm.2018.6293

Wang, F., Mullican, S.E., DiSpirito, J.R., Peed, L.C., Lazar, M.A., 2013. Lipoatrophy and severe metabolic disturbance in mice with fat-specific deletion of PPARγ. PNAS 110, 18656–18661. https://doi.org/10.1073/pnas.1314863110

Wang, W., Abualnaja, K.O., Asimakopoulos, A.G., Covaci, A., Gevao, B., Johnson-Restrepo, B., Kumosani, T.A., Malarvannan, G., Minh, T.B., Moon, H.-B., Nakata, H., Sinha, R.K., Kannan, K., 2015. A comparative assessment of human exposure to tetrabromobisphenol A and eight bisphenols including bisphenol A via indoor dust ingestion in twelve countries. Environment International 83, 183–191. https://doi.org/10.1016/j.envint.2015.06.015

Wang, Y., Kwon, G., An, L., Holmes, C.N., Haeba, M., LeBlanc, G.A., 2016. Differential interactions of the flame retardant triphenyl phosphate within the PPAR signaling network. MOJ Toxicol. Volume 2. https://doi.org/10.15406/mojt.2016.02.00039

Wang, Y.-X., Zhang, C.-L., Yu, R.T., Cho, H.K., Nelson, M.C., Bayuga-Ocampo, C.R., Ham, J., Kang, H., Evans, R.M., 2004. Regulation of Muscle Fiber Type and Running Endurance by PPARδ. PLOS Biol. 2, e294. https://doi.org/10.1371/journal.pbio.0020294

Werman, A., Hollenberg, A., Solanes, G., Bjørbæk, C., Vidal-Puig, A.J., Flier, J.S., 1997. Ligand-independent Activation Domain in the N Terminus of Peroxisome Proliferator-activated Receptor γ (PPARγ) DIFFERENTIAL ACTIVITY OF PPARγ1 AND -2 ISOFORMS AND INFLUENCE OF INSULIN. J. Biol. Chem. 272, 20230–20235. https://doi.org/10.1074/jbc.272.32.20230

West, A.G., Fraser, P., 2005. Remote control of gene transcription. Human Molecular Genetics 14, R101–R111. https://doi.org/10.1093/hmg/ddi104

Wettstein, G., Luccarini, J.-M., Poekes, L., Faye, P., Kupkowski, F., Adarbes, V., Defrêne, E., Estivalet, C., Gawronski, X., Jantzen, I., Philippot, A., Tessier, J., Tuyaa-Boustugue, P., Oakley, F., Mann, D.A., Leclercq, I., Francque, S., Konstantinova, I., Broqua, P., Junien, J.-L., 2017. The new-generation pan-peroxisome proliferator-activated receptor agonist IVA337 protects the liver from metabolic disorders and fibrosis. Hepatol. Commun. 1, 524–537. https://doi.org/10.1002/hep4.1057

White, R.J., Collins, J.E., Sealy, I.M., Wali, N., Dooley, C.M., Digby, Z., Stemple, D.L., Murphy, D.N., Billis, K., Hourlier, T., Enright, A.J., Busch-Nentwich, E.M., 2017. A high-resolution mRNA expression time course of embryonic development in zebrafish. eLife 6, e30860. https;//doi.org/10.7554/eLife.30860

Wilkening, S., Stahl, F., Bader, A., 2003. Comparison of Primary Human Hepatocytes and Hepatoma Cell Line Hepg2 with Regard to Their Biotransformation Properties. Drug Metab Dispos 31, 1035–1042. https://doi.org/10.1124/dmd.31.8.1035

Willy, P.J., Umesono, K., Ong, E.S., Evans, R.M., Heyman, R.A., Mangelsdorf, D.J., 1995. LXR, a nuclear receptor that defines a distinct retinoid response pathway. Genes Dev. 9, 1033–1045. https://doi.org/10.1101/gad.9.9.1033

Wojtowicz, A.K., Szychowski, K.A., Kajta, M., 2014. PPAR-γ Agonist GW1929 But Not Antagonist GW9662 Reduces TBBPA-Induced Neurotoxicity in Primary Neocortical Cells. Neurotox Res 25, 311–322. https://doi.org/10.1007/s12640-013-9434-z

Xu, H.E., Lambert, M.H., Montana, V.G., Parks, D.J., Blanchard, S.G., Brown, P.J., Sternbach, D.D., Lehmann, J.M., Wisely, G.B., Willson, T.M., Kliewer, S.A., Milburn, M.V., 1999. Molecular recognition of fatty acids by peroxisome proliferator-activated receptors. Mol. Cell 3, 397–403. https://doi.org/10.1016/s1097-2765(00)80467-0

Yamashita, D., Yamaguchi, T., Shimizu, M., Nakata, N., Hirose, F., Osumi, T., 2004. The transactivating function of peroxisome proliferator-activated receptor γ is negatively regulated by SUMO conjugation in the amino-terminal domain. Genes Cells 9, 1017–1029. https://doi.org/10.1111/j.1365-2443.2004.00786.x

Yang, C.F., Shen, H.M., Ong, C.N., 1999. Protective effect of ebselen against hydrogen peroxide-induced cytotoxicity and DNA damage in HepG2 cells. Biochemical Pharmacology 57, 273–279. https://doi.org/10.1016/S0006-2952(98)00299-8

Yin, N., Liang, Shaojun, Liang, Shengxian, Yang, R., Hu, B., Qin, Z., Liu, A., Faiola, F., 2018. TBBPA and Its Alternatives Disturb the Early Stages of Neural Development by Interfering with the NOTCH and WNT Pathways. Environ. Sci. Technol. 52, 5459–5468. https://doi.org/10.1021/acs.est.8b00414

Yozzo, K.L., McGee, S.P., Volz, D.C., 2013. Adverse outcome pathways during zebrafish embryogenesis: A case study with paraoxon. Aquat. Toxicol. 126, 346–354. https://doi.org/10.1016/j.aquatox.2012.09.008

Yu, C., Markan, K., Temple, K.A., Deplewski, D., Brady, M.J., Cohen, R.N., 2005. The Nuclear Receptor Corepressors NCoR and SMRT Decrease Peroxisome Proliferator-activated Receptor γ Transcriptional Activity and Repress 3T3-L1 Adipogenesis. J. Biol. Chem. 280, 13600–13605. https://doi.org/10.1074/jbc.M409468200

Yu, S., Matsusue, K., Kashireddy, P., Cao, W.-Q., Yeldandi, V., Yeldandi, A.V., Rao, M.S., Gonzalez, F.J., Reddy, J.K., 2003. Adipocyte-specific Gene Expression and Adipogenic Steatosis in the Mouse Liver Due to Peroxisome Proliferator-activated Receptor γ1 (PPARγ1) Overexpression. J. Biol. Chem. 278, 498–505. https://doi.org/10.1074/jbc.M210062200

Zechel, C., Shen, X.Q., Chambon, P., Gronemeyer, H., 1994. Dimerization interfaces formed between the DNA binding domains determine the cooperative binding of RXR/RAR and RXR/TR heterodimers to DR5 and DR4 elements. EMBO J. 13, 1414–1424.

Zhang, Y., Wang, X., Chen, C., An, J., Shang, Y., Li, H., Xia, H., Yu, J., Wang, C., Liu, Y., Guo, S., 2019. Regulation of TBBPA-induced oxidative stress on mitochondrial apoptosis in L02 cells through the Nrf2 signaling pathway. Chemosphere 226, 463–471. https://doi.org/10.1016/j.chemosphere.2019.03.167

Zhao, F., Kang, Q., Zhang, X., Liu, J., Hu, J., 2019. Urinary biomarkers for assessment of human exposure to monomeric aryl phosphate flame retardants. Environ. Int. 124, 259–264. https://doi.org/10.1016/j.envint.2019.01.022

Zhao, J., Sun, X.-B., Ye, F., Tian, W.-X., 2011. Suppression of fatty acid synthase, differentiation and lipid accumulation in adipocytes by curcumin. Mol Cell Biochem 351, 19–28. https://doi.org/10.1007/s11010-010-0707-z

Zhu, J., Huang, X., Jiang, H., Hu, L., Michal, J.J., Jiang, Z., Shi, H., 2018. The role of pparγ in embryonic development of Xenopus tropicalis under triphenyltin-induced teratogenicity. Sci. Total Environ. 633, 1245–1252. https://doi.org/10.1016/j.scitotenv.2018.03.313